REMOTE SENSING OF THE ELECTRODYNAMIC COUPLING BETWEEN THUNDERSTORM SYSTEMS AND THE MESOSPHERE / LOWER IONOSPHERE

A DISSERTATION

SUBMITTED TO THE DEPARTMENT OF ELECTRICAL ENGINEERING

AND THE COMMITTEE ON GRADUATE STUDIES

OF STANFORD UNIVERSITY

IN PARTIAL FULFILLMENT OF THE REQUIREMENTS

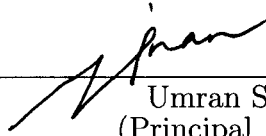FOR THE DEGREE OF

DOCTOR OF PHILOSOPHY

By

Steven Craig Reising

June 1998

I certify that I have read this dissertation and that in my opinion it is fully adequate, in scope and in quality, as a dissertation for the degree of Doctor of Philosophy.
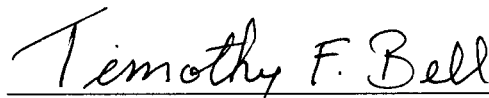
_____
Umran S. Inan
(Principal Adviser)

I certify that I have read this dissertation and that in my opinion it is fully adequate, in scope and in quality, as a dissertation for the degree of Doctor of Philosophy.
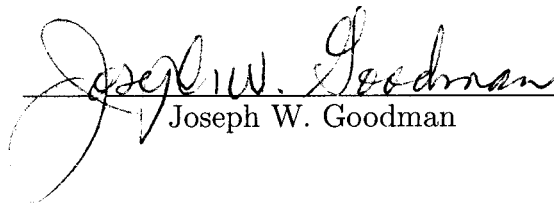
_____
Timothy F. Bell

I certify that I have read this dissertation and that in my opinion it is fully adequate, in scope and in quality, as a dissertation for the degree of Doctor of Philosophy.

_____
Joseph W. Goodman

Approved for the University Committee on Graduate Studies:

_____

iii

Dedication

In Memoriam

Flavian "Flip" Reising
(1912-1997)

M. Elizabeth "Betty" Reising
(1910-1988)

Joseph P. Bradley
(1895-1968)

J. Theresia Bradley
(1901-1981)

For the love and labor of those who preceded us,
May we deserve their legacy.

Abstract

In the past few years, dramatic experimental evidence has emerged, showing that tropospheric lightning discharges modify the mesosphere and the lower ionosphere through heating and ionization, producing gamma-ray bursts and optical emissions known as red sprites, blue jets, and elves. These transient electrodynamic coupling processes may have long-term effects such as chemical changes, persistent heating of ionospheric electrons, and increased production of mesospheric and stratospheric nitrogen oxides (NO_y). In order to assess the regional and global effects of the intense electrodynamic coupling of thunderstorms to the middle atmosphere, the occurrence rate of Sprites needs to be known over large areas of the Earth. Since continuous optical monitoring of Sprite occurrence on large spatial scales is not practical, a continuous proxy indicator for Sprite occurrence is needed.

Sprites are intense, transient luminous events in the mesosphere and lower ionosphere above thunderstorm systems. They extend from ∼40 to ∼90 km in altitude, are primarily red in color, and develop to full brightness in a few milliseconds. Sprites are nearly uniquely associated with positive cloud-to-ground lightning flashes, yet they occur in association with only a small subset of those flashes. The peak current of each flash, measured at high frequencies by the National Lightning Detection Network, is not a sufficient indicator of the likelihood of a positive cloud-to-ground lightning flash to produce a Sprite.

In this work, remote sensing of the electrodynamic coupling between thunderstorm systems and the mesosphere and lower ionosphere is accomplished by measurement of radio atmospherics in the ELF (extremely low frequency, here 15 Hz - 1.5 kHz) and VLF (very low frequency, here 1.5 - 22 kHz) ranges. Radio atmospherics ("sferics") provide a unique signature of each lightning return stroke and propagate efficiently in the waveguide bounded by the Earth's surface and the ionosphere. Novel digital signal processing techniques for ELF/VLF broadband measurements allow automated

detection and arrival azimuth determination of individual radio atmospherics. Arrival azimuth measurement is accomplished with $\pm 1°$ precision for radio atmospherics propagating from Nebraska to Palmer Station, Antarctica, a source-to-receiver distance of $\sim$12,000 km. Identification of the time of occurrence of sferics to $\sim$1-millisecond precision allows the identification of individual lightning discharges as the source of individual radio atmospherics. Broadband ELF/VLF measurements of radio atmospherics therefore allow the determination of characteristics of *those* lightning discharges which couple strongly to the middle atmosphere and lead to Sprite production.

Broadband measurements of sferics performed near Ft. Collins, Colorado, $\sim$500 km from the causative lightning, demonstrate that the ELF sferic energy is a proxy indicator which can be used to estimate the number of Sprites produced by a thunderstorm with an accuracy of $\pm 25\%$. In addition, simultaneous video observations of Sprites reveal variable delays of up to 100 milliseconds between the positive cloud-to-ground flash and Sprite onset. Comparison with high-resolution photometer measurements demonstrate the simultaneity of Sprite luminosity and an ELF "second pulse," radiated by electrical currents within the Sprite body [*Cummer et al.*, 1998]. Measurements of the second pulse are used to identify a quantitative relationship between the current in Sprites and total Sprite luminosity. Ultra-long range measurements at Palmer Station, Antarctica, show that Sprite-associated sferics have large ELF magnitudes in relation to non Sprite-associated sferics as measured at a range of $\sim$12,000 km [*Reising et al.*, 1996]. These results suggest that a few appropriately placed ELF/VLF sferics receivers may be sufficient for estimation of global Sprite occurrence rates.

Acknowledgements

Near the middle of this work, I realized that the proverbial had become true; I was and am standing on the shoulders of giants. Our accomplishments would be impossible without the legacy of our predecessors and the guidance and collaboration of our contemporaries. The least I can do is to recognize some of the persons who have participated in this work and in my development as a scientist and as an engineer.

First and foremost, I would like to express my unequivocal gratitude to Professor Umran Inan, my principal advisor, for leading me into the field and the fray of scientific inquiry, for showing me by example how to succeed as a researcher and a scholar, and for supporting and promoting our efforts with seemingly boundless energy and dedication. Secondly, I would like to give wholehearted thanks to Dr. Tim Bell, my co-advisor, for his cheerful guidance in the development of a discerning eye and mind and for his ever-present wit and insight in facing our everyday challenges in the world of science. Professor Bob Helliwell passed along to me, as to so many, the original enthusiasm and inquisitiveness with which he founded the VLF Group more than forty years ago. Dr. Vikas Sonwalkar provided initial advice on the subject of sferics and continuing encouragement as his career took him to the University of Alaska Fairbanks. Professor Don Carpenter was a continual source of encouragement and support. I thank Professor Tony Fraser-Smith for his scientific discussions, for serving on my orals committee and for his first-rate sense of humor. I give special thanks to Professor J. W. Goodman for serving as my orals chairman and third reader of this dissertation.

The staff of the VLF Group made this work possible. Shao Lan Min and June Wang provided outstanding proposal support and cheerful advice. Bill Trabucco gave me unparalleled training on field work in the Arctic and Antarctic regions and on building reliable, fail-safe hardware. Jerry Yarbrough taught me time-saving and

talented and dedicated support for the Palmer Station experiments which provided much of the data for this dissertation.

In closing, I cannot forget the people that play the most pivotal role in all of our lives, our families. I am grateful to my parents, Flavian and Mary Jo, for teaching me the value of education, of committing myself to a goal and of persisting to achieve it. I thank my sister, Kathy, for her unflagging love and support. Finally, my wife Kathleen Zaleski has been the most patient and the most steadfast in her belief in my potential for success. For all of these giants in my life, I am forever grateful.

Steven C. Reising

Stanford, California
May 31, 1998

Contents

List of Tables

List of Figures

Chapter 1

Introduction

Each lightning discharge dissipates a total energy of $\sim 10^9$ J, of which $\sim 10^6$ J is radiated as electromagnetic energy, during a duration of ~ 0.1 ms [*Uman*, 1987; pp. 322-323]. Energy released by a subset of lightning discharges couples to the mesosphere and the lower ionosphere, where the most dramatic visible effects are transient, luminous glows known as Sprites (see Figure 1.1), first recorded in 1989 [*Franz et al.*, 1990]. The characteristics of Sprites are described in Section 1.1. Each Sprite appears following a positive cloud-to-ground lightning discharge [*Boccippio et al.*, 1995; *Reising et al.*, 1996]. The characteristics of lightning discharges and the thunderstorm systems relevant to Sprites are described in Section 1.2. The intensity of the lightning discharge, which is measured routinely by the National Lightning Detection Network, is not a sufficient indicator of whether or not a given positive discharge is likely to initiate a Sprite. In this work, lightning discharges are remotely characterized via the measurement of their electromagnetic signatures, known as radio atmospherics, which propagate efficiently in the Earth-ionosphere waveguide. Measurement of radio atmospherics allows detection of the properties of *those* lightning discharges which lead to Sprites and, consequently, of the total number of Sprites produced by a thunderstorm. The characteristics of radio atmospherics are described in Section 1.3.

1.1 Sprites

Sprites are transient luminous glows in the middle atmosphere above thunderstorms, arguably the most dramatic visible evidence of electrodynamic coupling between thunderstorm systems and the overlying mesosphere and lower ionosphere (see Figure 1.1). Sprites extend from ~40 to ~90 km in altitude and have transverse extents of ~10 to ~50 km [*Sentman et al.*, 1995; *Lyons*, 1996]. They develop to full brightness in 1-3 ms [*Cummer et al.*, 1998], but their luminosity may last for 10-100 ms [*Fukunishi et al.*, 1996; *Winckler et al.*, 1996; *Lyons*, 1996]. Low light level video observations of Sprites have been conducted from the Space Shuttle [*Boeck et al.*, 1995], from aircraft [*Sentman and Wescott*, 1993; *Sentman et al.*, 1995] and from the ground [*Franz et al.*, 1990; *Lyons*, 1994; 1996; *Winckler et al.*, 1996].
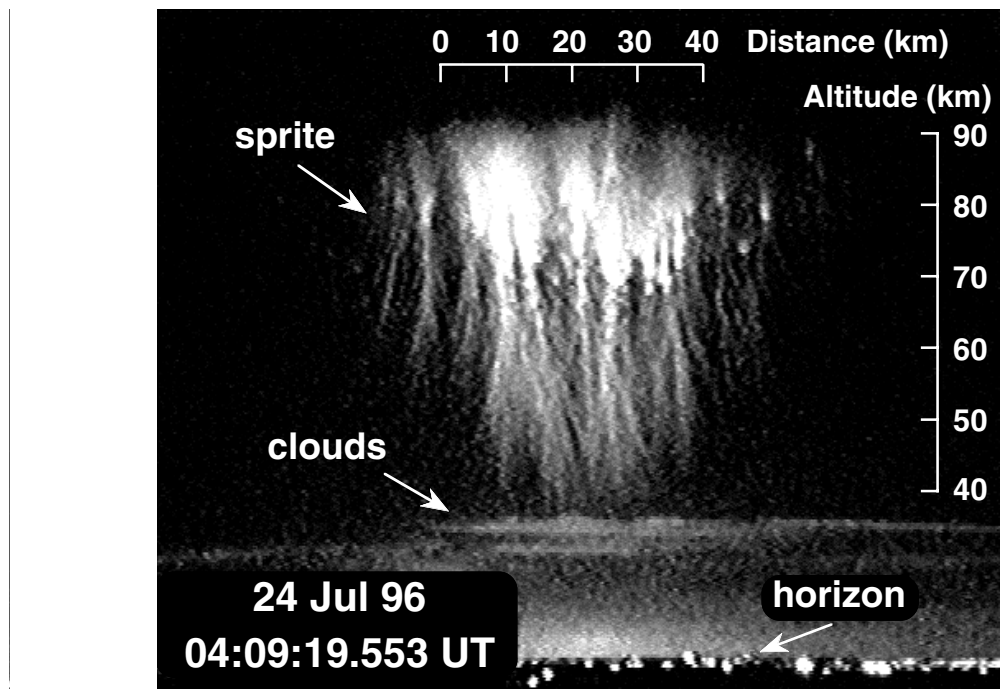
Figure 1.1: Image of a Sprite recorded by an intensified CCD video camera at Yucca Ridge, Colorado, at ~550 km range. Observations were made as a part of the Stanford University Fly's Eye Experiment.

Observations of other optical emissions provide additional evidence of electrodynamic coupling between thunderstorm systems and the middle atmosphere, including blue jets and blue starters from aircraft [*Wescott et al.*, 1995; 1996] and elves from the Space Shuttle [*Boeck et al.*, 1992] and from the ground [*Fukunishi et al.*, 1996; *Inan*

et al., 1997]. Other evidence of electrodynamic coupling includes VLF signatures of rapid changes in conductivity and ionization in the lower ionosphere [*Inan et al.*, 1988, 1993, 1995, 1996a; *Dowden et al.*, 1994] and radar detection of transient ionization patches above a thunderstorm [*Roussel-Dupré and Blanc*, 1997]. The observation of terrestrial gamma-ray flashes by the Burst and Transient Source Experiment is one of the most unexpected discoveries made by the Compton Gamma-Ray Observatory [*Fishman et al.*, 1994]. A number of satellite observations of gamma-ray flashes have been directly associated with individual sferics generated by positive CG discharges [*Inan et al.*, 1996b]. The gamma-ray photon energy extends above 1 MeV, indicating bremsstrahlung radiation from >1 MeV electrons, consistent with predictions of upward beams of runaway electrons accelerated by thundercloud electric fields [*Wilson*, 1925; *Bell et al.*, 1995; *Taranenko and Roussel-Dupré*, 1996; *Lehtinen et al.*, 1996; 1997].

Sprites are believed to be produced by intense quasi-electrostatic fields (tens of kV/m at ∼70 km altitude) which exist at high altitudes following positive CG discharges [*Pasko et al.*, 1995, 1996, 1997; *Boccippio et al.*, 1995; *Winckler et al.*, 1996; *Fernsler and Rowland*, 1996]. These quasi-electrostatic fields lead to ambient electron heating (up to ∼5 eV average energy), the ionization of neutrals and the excitation of optical emissions in the altitude range ∼40 to ∼90 km [*Pasko et al.*, 1997, and references therein]. The runaway electron mechanism may also play a role in Sprite generation [*Bell et al.*, 1995; *Taranenko and Roussel-Dupré*, 1996; *Lehtinen et al.*, 1996; 1997]. Another mechanism of interaction with the mesosphere and the lower ionosphere is the heating of ambient electrons by lightning electromagnetic pulses, which has been applied to explain the existence of elves [*Inan et al.*, 1991, 1996c; *Taranenko et al.*, 1993; *Rowland et al.*, 1995, 1996] and of Sprites [*Milikh et al.*, 1995].

For the quasi-electrostatic mechanism of Sprite production, the important parameters that determine whether or not a positive CG flash produces a Sprite are the altitude and magnitude of the thundercloud charge removed to ground. For a fixed altitude of removed charge, the single most important parameter in determining Sprite occurrence is the magnitude of the charge lowered to ground. The discharge duration plays a secondary role, as long as the charge removal time is shorter than the local relaxation time (ϵ_o/σ) at ∼70-90 km altitudes [*Boccippio et al.*, 1995; *Pasko et al.*, 1995; 1997].

1.2 Lightning Discharges and Thunderstorm Systems

In this dissertation we consider primarily cloud-to-ground (CG) lightning discharges, as opposed to intracloud discharges, which do not make electrical contact with the ground. This focus is appropriate because Sprites are nearly exclusively accompanied by CG flashes. In fact, the vast majority of prior research on lightning has also focused on CG discharges because of their potential for damage to property and living things, and because of their relative accessibility for study. It should be noted, however, that the number of intracloud discharges in a thunderstorm exceeds the number of CG discharges by a factor of ∼2-5 [*Uman*, 1987; pp. 44-45], and that the energy released in intracloud discharges may play an important role in electrodynamic coupling to the middle and upper atmosphere.

1.2.1 Positive and Negative Discharges

The polarity of a CG lightning discharge is classified as "positive" or "negative" based on the polarity of its net effect on the charge of the thundercloud. If the net effect of the discharge is to move negative charge (electrons) from the cloud to the ground, it is called a *negative CG*. If it has the net effect of transferring positive charge from the cloud to the ground (electrons moving upward), then it is called a *positive CG*. This terminology is in common use in the lightning literature [*Uman*, 1987; pp. 9-10]. The total CG discharge is called a *flash* and has a typical duration of 0.1 - 1 s. A CG flash consists of a series of leaders, typically three or four, each followed by *return strokes*, which occur each time there is a completion of the electrical connection between the cloud's charge reservoir and the ground. The first return stroke is initiated by the *stepped leader*, the visible channel following a high conductivity path formed by preliminary breakdown preceding the flash. If the flash ends when the first return stroke ceases, it is called a single-stroke flash. On the other hand, if additional charge is available in the cloud, a *dart leader* may propagate down the residual channel and initiate a subsequent return stroke. As many as 15 more return strokes may occur in the same flash, with typical delays between strokes of 30-100 ms [*Uman*, 1987; pp. 10-19].

Negative and positive CGs differ in their properties and occurrence rates. Positive

flashes are generally composed of a single stroke, sometimes followed by a period of continuing current (see Section 1.2.2). Positive CGs may dominate some winter storms, reportedly constituting up to 90-100% of the total lightning [*Brook et al*, 1989]. However, overall lightning rates in winter are low, and summer thunderstorms produce predominantly negative CG flashes [*Uman*, 1987; p. 20]. Consequently, negatives represented >97% of the CG flashes in the continental U.S. during 1989-1991, as recorded by the National Lightning Detection Network (see Section 1.2.4) [*Orville*, 1994]. An increase in the fraction of positive lightning in summer thunderstorms is correlated with increasing latitude and with increasing elevation above sea level [*Uman*, 1987; p. 20].

One of the most complete descriptions of return stroke currents is based on measurements of discharges to towers in Switzerland (e.g., [*Berger et al.*, 1975]). The currents were derived from measurements of the voltages induced in resistive shunts located on two towers reaching 55 m above the summit of Mt. San Salvatore [*Uman*, 1987; p. 120]. Based on these measurements, the average duration of negative first return strokes is ∼0.1 ms. The duration of positive first return strokes has more variability, with an average value of 0.2-0.6 ms [*Berger et al.*, 1975]. However, their recorded waveforms may have been altered by the electrical characteristics of the tower and measuring circuit and by the difference between discharges to tall objects and discharges to ground [*Uman*, 1987; p. 121]. Peak current magnitudes measured by *Berger et al.* [1975] were observed to fit a log-normal distribution. Negative first return strokes had a median peak current of 20-40 kA, with levels of 200 kA reached only 1% of the time. Subsequent return strokes carried approximately half the peak current of first strokes. Positive return strokes exhibited the same median peak current as first return strokes, but in extreme cases were much larger, with 5% of the positive peak currents exceeding 250 kA [*Uman*, 1987; pp. 122-125].

1.2.2   Continuing Currents

The total charge lowered from a thundercloud at a given altitude to the ground in a lightning discharge is believed to be the most important parameter in determining its potential for producing a Sprite (see Section 1.1 and [*Pasko et al.*, 1997]). The charge lowered to ground can be computed by integrating the current waveform over time. Typical values of charge transfer in the <0.1 ms duration of a negative return stroke

are ∼3-5 C for first strokes and ∼1 C for subsequent strokes [*Uman*, 1987; p. 125]. For positive return strokes, *Berger et al.* [1975] found that the median was ∼15 C, but that 5% of positive return strokes transferred more than 150 C to ground. Since peak currents rarely exceed 300 kA [*Brook et al.*, 1982], the charge transfer in a return stroke of ∼0.5 ms maximum duration is expected to be <120 C, assuming a simple approximation of a half-cycle of a sine wave for the time-dependence of current in the return stroke. *Continuing currents* are required for larger cloud-to-ground charge transfers. In these cases, current continues to flow in the cloud-to-ground channel for one to hundreds of milliseconds following the return stroke [*Uman*, 1987; pp. 13-14, 172]. Long-lasting continuing currents are of economic interest because they are responsible for the most serious heating damage due to lightning, including many electrical and forest fires [*Rakov and Uman*, 1990].

Brook et al. [1982] documented continuing currents associated with positive CGs from winter thunderstorms on the Hokuriku coast in Japan. They recorded field-change measurements for 12 positive CGs, ten of which were followed by continuing current. The two strongest continuing currents were sustained at a remarkably high level of 10-100 kA for several milliseconds, transferring a total charge to ground of ∼300 C in 4 ms and of ∼200 C in 10 ms. The current magnitude was observed to vary on a 1-ms time scale. A more recent study of winter thunderstorms in the same area of Japan measured >30 positive CGs. The three largest positive CGs were accompanied by continuing currents transferring 200-400 C of charge [*Goto and Narita*, 1995]. Based on observations of five summertime severe storms, *Rust et al.* [1981] reported continuing current durations of 30-240 ms in 31 positive CG flashes. *Brook et al.* [1982] observed continuing currents in association with negative CGs, but the magnitudes of continuing currents were an order of magnitude lower than those associated with positive CGs. Other measurements confirm that strong continuing currents are typically associated with positive CGs [*Uman*, 1987; p. 201].

In summary, removal of large amounts of charge, >120 C, in a single CG return stroke lasting <0.5 ms requires peak currents of >300 kA, a level which is rarely if ever reached. Continuing current of >1 ms duration after the first return stroke of the flash is required to transfer larger amounts of charge from cloud to ground.

OTD Lightning Observations for September 1995 through August 1996

Flash Density (flashes/km²/year)
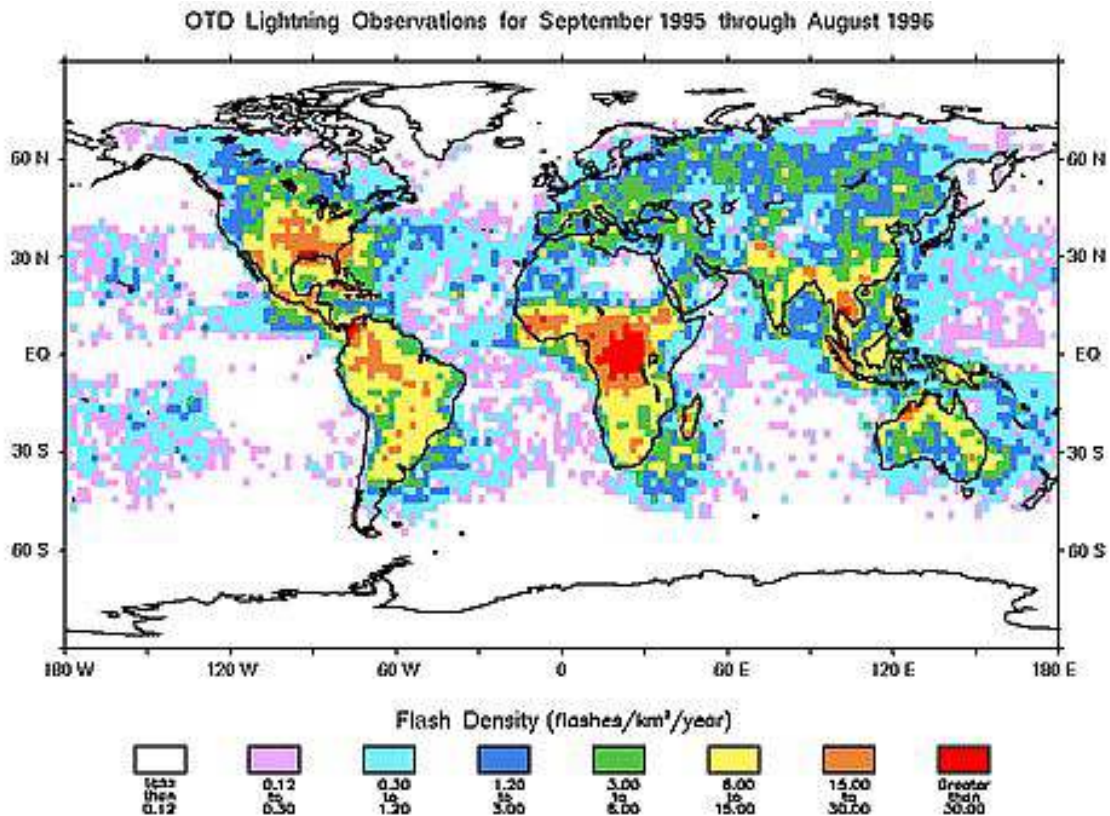
Figure 1.2: Worldwide flash density observations for a one-year period, measured by the Optical Transient Detector orbiting at 750 km altitude and 70° inclination. Courtesy of Dr. H. J. Christian. Available on the World Wide Web at http://thunder.msfc.nasa.gov/otd.html.

1.2.3 Global Lightning

The often-quoted global lightning occurrence rate of $\sim$100 flashes per second was reported in 1925, based on the product of the typical lightning rate for thunderstorms in England (200 flashes per hour), and the average number of thunderstorms on the globe (1800), which was derived from land and maritime records of the number of days per year during which thunder is heard [*Brooks*, 1925]. The first measurements of lightning from space were in general agreement with the rate of $\sim$100 flashes per second, based on an equivalent of five minutes of global lightning data measured at local midnight [*Orville and Henderson*, 1986]. A sufficient sample of global lightning data was not available to test the $\sim$100 flashes per second hypothesis until the launch of the Optical Transient Detector in April 1995 into a 750-km altitude, 70° inclination orbit. The Optical Transient Detector measurements indicate a rate of $\sim$40 flashes

per second worldwide, globally distributed as shown in Figure 1.2 [*Christian et al.*, 1996]. Lightning is preferentially produced over land because of the strong updrafts in continental clouds as opposed to oceanic clouds [*Goodman and Christian*, 1993].

1.2.4 The National Lightning Detection Network

The National Lightning Detection Network (NLDN) has provided real-time lightning data (within 40 seconds) covering the continental United States since 1989 [*Cummins et al.*, 1998]. The NLDN was created by merging regional networks covering the Western U.S. [*Krider et al.*, 1980] and the Midwest [*Mach et al.*, 1986] with the East Coast network operated by the State University of New York at Albany (SUNYA Network) [*Orville et al.*, 1983]. The sensors used in this network were gated, wideband magnetic direction finders manufactured by Lightning Location and Protection, Inc., and were designed to measure only CG lightning flashes [*Krider et al.*, 1976; 1980]. During the same period, a network based on time-of-arrival sensors manufactured by Atmospheric Research Systems, Inc., was installed nationwide [*Lyons et al.*, 1989]. During 1992, Lightning Location and Protection, Inc., developed the Improved Accuracy from Combined Technology method for locating lightning by combining information from both magnetic direction finders and time-of-arrival sensors. This allowed the NLDN to upgrade existing sensors of both types and to combine them with new sensors in order to form a new 106-station upgraded NLDN network, which was completed in 1995 [*Cummins et al.*, 1998].

The NLDN currently provides information on the time, location, intensity, number of strokes per flash and the location accuracy of each flash. The NLDN data used in this work is "flash data," i.e., the data contain timing, location and intensity information about only the first return stroke of each CG flash. The NLDN timing information is accurate to universal coordinated time to within 1 ms. The median accuracy of the CG location is 0.5 km, verified by triangulated video observations [*Idone et al.*, 1998a].

The single measure of return stroke intensity provided by NLDN is the return stroke peak current. The peak current measurement contains no information about the duration of the return stroke nor about continuing currents. Since the rise time of return strokes is ∼5 μs for negative strokes and ∼20 μs for positive strokes, this measurement contains an effective highpass filter at or above ∼50 kHz. However, in

positive CGs with continuing currents, the majority of the cloud-to-ground charge transfer occurs during the continuing current of >1 ms duration (see Section 1.2.2). Therefore the NLDN peak current measurement does not provide a reliable estimate of the total cloud-to-ground charge transfer. The peak current data are provided by NLDN in terms of the normalized magnetic signal strength (M_{peak}). In this work, we obtain the peak current (I_{peak}) from the M_{peak} by using the most recent calibration published prior to 1998, given by Equation 5 of *Idone et al.* [1993]:

$$I_{\mathrm{peak}}(\mathrm{kA}) = 4.20 + 0.171 \times M_{\mathrm{peak}}$$

Additionally, the NLDN data contain the polarity of the first return stroke of the lightning flash. *Brook et al.* [1989] confirmed correct polarity determination of the SUNYA lightning detection network, one of the predecessors of the NLDN, based on electric field change studies of lightning from winter storms in New York state. The authors emphasized the limitation that at >600 km range between the lightning and a magnetic direction finding sensor, the inverted "skywave" reflected from the ionosphere is often much stronger than the direct "ground wave," sometimes resulting in polarity misidentification. In most situations, though, multiple NLDN sensors are located within ~600 km from the source lightning.

In this work, the term "CG flash" is used when the literal meaning is "first return stroke of the CG flash." "Positive CG" or "negative CG" implicitly refer to the first return stroke of the flash.

1.2.5 Mesoscale Convective Systems

Mesoscale convective systems are intermediate-sized meteorological systems which are larger than individual cumulonimbus cells but smaller and shorter-lived than synoptic disturbances [*Barry and Chorley*, 1987; p. 203]. The mesoscale convective systems referred to in this work are midlatitude and subtropical systems which consist of nearly circular clusters of many interacting thunderstorm cells. They are not associated with weather fronts and usually develop during weak synoptic-scale flow. Mesoscale convective systems span transverse scales of >10,000 km^2 and have lifetimes of 6-24 hours. When a mesoscale convective system exceeds a horizontal extent of 100,000 km^2, it is classified as a mesoscale convective complex. These complexes
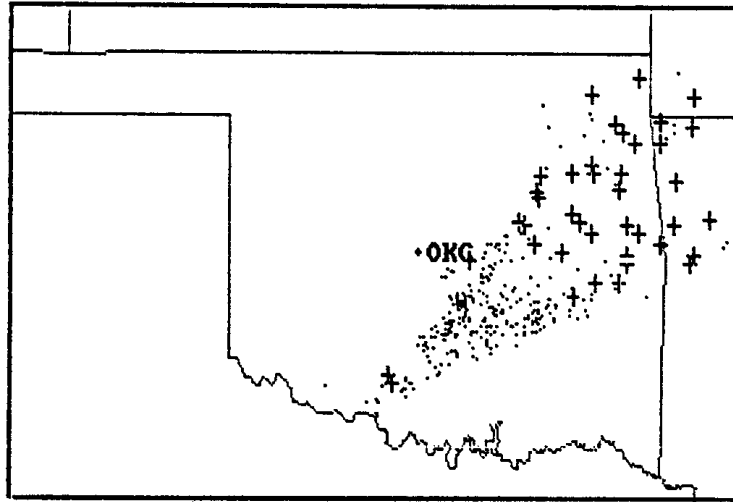
Figure 1.3: From *Brook et al.* [1989]. Winter thunderstorm of January 17, 1988. The storm started at the Oklahoma-Texas border and continued as it moved northeast for a period of 14 hours. The negative (dots) and positive (crosses) CG return strokes are separated into two distinct regions.

are common over the Great Plains and the midwestern U.S. during the spring and summer where they account for perhaps 80% of growing season rainfall [*Barry and Chorley*, 1987; pp. 203-207; *Moran and Morgan*, 1997; pp. 311-313].

   Orville et al. [1988] first reported a "bipolar" pattern in the geographical distribution of positive and negative CGs in many mesoscale convective systems. They found that CG locations were "polarized" into two regions, one predominantly composed of positive CGs and the other of negative CGs, separated by 60-200 km (see Figure 1.3). The direction between the two "bipoles" is that of the upper level (geostrophic) wind, with the positive CGs occurring on the downwind side of the storm. The bipolar pattern was observed in all seasons, with the clearest defined separation of the polarities occurring in winter [*Orville et al.*, 1988]. *Rutledge et al.* [1990] found that negative CGs are concentrated in the convective core of the storm, where the updrafts and rain rates are strongest, and that positive CGs are predominant in the stratiform region. The classical model of thunderstorm electrification, with an area of distributed positive charge overlying an area of negative charge, explains the dominance of negative CGs in the convective core (see top left of Figure 1.4). *Rutledge et al.* [1990] modeled the stratiform region electrification as an inverted dipole, with positive charge on the bottom and negative charge on top (see top right of Figure 1.4), as a result of *in-situ* charging processes independent of those in the convective core.
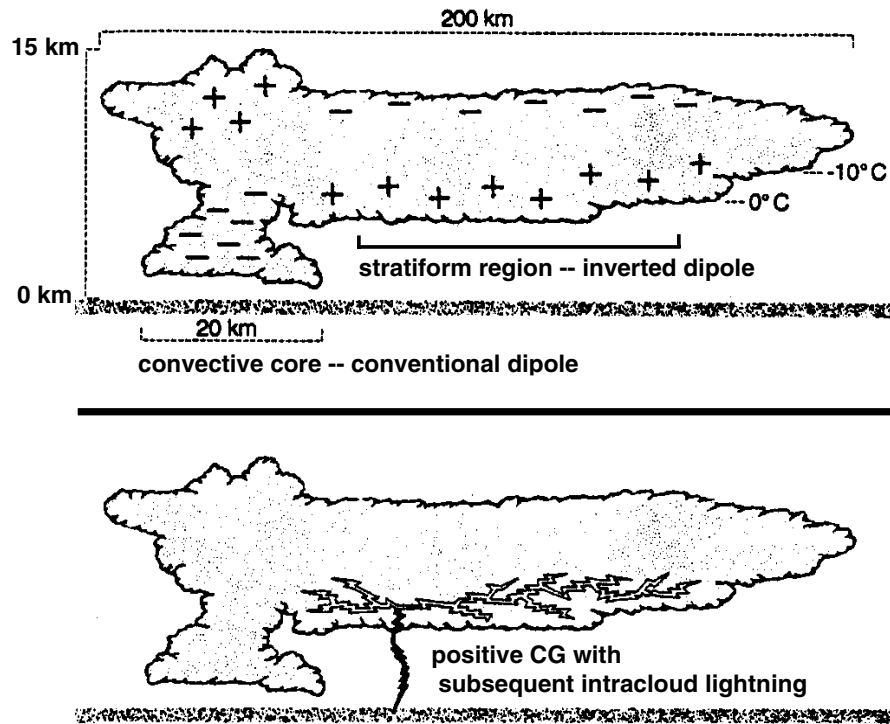
Figure 1.4: Adapted from *Lyons* [1996]. (Top) Schematic of the typical Great Plains mesoscale convective system associated with Sprites. Models of electrification are shown for the convective core on the left and stratiform region on the right. (Bottom) Positive CG causes charge rearrangement in the cloud, which may induce subsequent intracloud "spider" discharges in the stratiform region.

Related work indicates that in the convective core, extensive vertical growth of the thundercloud leads to the creation of a mixed-phase layer between 0°C and −40°C, where graupel particles (1-10 mm snowballs) form and contribute significantly to the charging of the thundercloud [*Williams*, 1995; pp. 36-38]. These "deep convective regions" may be necessary for the formation of downwind horizontally extensive stratiform regions, where the highest percentage of positive CGs occur [*Rutledge et al.*, 1993]. Electric field soundings aboard balloons indicate that the stratiform regions of mesoscale convective systems have multiple vertical layers of space charge, which are nearly uniform in the horizontal dimension and each hold up to ∼1000 C of charge [*Stolzenburg et al.*, 1994; *Marshall et al.*, 1996]. In light of observations of large continuing currents associated with positive CGs (see Section 1.2.2), this charge structure indicates that large reservoirs of positive charge exist in the horizontally extensive (>100 km) stratiform regions of mesoscale convective systems. In some cases, a positive CG and continuing currents may drain charge from only part of the reservoir,

and the resulting charge rearrangement in the stratiform region may induce subsequent intracloud discharges, known as "spider" lightning [*Williams*, 1995; pp. 50-52; *Lyons*, 1996] (see also Section 3.3). Sprites are associated with the occurrence of positive CGs, and most Sprites have been observed overlying the stratiform regions of mesoscale convective systems in the mature or decaying phases (e.g., [*Lyons*, 1996]). The predictions of quasi-electrostatic models of Sprite production (see Section 1.1) are consistent with the hypothesis that large reservoirs of positive charge exist in the stratiform regions of mesoscale convective systems.

1.3   Radio Atmospherics

In this dissertation, broadband ELF/VLF measurements of radio atmospherics are used to assess the characteristics of individual lightning discharges from distances of up to ∼12,000 km. Lightning radiates electromagnetic energy from a few Hz [*Fukunishi et al.*, 1997] up to many tens of MHz [*Weidman and Krider*, 1986]. Consistent with the time and spatial scales of lightning discharges, the peak power radiated by a lightning discharge is in the ELF (extremely low frequency, here 15 Hz - 1.5 kHz) and VLF (very low frequency, here 1.5 kHz - 22 kHz) ranges [*Uman*, 1987; p. 118]. Radio atmospherics are the electromagnetic signals in the ELF/VLF frequency ranges that are launched into the Earth-ionosphere waveguide by lightning discharges [*Budden*, 1961; pp. 5,69]. Radio atmospherics are commonly called "sferics," where the modified spelling is used to avoid confusion with terms such as "spherical geometry." Sferics propagate with low but variable attenuation, typically ∼2-3 dB/1,000 km, depending upon day/night, land/ocean and east/west propagation conditions, and can therefore be observed at large distances (>12,000 km) from the source [*Davies*, 1990; pp. 367, 387-389]. The parallel-plate waveguide which guides the propagation of sferics has as its boundaries the ground and the lower boundary of the D-region of the ionosphere, which at VLF frequencies is ∼70 km altitude during the day and ∼80-85 km altitude at night [*Thomson,* 1993; *Cummer*, 1997].

Radio wave propagation at these frequencies is typically analyzed in terms of waveguide modes, characterized as quasi-transverse electric and quasi-transverse magnetic modes in the VLF frequency range [*Budden*, 1962]. All of the modes except one have cutoff frequencies at integer multiples of ∼1.8 kHz, the frequency with a free-space wavelength equal to the twice the height of the Earth-ionosphere waveguide,

∼80-85 km at night [*Cummer*, 1997]. The single mode which has no cutoff frequency and which propagates in the Earth-ionosphere waveguide at frequencies below ∼1.8 kHz is the quasi-transverse electromagnetic mode. Models of the quasi-transverse electromagnetic mode of propagation have been used previously to obtain estimates of the current moment of the source lightning, and to infer the magnitude of the charge lowered from the cloud to ground [*Bell et al.*, 1996, 1998; *Cummer and Inan*, 1997]. The quasi-transverse electromagnetic mode does not overlap the VLF frequency range because its attenuation increases exponentially with frequency, and most quasi-transverse electromagnetic signals are strongly attenuated above ∼1 kHz [*Greifinger and Greifinger*, 1986; *Sukhorukov and Stubbe*, 1997].

At long ranges (e.g., 5,000-12,000 km), sferics are repeatedly observed to have an oscillating VLF portion lasting ∼1 ms, sometimes followed by an ELF "slow tail" (e.g., [*Hepburn*, 1957; *Taylor and Sao*, 1970; *Sukhorukov*, 1992; *Sukhorukov and Stubbe*, 1997]). The term "slow tail" denotes its late arrival; the first maximum of the ELF slow tail is delayed in time with respect to the VLF onset by an amount related to the propagation distance [*Wait*, 1960; *Sukhorukov*, 1992]. This delay is a simple result of the difference in phase velocities; the ELF slow tail propagates in the quasi-transverse electromagnetic mode with a phase velocity of ∼0.9 c, while the VLF portion propagates in the quasi-transverse electric and quasi-transverse magnetic modes with a phase velocity much closer to c, the speed of light [*Sukhorukov and Stubbe*, 1997; *Cummer*, 1997]. Theoretical calculations show that the ELF slow tail is excited at significant levels only by source lightning discharges with a continuing-current component with significant variations on the time scale of ∼1-3 ms [*Wait*, 1960]. In this dissertation, we make use of this fact to deduce the strength of continuing currents with duration ∼1-3 ms based on remote measurements of the ELF slow tails of sferics at large source-to-receiver distances (∼12,000 km).

1.4 Contributions of this Work

The contributions of this dissertation are as follows:

- Developed novel digital signal processing techniques for automated detection and arrival azimuth determination of radio atmospherics ("sferics") in broadband ELF/VLF data on a continuous basis. Determination of the arrival azimuth of sferics is based on the VLF Fourier Goniometry technique [*Burgess*, 1993]. We demonstrated arrival azimuth measurement with $\pm 1°$ precision for sferics propagating from Nebraska to Palmer Station, Antarctica, a source-to-receiver distance of $\sim$12,000 km.

- Based on ELF measurements of sferics at Palmer Station, Antarctica, demonstrated the first evidence of continuing currents in Sprite-producing positive CG lightning flashes. The continuing currents flow from cloud to ground for $\sim$1-3 ms following the positive return stroke. The radiation from these currents enhances the ELF slow tails of sferics, which are observed at $\sim$12,000 km from their source lightning.

- Based on ELF measurements of sferics at Yucca Ridge, Colorado, developed a proxy indicator for Sprite occurrence which can estimate the number of Sprites produced above a mesoscale convective system.

- Through measurements of ELF energy radiated from Sprites themselves, identified a quantitative relationship between the current in Sprites and total Sprite luminosity.

Chapter 2

Broadband ELF/VLF Lightning Detection and Location

In this chapter we describe the systems used for remote sensing of radio atmospherics ("sferics"), the impulsive radio signals emitted by lightning discharges. We describe the broadband ELF/VLF measurements and algorithms used for automated identification and arrival azimuth determination of sferics. We then demonstrate the utility and accuracy of this technique at ultra-long range ($\sim$12,000 km) using data acquired at Palmer Station, Antarctica.

The basic data used for measurement of radio atmospherics is broadband ELF/VLF data recorded in digital form on magnetic tape. In some cases, the data are highpass filtered to avoid unwanted interference from 60 Hz ac power and its harmonics. In other cases, the lower end of the frequency range measured extends below 60 Hz so that the power line interference is unavoidable and must be removed in post-processing. The sferic data analysis procedures are summarized in block diagram form in Figure 2.1. First, interference from 60 Hz and its harmonics is removed using a 10th-order highpass IIR Butterworth filter [*Strum and Kirk*, 1988; pp. 623-659]. All filters described in this chapter use the same basic realization. The cutoff frequency of the highpass filter is 1.5 kHz. Second, a 4 kHz bandwidth of interest is chosen to maximize signal-to-noise ratio, as described below. Third, threshold and coherence criteria are used to identify the time of occurrence of sferics. Fourth, the arrival azimuths of the identified sferics are determined using the VLF Fourier Goniometry method (see Section 2.3) [*Burgess*, 1993]. In the final step, the peak value of the magnitude in both the VLF and ELF frequency bands and the average energy in
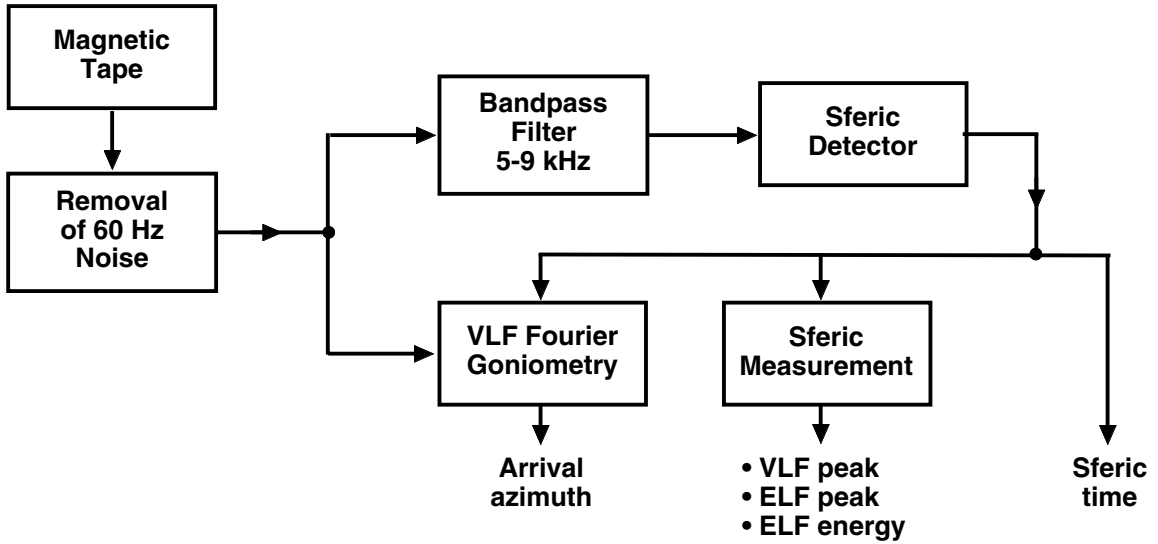
Figure 2.1: ELF/VLF sheric data analysis.

the ELF band are measured and stored. These measurements result in five quantities identified for each sheric. The azimuth measurements are then triangulated with measurements of the same sherics at other stations in order to determine lightning location.

2.1   Broadband ELF/VLF Receiving Systems

In this section we describe the Stanford University ground-based broadband ELF/VLF receiving systems that were used to acquire the data analyzed in this dissertation. These systems measure electromagnetic waves in the Earth-ionosphere waveguide in the frequency range between 15 Hz and 22 kHz. A block diagram of a broadband receiver and recording system is shown in Figure 2.2. At each receiver location, two orthogonal loop antennas are used to detect both components of the horizontal magnetic field, normally oriented geomagnetic north-south (labelled "N/S") and geomagnetic east-west (labelled "E/W"). The antenna terminals are connected to a matched preamplifier to yield flat system frequency response and maximum sensitivity for a particular antenna. The line driver-line receiver combination is used to isolate the antennas and preamplifiers from the nearest sources of power line interference by ∼1000-3000 feet.

The output voltage of the line receiver is a scaled version of the broadband
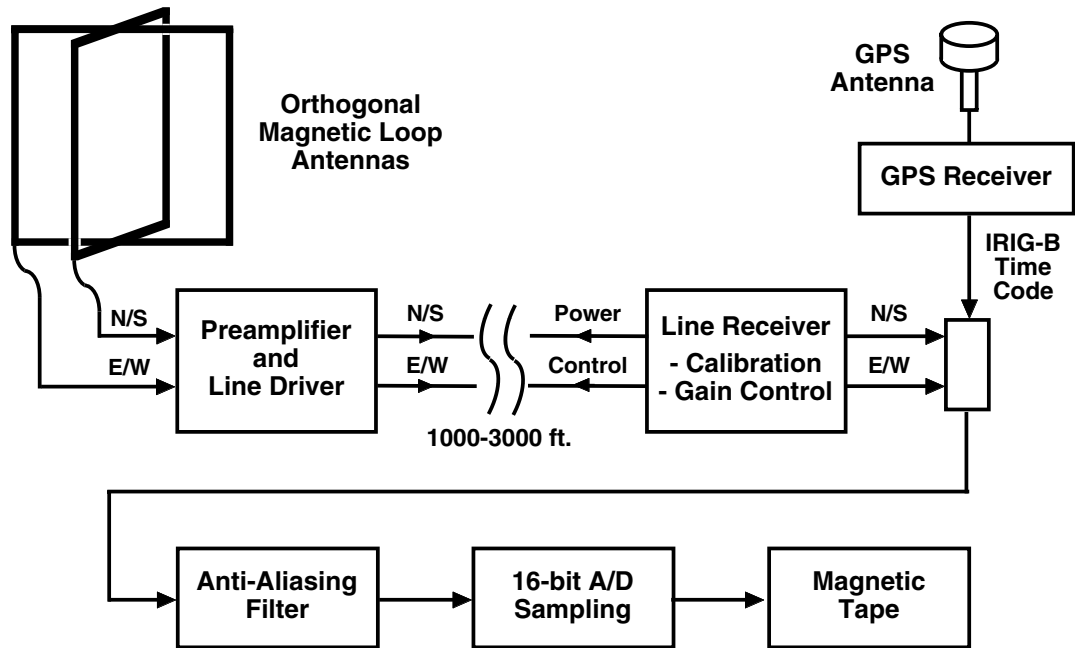
Figure 2.2: ELF/VLF sferic receiver.

ELF/VLF signal of interest. This voltage is sampled at 44.1 kSamples per second using analog-to-digital (A/D) converters at 16-bit precision, providing sufficient dynamic range for the removal of 60 Hz interference in post-processing. For systems with built-in highpass filtering of power line interference (e.g., Section 2.1.1), large dynamic range provides for low-noise monitoring of sferics from both nearby and distant lightning sources without the need for gain adjustment. The gain of the receiver is chosen so that the quantization noise due to sampling is nearly equal to the electronics noise of the receiver. Anti-aliasing filters condition the signals before A/D conversion by applying a sharp lowpass filter at $\sim$20 kHz. The digital samples are archived on magnetic media and later retrieved for post-processing.

2.1.1 ELF/VLF Receiver at Palmer Station, Antarctica

The Stanford University broadband ELF/VLF receiver at Palmer Station, Antarctica ($64°46'26''$S, $64°02'12''$W) is primarily used to measure characteristics of magnetospheric signals such as lightning-generated whistlers [*Burgess and Inan*, 1993]. The use of the Palmer Station receiver for monitoring sferics began in the early 1990's as part of an effort to track lightning over large areas of the Western Hemisphere
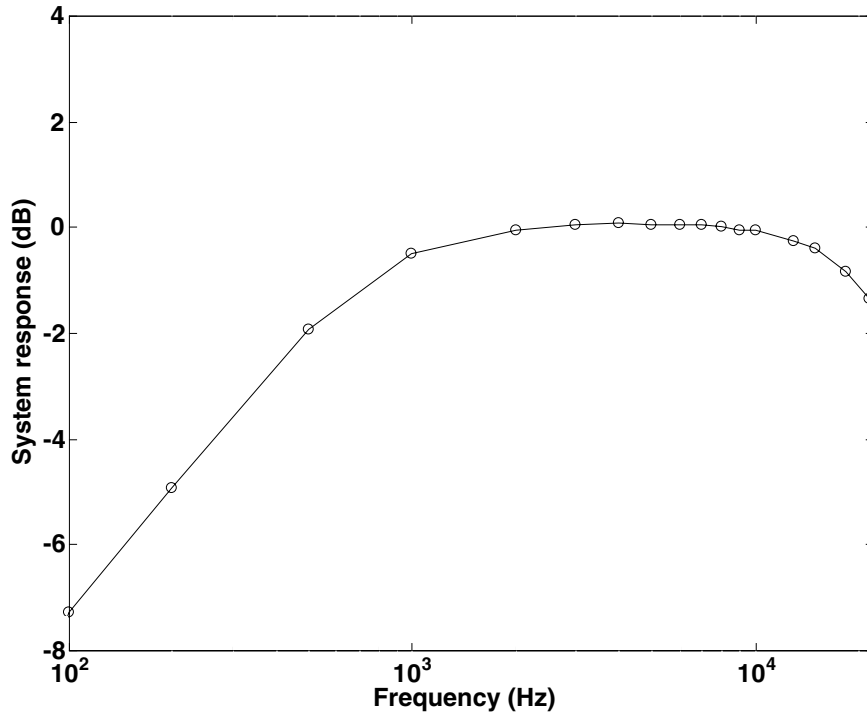
Figure 2.3: Palmer Station ELF/VLF receiver frequency response.

[*Hakeman et al.,* 1993].

Calibration of the ELF/VLF receiver is performed to determine the conversion factor between the output voltage and the equivalent magnetic field of a wave incident on the loop antenna and to measure the system frequency response [*Paschal,* 1988]. To perform the calibration procedure, one injects a sinusoidal current of known amplitude at the antenna terminals and measures the output with a true-rms digital multimeter. During this measurement, each loop antenna is disconnected in turn and replaced by a "dummy loop" that has inductance and dc resistance equivalent to that of the loop antenna. This method was used to obtain the system frequency response for the Palmer Station ELF/VLF receiver, shown in Figure 2.3. At the lower frequencies, the Palmer response is flat within ±1 dB down to 1 kHz, then it decays at ∼10 dB/decade, with a -3 dB point at ∼300 Hz. At higher frequencies the system response is flat within ±1 dB until the frequency exceeds the ∼20 kHz cutoff frequency of the lowpass anti-aliasing filters.

At Palmer the data are sampled using a Sony PCM 601-ESD encoder, which samples two analog audio input signals continuously and encodes the resulting digital

data onto one output video signal using pulse code modulation. Upon playback, the pulse code modulation decoder allows error-free recovery of the two streams of digital samples at 44.1 kSamples per second. A video cassette recorder is used to write the video signal onto magnetic tape. The audio input of the same recorder allows simultaneous recording of an IRIG-B timing signal [*Burgess*, 1993]. IRIG-B is a 1-ms resolution time encoding standard, which in this work is derived from signals received by GPS or GOES receivers, which are both synchronized to coordinated universal time by the National Institute of Standards and Technology, formerly the National Bureau of Standards.

2.1.2   ELF/VLF Sferic Receiver at Yucca Ridge, Colorado

A new ELF/VLF Sferic Receiver was designed and built at Stanford University and installed at Yucca Ridge Field Station ($40°40'06''$N, $104°56'24''$W), 15 km northeast of Fort Collins, Colorado, during July 1996. The sensitivity of the antenna-preamplifier combination is ten times lower than the Palmer system to avoid saturation of the preamplifier due to strong sferics from nearby ($\sim$500 km or nearer) lightning. The motivation for the design of a new system was to extend the low end of the frequency response further into the ELF band to enable accurate measurement of electromagnetic radiation produced by lightning continuing currents (see Section 1.2.2) on time scales longer than $\sim$3 ms. The Yucca Ridge system frequency response is flat to $\pm$1 dB down to $\sim$30 Hz, with a -3 dB point of $\sim$15 Hz, as shown in Figure 2.4. Table 2.1 compares the characteristics of the Palmer and Yucca Ridge systems.

Table 2.1: Comparison of Palmer and Yucca Ridge broadband systems

Parameter	PA system	YR system
Shape	triangle	square
Length of sides	9 x 18 m	81 x 81 cm
Number of turns	1	146
Wire gauge	# 6	# 18
Resistance	61.5 mΩ	10Ω
Inductance	65 μH	60 mH
Cutoff frequency	$\sim$300 Hz	$\sim$15 Hz
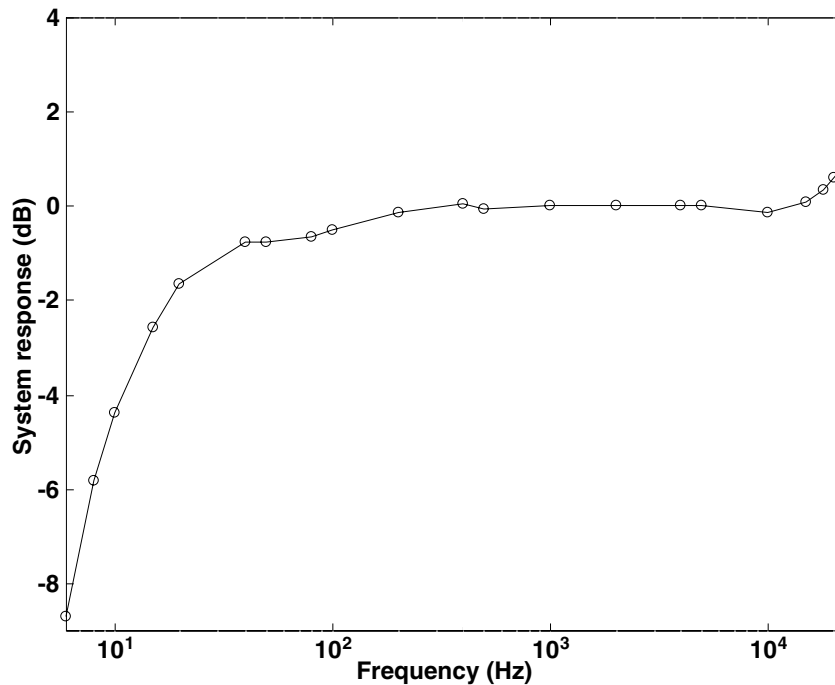
Figure 2.4: Yucca Ridge ELF/VLF sferic receiver frequency response.

At Yucca Ridge, the ELF/VLF data are recorded on two Digital Audio Tape recorders. The first recorder samples the output of both N/S and E/W channels. The second recorder duplicates the N/S channel recording while simultaneously sampling the IRIG-B time signal. The two tapes are resynchronized during post-processing.

2.2 Sferic Detection

After the broadband ELF/VLF data are retrieved from magnetic tape, an algorithm is needed to identify sferics and discriminate them from noise sources. The sferic detector (see Figure 2.1) accomplishes this by requiring a signal to pass two tests in order to be considered a sferic. These two tests are the threshold test and the coherence test. For the first test, the peak amplitude of a sferic must exceed a given threshold. This allows the threshold to be chosen so that a reasonable quantity of output data is produced, depending on the time duration under consideration and on the available computer memory. The second test is a coherence test which discriminates against noise that is not strictly coherent between the two sensors, as defined below.
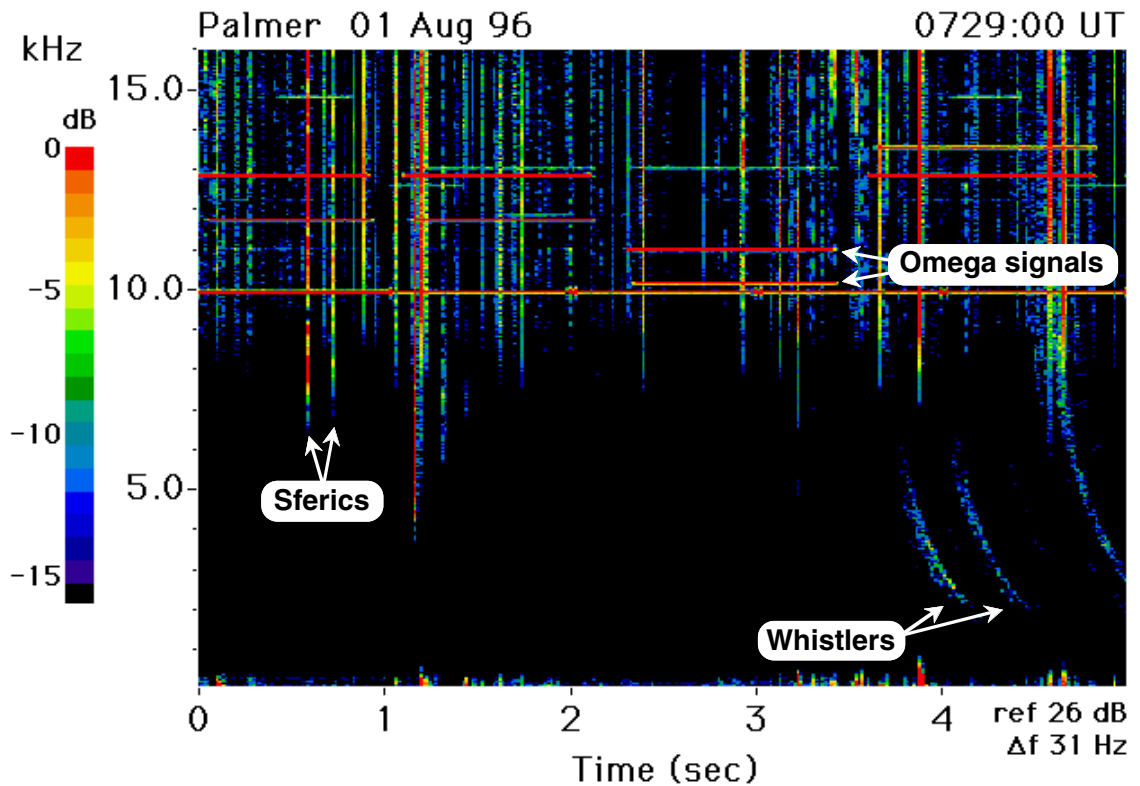
Figure 2.5: Spectrogram of broadband data from Palmer Station, Antarctica.

For automated detection of sferics in broadband ELF/VLF data, it is necessary to take into account the characteristics and variability of other electromagnetic signals in the same frequency range. Figure 2.5 is a spectrogram from 100 Hz to 16 kHz of five seconds of broadband data recorded at Palmer Station, Antarctica, during typical summer nighttime conditions. The vertical lines are sferics, which are broad in frequency and short in duration. They exceed the minimum amplitude in the spectrogram above ∼5-7 kHz, and the ELF component of some sferics is clearly visible below ∼500 Hz. The horizontal segments of approximately one-second duration with frequency between 10 and 14 kHz are the Omega navigation transmitter signals [*Burgess*, 1993]. The single horizontal line at 10 kHz is a locally injected amplitude-modulated clock signal for redundancy in timing. Finally, the gently curving lines in the lower right corner are whistlers, the component of lightning energy which has propagated within the density inhomogeneities called "ducts" in the earth's magnetosphere and is received on the ground [*Helliwell*, 1965]. Their "whistling" quality is

due to dispersion experienced in propagation through the cold plasma in the magnetosphere [*Davies*, 1990; pp. 368-370]. If one wishes to detect only sferics, whistlers constitute a naturally-generated "noise source."

In the frequency band between 5 and 9 kHz there is strong sferic energy and little interference from natural or anthropogenic sources (see Figure 2.5). We implement the threshold test, which is the first of the two tests, in this frequency band. For the threshold test, we load a two-second block of data into memory, use a bandpass filter to eliminate all but the 5 to 9 kHz band, compute the total magnetic field and detect peaks exceeding a selectable threshold. Explicitly, where B_{NS} represents the measured N/S component of wave magnetic field and B_{EW} represents the measured E/W component of the wave magnetic field, we find the magnitude of the incident wave magnetic field as $B = \sqrt{B_{\mathrm{NS}}^2 + B_{\mathrm{EW}}^2}$. Maxima in B which exceed the given threshold are recorded as possible sferic occurrences. This test is performed in two-second blocks for the entire data set under analysis.

To verify sferic occurrence, the possible sferic data sets are also subjected to the coherence test to discriminate between sferics and random noise sources. This coherence test requires the signals on each antenna to be in phase or 180 degrees out of phase. To implement the coherence test, for each of $B_{\mathrm{NS}}(t)$ and $B_{\mathrm{EW}}(t)$, we take the Fast Fourier Transform (FFT) of 4 ms of data using a Hamming window [*Oppenheim and Schafer*, 1989; p. 447], and save the 17 frequency domain samples in the 5 to 9 kHz frequency band. The coherence test compares the phases of $B_{\mathrm{NS}}(f)$ and $B_{\mathrm{EW}}(f)$ and finds the number of the frequency domain samples having phase coherence. A sample i is said to have phase coherence if either

$$|\angle B_{\mathrm{NS}}(f_i) - \angle B_{\mathrm{EW}}(f_i)| < \epsilon, \ or$$

$$|\angle B_{\mathrm{NS}}(f_i) - \angle B_{\mathrm{EW}}(f_i)| - 180° < \epsilon$$

is true. We use $\epsilon \sim 5°$, and a sferic passes the coherence test if at least a fixed percentage of the frequency domain samples between 5 and 9 kHz have phase coherence. The fixed percentage is chosen to be 35% based on the particular features of sferics and of the ambient noise background.

Each waveform that passes both the threshold and the coherence tests is identified as a sferic. The time of the sferic is recorded with $\sim$1 ms precision.

2.3   Sferic Arrival Azimuth Determination

After identification of each sferic, we need to determine the location of its source lightning discharge. This section describes arrival azimuth determination at a single receiving station. In order to determine the actual location of a lightning flash, one needs to perform triangulation of measurements at multiple locations. Triangulation algorithms are readily available [*Orville Jr.*, 1986], therefore in this dissertation we address the method and results of arrival azimuth determination at a single receiving station.

VLF Fourier Goniometry is a VLF direction-finding method using two orthogonal magnetic loop antennas to find the major axis of the polarization ellipse of the incoming wave [*Burgess*, 1993; *Inan et al.*, 1996b; *Reising et al.*, 1996]. *Burgess* [1993] verified the accuracy of VLF Fourier Goniometry by comparing the measured arrival azimuths of signals from eight Omega navigation transmitters to their expected arrival azimuths at Palmer Station, Antarctica. He found agreement between expected and actual bearings of $\pm 5°$ and applied VLF Fourier Goniometry to direction finding on whistlers. In this section we apply the same method to determine the arrival azimuth of sferics at Palmer Station. This implementation assumes that the sources of the waves are on or near the ground so that the elevation angle of arrival at the receiver (>1000 km away) is nearly zero [*Cousins*, 1972].

VLF Fourier Goniometry uses the Fourier Transform to synthesize a rotating antenna, or goniometer, over a range of frequencies in the band of interest. A wave with time dependence $\cos(2\pi f_0 t)$ incident on a goniometer rotating at a frequency f_0 produces a phase-shifted output dependent upon the direction of arrival. For a zero phase reference corresponding to the goniometer pointing north, the phase shift of the output is equivalent to the bearing of the incoming signal. To implement the same goniometer at frequency f_0 with two fixed orthogonal antennas, we synthesize a Fourier Goniometer signal B_{FG} using the outputs of the two antennas, B_{NS} and B_{EW}, as

$$B_{\mathrm{FG}}(f_0) = \frac{1}{\tau} \int_0^{\tau} [B_{\mathrm{NS}} \cos(2\pi f_0 t) + B_{\mathrm{EW}} \sin(2\pi f_0 t)] dt$$

The integral averages the signal over the duration of the sferic, τ. For a general frequency f, we have,

$$B_{\mathrm{FG}}(f) = \frac{1}{\tau} \int_0^{\tau} (B_{\mathrm{NS}} - jB_{\mathrm{EW}})\, e^{\, j2\pi ft} dt$$

Hence $B_{\text{FG}}(f)$ is the Fourier transform of the complex quantity which has real part B_{NS} and imaginary part $-B_{\text{EW}}$. The phase of this complex quantity is the bearing of the received signal, and its magnitude is the magnitude of the total magnetic field, B.

For computational efficiency the Fourier Goniometer signal, $B_{\text{FG}}(f)$, is computed using the Fast Fourier Transform algorithm. We use N samples in the frequency domain for 5 kHz $< f_i <$ 9 kHz. In this case we use the same frequency range for sferic detection (see Section 2.2) and arrival azimuth determination. Since the Omega navigation transmitters were decommissioned during 1997, the 10-14 kHz frequency range may be more useful for arrival azimuth determination in future work. The arrival bearing of each sferic is estimated by averaging the arrival direction in each frequency bin, using the magnitude in that bin as a weighting function. Expressing the arrival azimuth of a sferic as Φ, we have,

$$\Phi = \frac{\displaystyle\sum_{i=0}^{N-1} |B_{\text{FG}}(f_i)| \, \angle B_{\text{FG}}(f_i)}{N \displaystyle\sum_{i=0}^{N-1} |B_{\text{FG}}(f_i)|}$$

.

With two orthogonal magnetic loop antennas, if a signal is deduced to arrive at a certain bearing, it is not possible to determine if it actually arrived from this bearing or from $\Phi \pm 180°$. Therefore, we have a 180° ambiguity in arrival azimuth determination. In practice, since VLF propagation over ice is highly lossy [*Rogers and Peden*, 1975], nearly all sferics measured at Palmer Station, Antarctica, arrive from bearings between -90° and +90° (see Figure 2.6). Therefore, the arrival azimuth of each sferic observed at Palmer is recorded in the domain $[-90°, +90°]$, along with its time of occurrence and total magnitude.

2.4 Precision of Sferic Arrival Azimuth Determination

Analysis of broadband VLF measurements at Palmer Station, Antarctica, as described in Sections 2.2 and 2.3, allows detection of sferics from lightning at least as
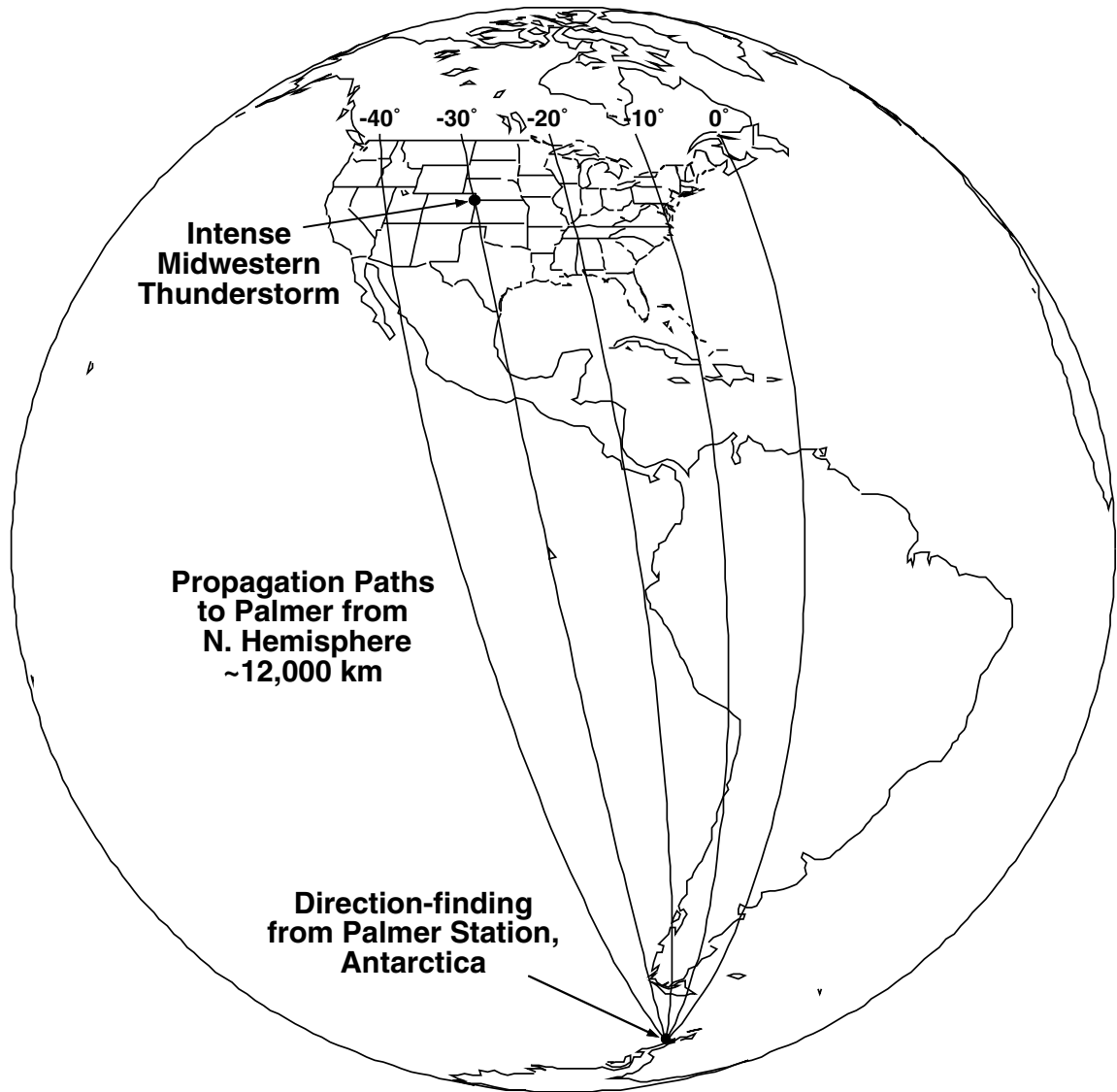
Figure 2.6: View of great circle propagation paths from North America to Palmer Station, Antarctica.
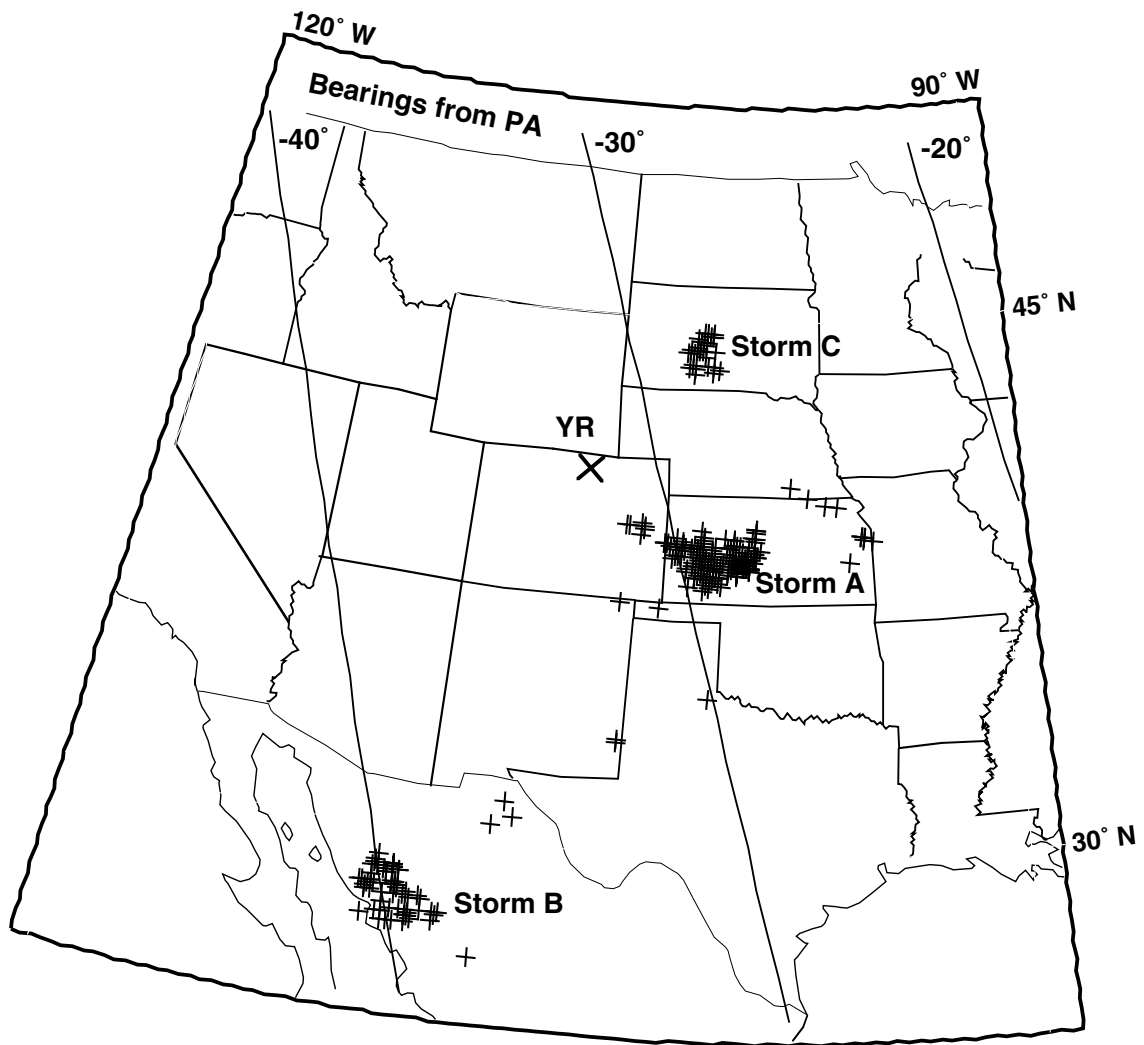
Figure 2.7: Thunderstorm activity from 0644 to 0800 UT on August 1, 1996. Pluses show locations of positive cloud-to-ground flashes observed by the NLDN with peak current exceeding 23 kA. The Yucca Ridge Field Station in Colorado is denoted by "YR."

far as the Great Plains, at a range of ~12,000 km from Palmer (see Figure 2.6). In order to determine the precision of the arrival azimuth determination method presented in Section 2.3, we compare the measured arrival azimuth, Φ, of individual sferics with the expected arrival azimuth derived from the known locations of their source lightning discharges. Since those locations of CG discharges in the continental U.S. are measured to ~0.5 km precision by the NLDN (see Section 1.2.4), we choose thunderstorms in the continental U.S. to verify the precision of sferic arrival azimuth determination.

Several storms occurring on August 1, 1996, were studied using lightning location
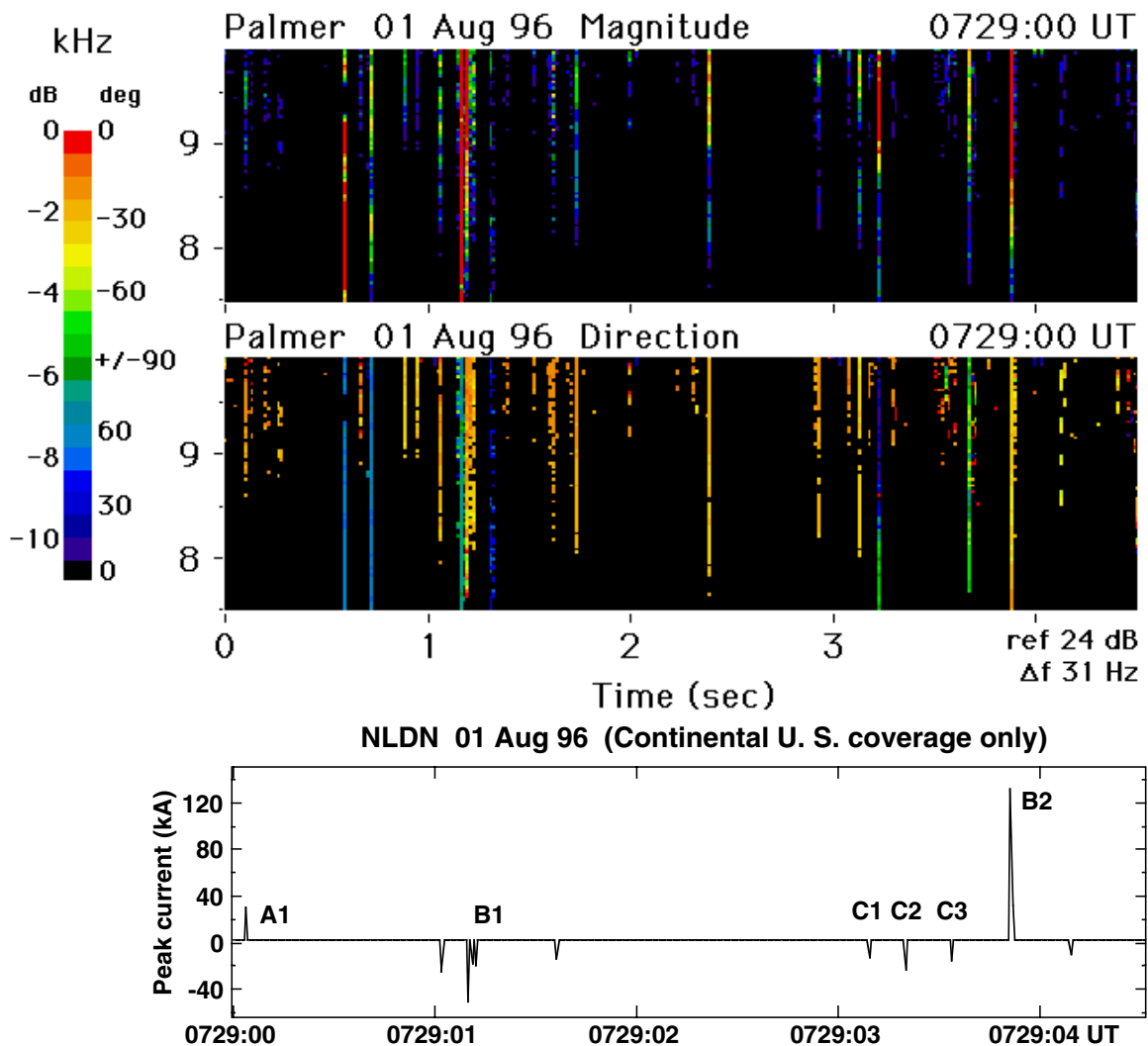
Figure 2.8: Magnitude and arrival direction spectrograms for 5 seconds of VLF data (7.5-10 kHz) and concurrent NLDN data on time of occurrence and peak current of CG flashes.

data from the NLDN, as shown in Figure 2.7 (see also [*Bell et al.*, 1998]). This figure shows only positive CG flashes occurring during a 75-minute period from 0644 to 0800 UT and exceeding 23 kA peak current (see Section 1.2.4). The western Kansas storm denoted 'Storm A' is discussed in the context of Sprite observations in Sections 3.2 and 4.2. The other two active storms in North America at that time are labelled 'Storm B' in Sonora, Mexico, and 'Storm C' in South Dakota (see Section 4.3.4).

Five seconds of Palmer broadband VLF data from this period are shown in Figure 2.8. The top panel is a spectrogram of the magnitude of the wave magnetic field
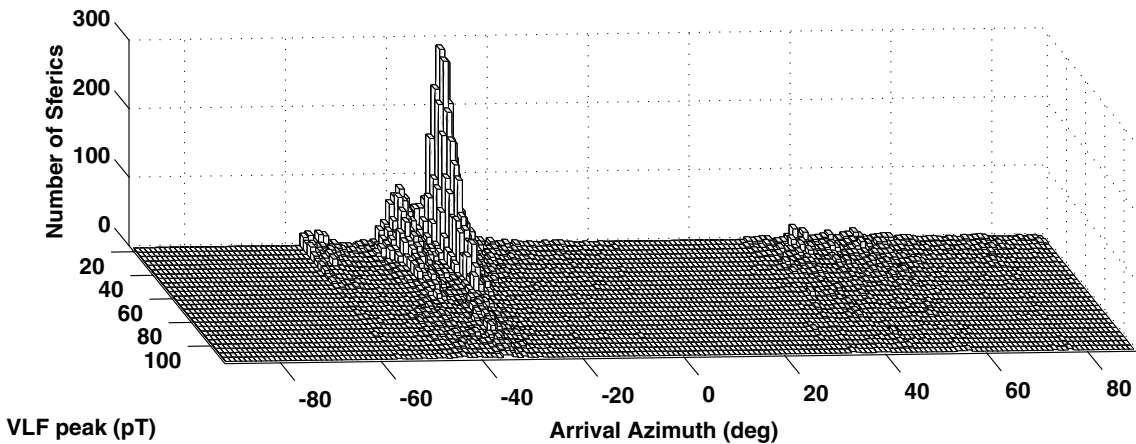
Figure 2.9: Histogram of the number of sferics as a function of both the peak value of the VLF magnetic field intensity and the arrival azimuth (see Figure 2.6). The observation period was from 0715 to 0730 UT on August 1, 1996.

measured in the 7.5 to 10 kHz band. The magnitude scale is shown in dB on the left side of the color bar. The middle panel is a spectrogram of the direction of arrival in the same frequency range. The arrival bearing is given rotating from 0° north as red, to the west as green, then from the east equivalently as green, and back to the north as purple. All azimuth values are given in the domain $[-90°, +90°]$, due to the 180° ambiguity (see Section 2.3). The bottom panel shows the peak current of CG lightning flashes observed by the NLDN during the same time period. The sferic labelled A1 arrives at Palmer from Storm A at -29° bearing, in agreement with its orange color in the direction spectrogram. Similarly, sferic B2 arrives at Palmer from Storm B at -40° bearing, and has a yellow-orange color in the direction spectrogram.

All sferics detected within a 15-minute interval are shown in Figure 2.9 as a histogram of the number of sferics versus both the magnitude of the sferic (given as peak value of the VLF magnitude) and the arrival azimuth at Palmer. Storm B is clearly visible from -41° to -38° bearing, and Storms A and C combine to form the highest peak, between -31° and -25° bearing.

To determine the precision of sferic arrival azimuth determination, lightning locations measured by NLDN with ~0.5 km precision were compared to the bearings measured at Palmer. Using the NLDN locations as the source, and assuming that most of the sferic energy propagated directly along the great circle path from the lightning discharge to the receiver at Palmer, the difference between the expected and measured arrival azimuths was determined for each of 328 flashes. The resulting
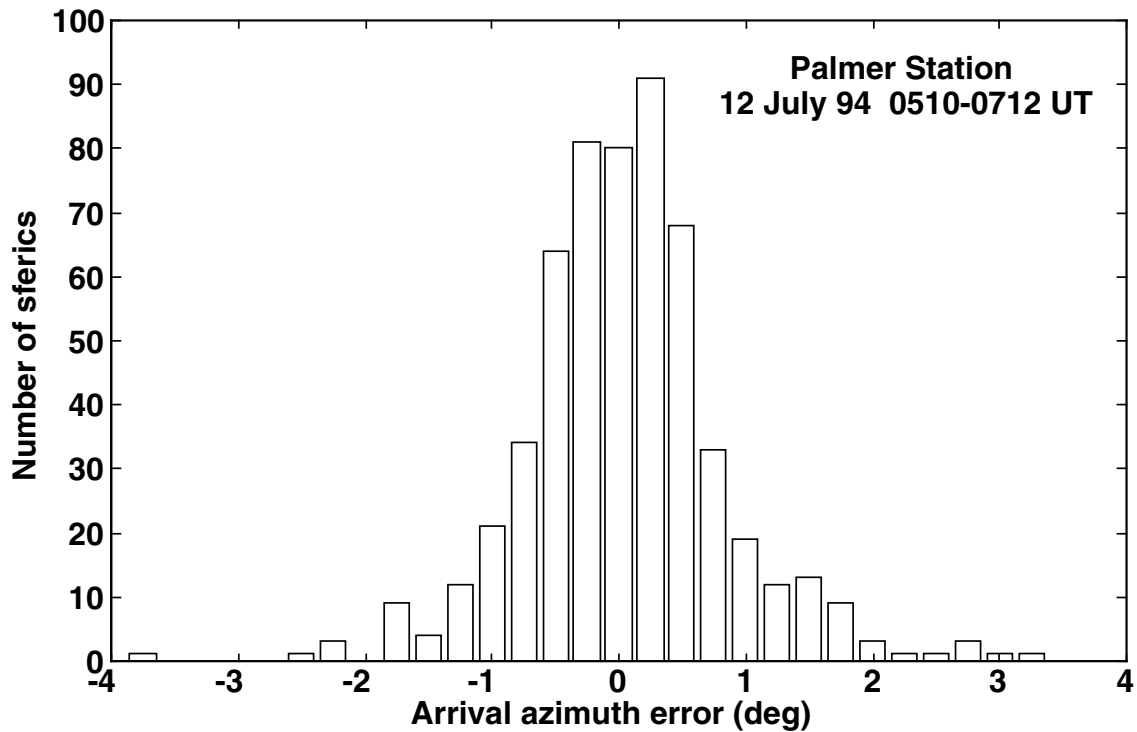
Figure 2.10: Arrival azimuth error of 328 sferics received at Palmer Station, Antarctica, from source lightning in Nebraska, a source-to-receiver distance of ∼12,000 km.

statistics are shown as a histogram of number of sferics as a function of arrival azimuth error in Figure 2.10. Over 90% of the sferics have a bearing error of $\pm 1°$ or less. At a range of ∼12,000 km, $\pm 1°$ bearing error corresponds to ± 200 km in transverse distance error.

In this chapter we have described the receiving systems and algorithms used for broadband ELF/VLF remote sensing of sferics originating in lightning. Using a single broadband ELF/VLF receiving station, this technique identifies lightning flashes at a source-to-receiver distance of at least ∼12,000 km and measures arrival azimuth with an accuracy of $\pm 1°$.

Chapter 3

Association of Sprites and Cloud-to-Ground Lightning

This chapter describes the temporal association of visually observed Sprites in the mesosphere and lower ionosphere with cloud-to-ground lightning in the troposphere. The association of Sprites with positive CG lightning has been reported previously [*Boccippio et al.*, 1995; *Winckler et al.*, 1996; *Reising et al.*, 1996; *Lyons*, 1996]. This study extends previous work by analyzing a large number of Sprites and by measuring the delay between a positive CG return stroke and the occurrence of a Sprite with high time resolution (~17 ms).

3.1   Identification of Sprite Onset Time

We rely exclusively on ground-based observations of Sprites, which have the advantage of recording all Sprites above a thunderstorm on a continuous basis. In this context, "all Sprites" means those Sprites which are in the field of view and are detectable above the noise level of the intensified charge-coupled device (CCD) camera. For the ground-based observations, we use an image-intensified black-and-white Pulnix CCD camera with a ~19° wide by ~14° high field of view. In order to be detected, a Sprite must emit enough photons to exceed noise generated in the imaging system and recorded on the videotape. This noise appears to the observer as "speckle" on the video screen. Weak Sprites are best detected by watching a video in motion, as opposed to single images, because the human eye is more sensitive to temporal changes than to stationary pattern differences.
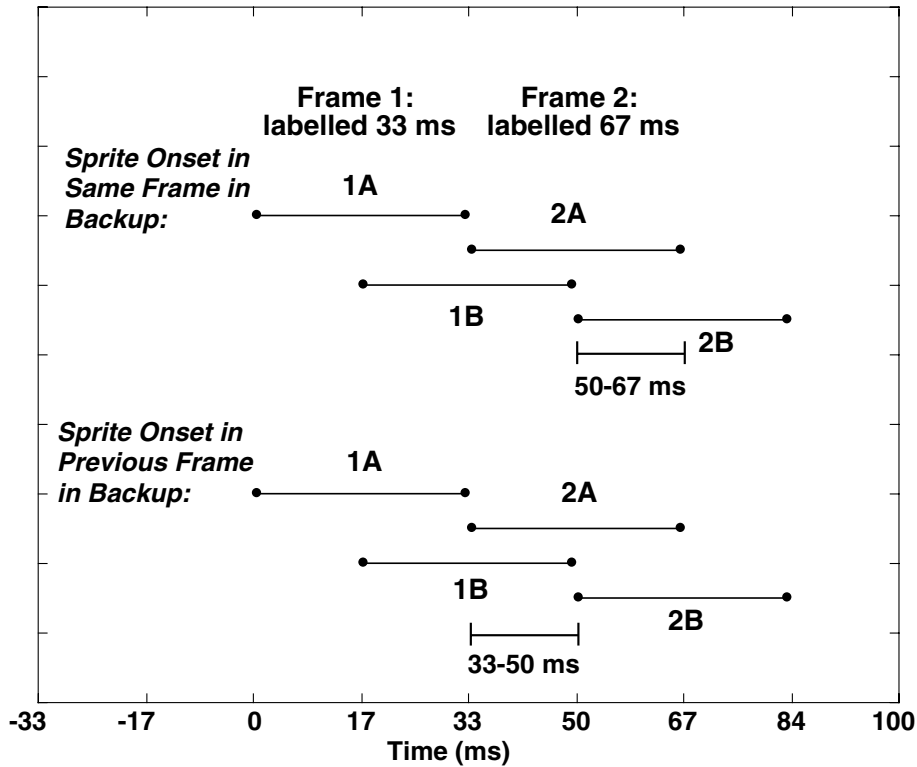
Figure 3.1: Determination of time of Sprite onset to 16.7 ms precision (see text for detail).

Current video hardware is still based on a variation of the RS-170 video standard adopted by the broadcast industry in 1957. RS-170 is a 30 frames per second, 2:1 interlaced format that accomplished flicker-free video within a broadcast bandwidth that could be transmitted in the 1950s [*Burke,* 1996; p. 736]. Interlacing is accomplished by reading first the odd horizontal scan lines, or "first field," and then the even scan lines, or "second field." In the normal frame-integration mode, the first and second fields each last 1/30 sec (33 ms), but they are offset in time from each other by 1/60 sec (16.7 ms) [*Burke,* 1996; p. 775]. As shown in Figure 3.1, field 1A is sensitive to illumination from $t = 0$ to 33.3 ms, and field 1B is active from $t = 16.7$ to 50 ms. Frame 2 begins at $t = 33.3$ ms, giving a video rate of 30 frames/sec.

For Sprite monitoring, the intensified CCD camera signal is recorded on a standard VHS video cassette recorder (VCR). A TrueTime video time inserter card writes the time across the bottom of the video frame with 1-ms resolution, as shown in Figure 1.1. The time stamp is delayed by 33 ms from the beginning of the frame, so that if a frame starts at the beginning of second S, the time stamp reads S.033. The video inserter card derives its time from a GPS clock with time referenced to universal

coordinated time to better than 200 ns.

Since the vertical extent of Sprite images is greater than one horizontal scan line, individual fields can be used to find the onset time of Sprite luminosity with a time resolution of 16.7 ms. A single field of each frame is viewed using the pause function on a standard VCR. In order to view the other field of each frame, the videotape was played on one VCR, and the output was recorded on a second VCR from a different manufacturer. The resulting backup videotape, when viewed using the pause function, displayed a different field of each frame, compared to the original videotape. We can therefore view each field independently using both the original and backup videotapes.

We illustrate the determination of Sprite onset time to 16.7 ms resolution in Figure 3.1, where two consecutive frames are labelled 1 and 2, while the first and second fields within each frame are labelled A and B, respectively. The horizontal axis gives the time relative to the beginning of frame 1, and the time stamp shown on each frame is 33 ms after the beginning of exposure of its first field. When using the pause function, we view field A on the original tape and field B on the backup tape. Referring to Figure 3.1, if the Sprite onset is observed on the same frame (here frame 2) on both the original and the backup, the Sprite onset is during the second half of field 2A or, equivalently, the first half of field 2B. If the Sprite onset is observed on frame 2 of the original tape and frame 1 of the backup tape, then the Sprite onset is during the second half of field 1B or, equivalently, the first half of field 2A. This method enables the determination of the onset time of any observed Sprite with a precision of ∼17 ms.

3.2 Association of Sprites and Positive Cloud-to-Ground Flashes

In order to determine the association of Sprites and cloud-to-ground (CG) flashes, the time of Sprite onset can be compared to the onset time of sferics recorded at the same location. The VLF sferics reported here are *those* sferics which are generated by CG lightning flashes. VLF sferics propagate at a phase velocity nearly equal to c, the speed of light [*Cummer,* 1997]. Since both the VLF sferic and the visible light of the Sprite travel nearly the same distance at nearly the same propagation speed (c), the

relative times of their occurrence can be considered equal to the relative times of their arrival at the receiving location, within an error of <0.1 ms. As a result, measurement of the time between sferic onset and Sprite onset yields the delay between a CG flash and a subsequent Sprite.

To illustrate the association between Sprites and positive CG flashes, we report results of observations of Sprites above a mesoscale convective system in western Kansas on August 1, 1996 (see Figure 3.2). Continuous video observations of Sprites were conducted at Yucca Ridge (see Section 2.1.2) as part of the Stanford / Lockheed Fly's Eye experiment [*Inan et al.*, 1997]. Simultaneously, the signals from two orthogonal magnetic loop antennas oriented geographic N/S and E/W were recorded digitally on a continuous basis (see Section 2.1).

During the August 1 observations, the intensified CCD camera was pointed southeast, with a field of view bounded by the segments shown in Figure 3.2. The NLDN-recorded flash locations are denoted by dots for negative CG flashes and by pluses for positive CG flashes. The color code indicates the strength of the flash in terms of NLDN-measured peak current, and the red circles indicate the locations of positive CGs which are associated with Sprites. The CG lightning polarity exhibits the expected "bipolar" pattern for a mesoscale convective system, as described in Section 1.2.5. The convective core of the storm is to the southwest, where negative CGs are concentrated, and the downwind stratiform region is to the northeast, where most positive CGs occurred [*Orville et al.*, 1988; *Rutledge et al.*, 1990]. All Sprites were observed over the trailing stratiform precipitation region of the mesoscale convective system, consistent with previous observations [*Sentman et al.*, 1995; *Winckler et al.*, 1996; *Lyons*, 1996]. Previous studies have shown that the center of the Sprite may be displaced from the NLDN-detected CG location by as much as ∼40 km [*Winckler et al.*, 1996; *Lyons*, 1996], which explains the observation of one Sprite associated with a CG location just outside (north of) the camera field of view (see Figure 3.2).

During the period 0644-0907 UT, or 1:44 to 4:07 a.m. local (CDT) time, the intensified CCD camera observed 98 Sprites above the mesoscale convective system in western Kansas, giving an average occurrence rate of one Sprite every ∼90 seconds. A three-minute period from ∼0815-0818 UT was eliminated from the analysis because no video data were available. During the 139-minute observation period, there were ∼9400 CGs recorded by NLDN above a peak current threshold of 10 kA, and 12% of these CG flashes were of positive polarity.
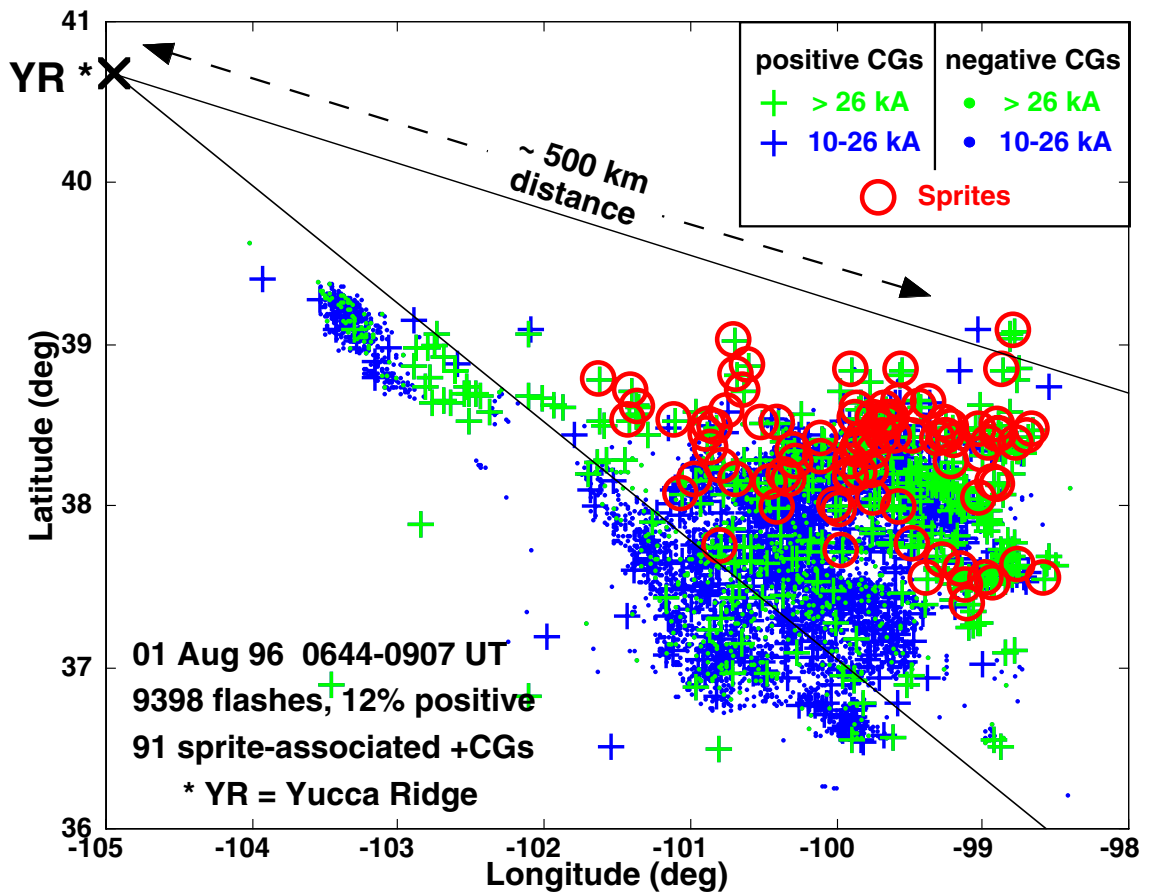
Figure 3.2: NLDN lightning locations and camera field of view for observations from Yucca Ridge, Colorado on August 1, 1996.

The onset times of all 98 Sprites were compared to occurrence times of sferics and NLDN-recorded CG flashes. In 94 (96%) of the cases, the Sprite was associated with a positive CG. Of these 94, 85 of the Sprite onset times were within 200 ms after the occurrence of the positive CG. Four of the other Sprites occurred 200-400 ms after the positive CG. In each of three other cases, two Sprites were observed within ∼200-300 ms following a single positive CG. For two of the 94, the NLDN did not detect the CG, but a sferic of positive polarity and CG characteristics [*Inan et al.*, 1996b] was observed in association with the Sprite. In the remaining four of 98 Sprites, the association is unclear because no positive CGs occurred for at least 1 second before the Sprite onset. However, *after* the Sprite appeared there was a subsequent positive CG, within 150-300 ms in three of the four cases, and ∼700 ms later in the fourth case. The association of the Sprites and the subsequent positive CGs is unclear; yet the process that triggered the Sprite may be part of an

extensive intracloud process ("spider" lightning) that can last as long as ~600 ms and may be connected to the subsequent occurrence of positive cloud-to-ground lightning (see Figure 1.4) [*Williams*, 1995, pp. 50-52; *Lyons*, 1996]. It is known that the stratiform precipitation region of large mesoscale convective systems is favorable to horizontally extensive regions of positive charge generation and leads to large positive CGs [*Rutledge et al.*, 1993]. Our understanding of these events is limited by a lack of data, but the Lightning Detection and Ranging system at Kennedy Space Center is capable of three-dimensional mapping of intracloud processes and is being used to investigate horizontally extensive intracloud and CG processes [*Stanley et al.*, 1997].

All Sprite onset times were checked for possible association with negative CGs. Negative CGs were recorded by NLDN within ~400 ms of nearly half of the Sprite onsets. However, in all except two cases, a stronger association of the Sprite with the positive CG than with the negative CG is demonstrated by one of the following: (1) the negative CG is out of the camera field of view, (2) the positive CG is closer in time to the Sprite onset than the negative CG, or (3) the positive CG occurs before the Sprite and the negative CG occurs afterward. In the first of the two cases where a negative CG is closer in time to the Sprite onset than any NLDN-recorded positive CG, there is a positive CG not detected by the NLDN but detected by identification of a sferic at that time with positive CG characteristics. Sferics generated by CGs have characteristics which distinguish them from other sferics produced by intracloud lightning, and the polarity of a sferic can be uniquely identified [*Inan et al.*, 1996b]. The positive CG identified by a sferic is closer in time to Sprite onset than the negative CG. In the second exceptional case, the positive CG occurs ~150 ms before the Sprite onset and the negative CG occurs ~60 ms before the Sprite onset, indicating a more likely temporal association between the negative CG and the Sprite.

In summary, for the 139 minutes of observation on August 1, 1996, in 96% of the cases a positive CG occurs before Sprite onset, usually within ~200 ms. In the remaining 4% of cases, a positive CG follows Sprite onset, and may be involved in an interconnected intracloud process ("spider" lightning) triggering both the Sprite and the positive CG. There was only one case out of 98 in which a Sprite was temporally associated more closely with a negative CG than any positive CG.

These results are consistent with previous work. Two midwestern mesoscale convective systems were studied using video observations of Sprites at Yucca Ridge and sferics measurements at Palmer Station, Antarctica [*Reising et al.*, 1996] (see also

Sections 4.3.2 and 4.3.3). During 122 minutes of observation on July 12, 1994, 44 Sprites were observed, and sferics of positive CG polarity were observed at Palmer Station in association with 95% of the Sprites. The NLDN recorded positive CGs within ±100 ms of the Sprite event in only 70% of the cases; however, upgrade of the NLDN upgrades to the Improved Accuracy from Combined Technology between 1994 and 1995 improved its detection efficiency for complex events (see Section 1.2.4) [*Cummins et al.*, 1998; *Idone et al.*, 1998b]. On July 15, 1995, 35 Sprite events were observed in 104 minutes, and sferics of positive CG polarity were measured at Palmer Station in association with 97% of the Sprites. The NLDN recorded positive CG flashes in 83% of the cases, showing the improvement due to the NLDN upgrade. Similarly, *Boccippio et al.* [1995] reported positive CGs recorded by NLDN in association with 86% and 82% of Sprites, for mesoscale convective systems on July 12, 1994, and September 7, 1994, respectively. *Lyons* [1996] reports that 94% of 36 Sprites observed during a 4.5 hour period on August 6, 1994, were temporally associated with positive CGs recorded by the NLDN.

3.3   Delays between Positive CG Flashes and Sprite Onsets

A subset consisting of 17 of the 98 Sprites observed on August 1, 1998, and occurring from 0817 to 0832 UT, were analyzed by *Bell et al.* [1996; 1998]. In Figure 3.3 we illustrate the broad range of delays between the positive CG and the onset of each Sprite. For 17 Sprites observed by the intensified CCD camera during the 15 minute period, the delays ranged from ∼1 ms to ∼110 ms. The *Bell et al.* [1998] study also used the ELF portion of sferics observed at Yucca Ridge to determine the magnitude of the continuing currents (see Section 1.2.2) that followed the first return strokes of these positive CG discharges. This task was accomplished by using a well established model of ELF wave propagation in the Earth-ionosphere waveguide [*Greifinger and Greifinger*, 1986; *Sukhorukov*, 1992].

The total charge removed from the cloud to the ground can be derived from the time-integral of the current waveform, denoted by the following expression:

$$Q_T = \int_o^\tau I(t)dt$$
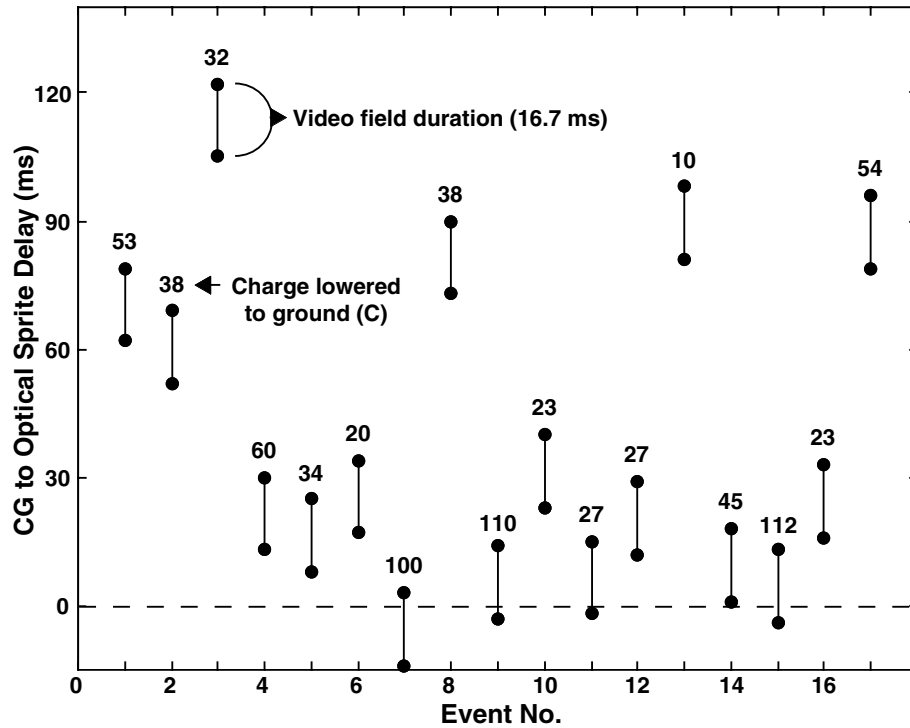
Figure 3.3:   From [*Bell et al.*, 1998]. Time delay between the causative positive CG discharge ($t = 0$) and the video field in which the Sprite first appeared, for each of the 17 events. The time duration of the video field is indicated by two dark circles connected by a vertical line. The number immediately above each video field marker represents the positive charge (Q_T) lowered to ground during the intense continuing currents that followed the first positive return stroke, assuming $l = 10$ km.

where the discharge begins at $t = 0$ and τ represents the time at which the measured sferic falls below the RMS noise level. The charge lowered to ground, assuming a cloud-to-ground distance of $l = 10$ km, is given by the number above each segment in Figure 3.3, from *Bell et al.* [1998]. Most of these 17 events exhibit delays of <30 ms between the positive CG and subsequent Sprite. The average value of Q_T for the eight discharges that occurred within 15 ms of the beginning of the video field is $\bar{Q}_T \sim 65C$, while for the others, $\bar{Q}_T \sim 30C$, and the average time delay until the beginning of the video field was ~55 ms. These observations indicate that there may be at least two ways by which a Sprite is produced. The first mechanism requires the transfer of a large amount (~100 C) of positive charge from a thundercloud during a positive CG return stroke and subsequent continuing current, in which case a Sprite is produced shortly thereafter. This mode applies to events 7, 9, and 15 in Figure 3.3. Alternatively, a positive CG which transfers a smaller amount of charge (~10-50 C)

from the cloud to the ground may induce subsequent intracloud "spider" lightning discharges in nearby regions of the cloud (see Figure 1.4). These intracloud discharges may lead to Sprite production, where the Sprite appears >40 ms after the positive CG. This mode applies to events 1, 2, 3, 8, 13, and 17 in Figure 3.3. An example of connected positive CG and intracloud "spider" discharges is shown schematically in Figure 1.4 (see also Figure 1 of *Marshall et al.* [1996]).

The following chapter addresses the question of *which* positive CGs lead to Sprites by developing a proxy measure for Sprite occurrence based solely on broadband ELF/VLF measurements of the sferic launched by each positive CG.

Chapter 4

ELF Sferic Energy as a Proxy Indicator for Sprite Occurrence

As was discussed in Section 3.2, Sprite occurrence is nearly always associated with a positive cloud-to-ground flash (CG). However, on average only ∼15-20% of positive CGs during the Sprite-producing phase of mesoscale convective systems are associated with Sprite occurrence [*Reising et al.*, 1996; *Lyons*, 1996]. The assessment of the salient characteristics of those CG flashes which lead to Sprite production is therefore an outstanding question, which we address in this chapter. There are many characteristics of CG discharges which may be important for Sprite production, including the amount of charge removed from the cloud, the strength of the discharge as measured by radiated sferic intensity, and the altitude and lateral extent of the active thundercloud. The most readily accessible parameter is the peak lightning current as measured by the NLDN; however, the NLDN-recorded peak current has been shown not to be a good indicator of the Sprite-producing capacity of a positive CG (see Section 4.2 and *Reising et al.* [1996]).

Video observations are often limited by foreground clouds which obscure the observer's view of the area of the sky where Sprites occur. For example, at Yucca Ridge during summer 1996 (see Section 2.1.2), clouds reduced visibility of the area of the sky where Sprites were expected to occur on >40% of possible evenings of observation. In addition, video observations are limited to line-of-sight visibility and to ∼1000 km range from the observation camera [*Lyons*, 1996]. In order to determine the total rate of Sprite occurrence on continental and global scales, as well as the characteristics of storms which lead to Sprite production, one needs a proxy for Sprite occurrence that

is based on remote measurements and is independent of direct video observations. This chapter describes a proxy for Sprite occurrence based on individual CG flashes using sferics measurements at both medium range ($\sim$600 km) and at ultra-long range ($\sim$12,000 km) from the source lightning.

Other techniques have been explored as possible indicators of Sprite occurrence, including excitation of the resonances of the Earth-ionosphere cavity (also known as "Schumann resonances") [*Boccippio et al.*, 1995; *Füllekrug and Reising*, 1997]. *Boccippio et al.* [1995] reported that 95% and 78% of Sprites were accompanied by ELF transients in the Schumann resonance frequency range in the storms studied on July 12, 1994, and September 7, 1994, respectively (see Section 4.3.2). In order to use ELF transient events as a proxy indicator for Sprite occurrence, one would also need to know the number of ELF transients which were *not* accompanied by Sprites. The only information that the authors provide in this context is that the interval between successive transients was several seconds and that a total of 97 Sprites were observed over a combined study duration of $\sim$7 hours, indicating that many other ELF transients exceeded their detection threshold. *Füllekrug and Reising* [1997] found that in a 97-minute period, 30 discrete excitations of the Earth-ionosphere cavity resonances associated with CG flashes in a Kansas Sprite-producing storm were simultaneously detected in Hollister, California, and in Silberborn, Germany. A full 80% of these 30 Earth-ionosphere cavity resonance events were associated with Sprite-producing positive CG flashes, suggesting the possibility of using ultra-long range Earth-ionosphere cavity resonance event detection as a proxy for Sprites.

In this chapter we describe a proxy indicator for Sprite occurrence that allows the estimation of the number of Sprites produced by a mesoscale convective system to within $\pm$25% (see Section 4.2). This proxy indicator is based on continuous recordings of ELF/VLF broadband data in which sferics are detected in association with >95% of positive CGs with peak current >20 kA at a range of $\sim$12,000 km (see Section 3.2), with >98% detected at $\sim$1000 km range. Since all Sprite-associated positive CGs have peak currents exceeding 20 kA, this proxy indicator has greater sensitivity than the Earth-ionosphere cavity resonance Sprite detection described by *Füllekrug and Reising* [1997]. The proxy indicator described in this chapter is based on the ELF energy of a sferic, which is enhanced by continuing currents, i.e., currents which continue to flow following the positive CG return stroke (see Section 1.2.2).

4.1 Quantitative Analysis of VLF and ELF sferics

When the bandwidth of broadband ELF/VLF receivers extends below ~300 Hz, as the Yucca Ridge system does (see Section 2.1.2), the recorded data is contaminated by the power line interference at 60 Hz (50 Hz in Europe) and its harmonics. Although it is possible to substantially remove this interference prior to recording using selective notch filtering of the fundamental frequency and its harmonics, such filtering necessarily contaminates data in adjoining frequency regions. At the same time, measurements sampled with 16-bit resolution provide sufficient dynamic range for the removal of the interference in post-processing. With this in mind, we have chosen to record the raw data with 60 Hz interference. In our work, we are interested in quantitative sferics measurements extending into the ELF frequency range (here ~15 Hz - 1.5 kHz), overlapping the frequencies of power line interference. Therefore the removal of interference cannot be accomplished by highpass filtering. We instead remove the 60 Hz interference by choosing a single cycle of 60 Hz interference that is free of sferics and is within a time window during which the power-line frequency is stable, ~2-3 seconds. We replicate the single cycle to produce a waveform of sufficient length, and phase align it with the unfiltered sferic [*Cummer*, 1997]. Then we subtract this synthesized 60 Hz waveform (dotted line in the top panel of Figure 4.1) from the unfiltered sferic (solid line in the top panel of Figure 4.1) to remove the power line interference. We show the resulting noise-removed sferic launched by a Sprite-associated positive CG at 08:31:28 UT on August 1, 1996, in the bottom panel of Figure 4.1. All sferics recorded at Yucca Ridge are filtered using this technique.

In the ELF frequency band below ~1.5 kHz, only the quasi-transverse electromagnetic mode propagates in the Earth-ionosphere waveguide, while all other modes are evanescent (see Section 1.3). In our analysis we extract this single mode (hereafter referred to as "ELF sferic") from the sferics data in hand by digital lowpass filtering with a cutoff frequency of 1.5 kHz. This digital filter and all other filters mentioned in this chapter are implemented as 30th-order FIR filters windowed by the Hamming function [*Oppenheim and Schafer*, 1989; p. 447]. Likewise, we extract all other modes (referred to as "VLF sferic") from the sferics data in hand by digital highpass filtering with a cutoff frequency of 1.5 kHz, clearly below the cutoff frequency of the lowest-order VLF mode [*Bell et al.*, 1998]. The VLF and ELF components of a sferic launched by a Sprite-producing positive CG at 08:26:09 UT are shown in Figure 4.2.
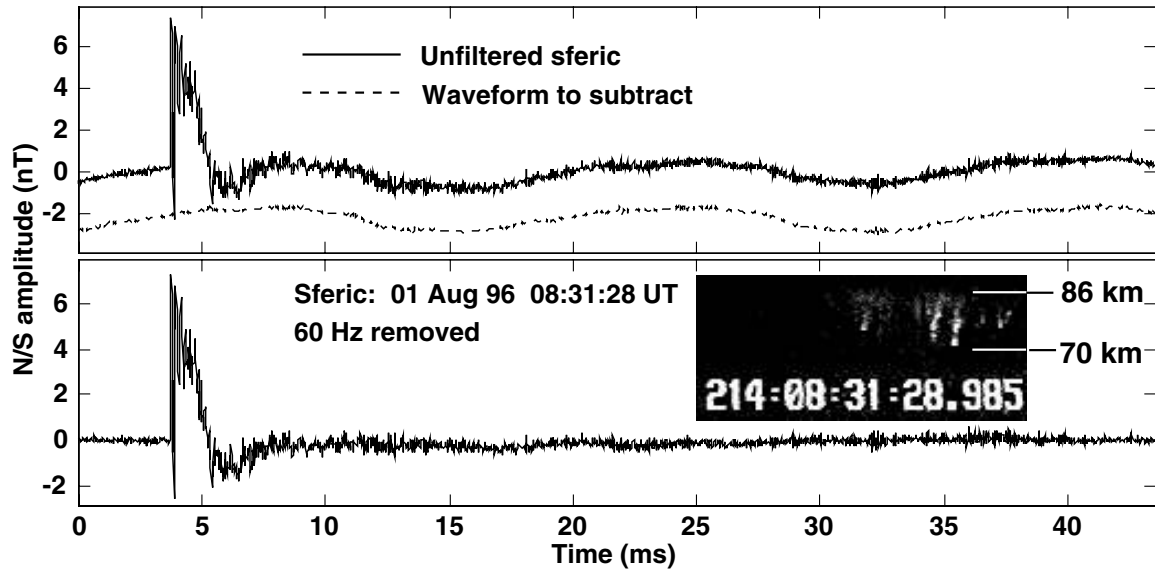
Figure 4.1: (Top) The ELF/VLF waveform of a sferic generated by a 61-kA positive CG discharge at 08:31:28 UT on August 1, 1996. (Bottom) The resultant sferic waveform after subtraction of the power line interference (shown above as dashed line). The associated Sprite is shown in the inset, with top and bottom altitudes which were calculated assuming the Sprite was centered over the associated positive CG discharge. This approximation is typically correct to within ±5 km in altitude and is used to calculate the altitudes of all other Sprite images shown in this chapter.

Several definitions are needed for quantitative analysis of the ELF and VLF components of sferics. As defined in Section 2.2, the magnitude of the wave magnetic field is computed as the vector sum of the measured N/S and E/W magnetic field components. The magnitude of the wave magnetic field is used so that direct quantitative comparisons are possible among sferics arriving from different directions. The peak values of the magnitude of both the ELF and VLF components of sferics are denoted as ELF peak and VLF peak respectively in Figure 4.2.

The intensity and duration of the ELF sferic measured at Yucca Ridge is related to the strength and duration of the continuing current following the first return stroke of the CG flash, as shown by *Bell et al.* [1998]. Since the total charge transferred to ground is the integral of the current waveform, we compute the integral of the magnitude of the wave magnetic field to provide a measure related to total charge transfer. We divide the result by the duration of integration to yield a time average and square the result for expression in units of energy. Explicitly, the ELF sferic energy is defined as the square of the average value of the vector sum between $t = -2$ ms and $t = 20$ ms, where $t = 0$ is the sferic onset, for all sferics measured at Yucca Ridge.
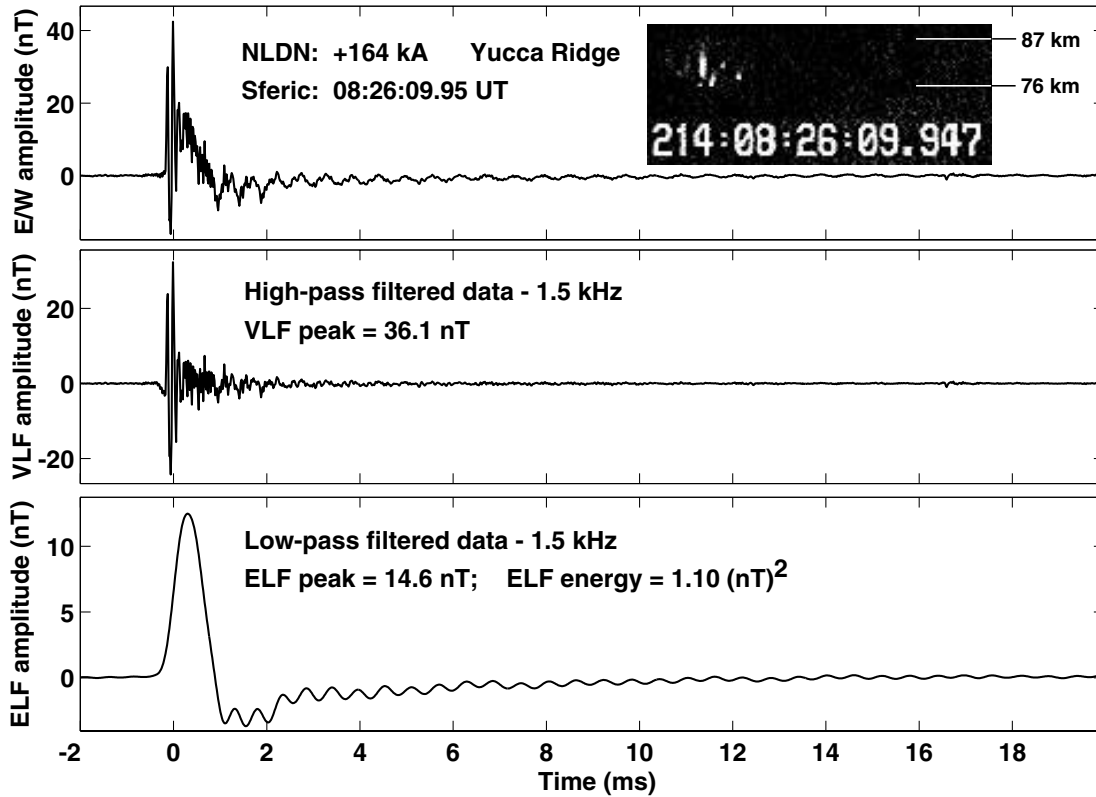
Figure 4.2: The sferic waveform launched by a 164-kA positive CG discharge at 08:26:09 UT on August 1, 1996. (Middle) The VLF component of the same sferic after digital highpass filtering with a cutoff frequency of 1.5 kHz. (Bottom) The ELF component of the same sferic after digital lowpass with a cutoff frequency of 1.5 kHz. The Sprite associated with this sferic is shown in the inset.

This definition of ELF sferic energy gives the average energy over the duration of the sferic, except in cases where a second ELF pulse is generated by a Sprite with a long (>20 ms) delay after the CG (see Section 4.4). The ELF "slow-tail magnitude" was defined by *Reising et al.* [1996] for Palmer Station measurements as the average value of the magnitude (vector sum of N/S and E/W) of the magnetic field between $t = -2$ ms and $t = 10$ ms. This slow-tail magnitude (see Section 4.3) is simply the square-root of the ELF sferic energy. In summary, the ELF sferic energy is defined as an indicator of the charge transfer from the cloud to the ground in the continuing current. In the next section we use the ELF sferic energy to form a proxy indicator for Sprite occurrence.

4.2 Medium Range Measurements at Yucca Ridge, Colorado

From 0644 to 0907 UT on August 1, 1996, 98 Sprites were observed above a mesoscale convective system in western Kansas, as discussed in Section 3.2 (see Figure 3.2). The peak currents of the 94 Sprite-producing positive CGs (see Section 3.2) ranged from 19 to 164 kA, as measured by the NLDN. We chose a threshold peak current of 26 kA and analyzed all NLDN positive CGs above this threshold. In addition, to confirm association with the Sprite, we required the positive CGs to occur within 200 ms before the Sprite onset. Of the 94 Sprite-producing positive CGs, 81 met both the threshold and the timing criteria. The distribution of the NLDN peak currents of these 81 Sprite-producing positive CGs is shown in the shaded bars of Figure 4.3. The unshaded portions of the bars show the distribution of the NLDN peak currents for all other positive CGs exceeding the 26-kA threshold and in the camera field of view, which includes most of the Sprite-producing storm (see Figure 3.2). The location criterion for CGs "in the camera field of view" was extended to include all NLDN-recorded CGs which could have produced Sprites anywhere in the field of view, even if the causative flash was just outside the nominal field of view. This criterion is identical to that used in the study of Sprite-producing storms from 1994 and 1995 [*Reising et al.*, 1996].

The ELF sferic energy, as defined in Section 4.1, is the integrated energy of the sferic in the ELF band (here $\sim$15 Hz - 1.5 kHz). This quantity is an indicator of total charge transfer in the continuing current following the first return stroke of a CG flash (see Section 4.1). Figure 4.4 shows the distribution of ELF sferic energy for the same 334 positive CGs whose NLDN peak current distribution is shown in Figure 4.3. The 0 decibel reference for the logarithmic scale is chosen to be equal to the mean of the distribution. For this population of sferics, one standard deviation is found to be $\sim$7 dB, as noted in the figure.

From Figure 4.4 it is evident that mean of the of the Sprite-associated ELF energy (shaded bars) is approximately one standard deviation greater than the mean of the distribution of ELF energy for the entire storm. Both ELF sferic energy distributions exhibit a log-normal distribution, consistent with the distribution of the peak currents of CG lightning flashes [*Berger et al.*, 1975]. The deviation from a log-normal
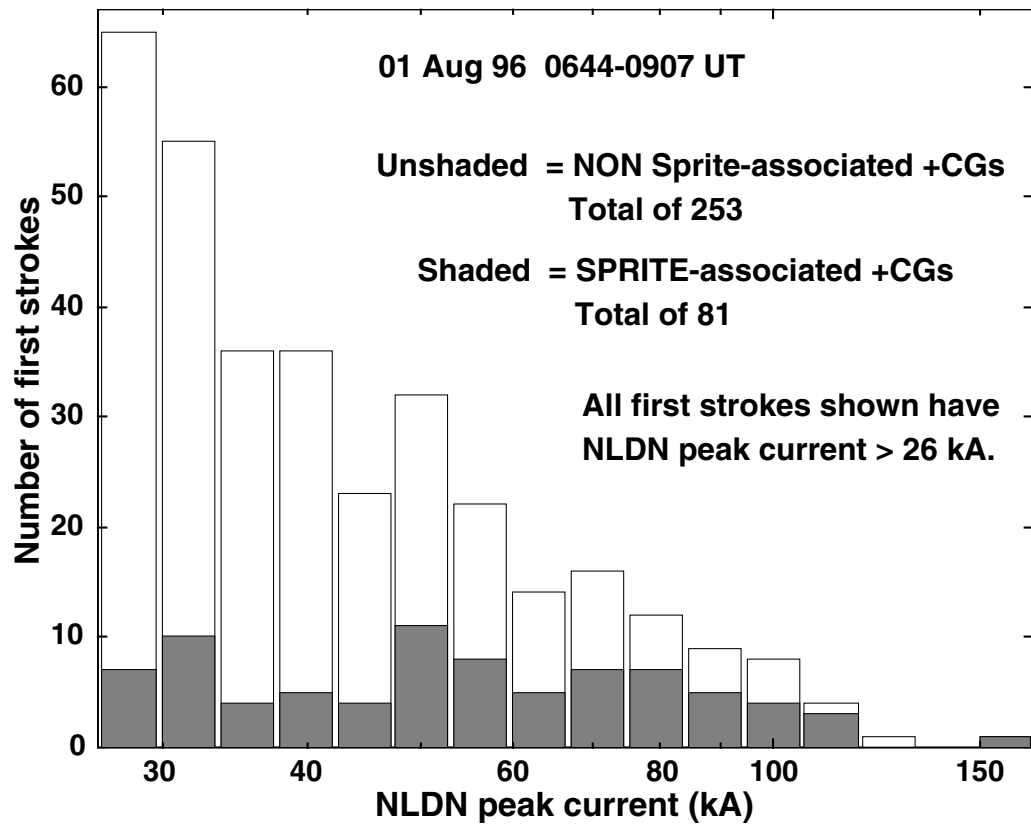
Figure 4.3: Histogram of the number of first strokes of positive CG flashes recorded by the NLDN with peak current ≥26 kA. Sprite-associated CGs are shown as shaded bars, and all other positive CGs are shown as unshaded bars.

distribution above ∼12 dB is due to the "second ELF pulse" observed in ∼20% of Sprites at 500-600 km range (see Section 4.4). The use of an absolute threshold criterion for prediction of Sprite production by individual positive CGs is shown in Figure 4.5. The histogram bars are identical to the distribution of the overall storm shown in Figure 4.4. The numbers on each histogram bar in Figure 4.5 correspond to two "quantized" cumulative distributions which can be used to measure the success of an absolute threshold method. The black numbers above each bar show the percentage of CGs which lead to Sprites, out of all CGs which launch sferics with ELF energy greater than or equal to that of each histogram bin. The red numbers inside each bar show the percentage of Sprites produced by CGs which launch sferics with greater than or equal to the ELF sferic energy of each histogram bin. For example, if one predicts that all positive CGs which launch sferics with >7 dB ELF energy are Sprite-producing CGs, then one is 83% correct, and one predicts a number of Sprites equal
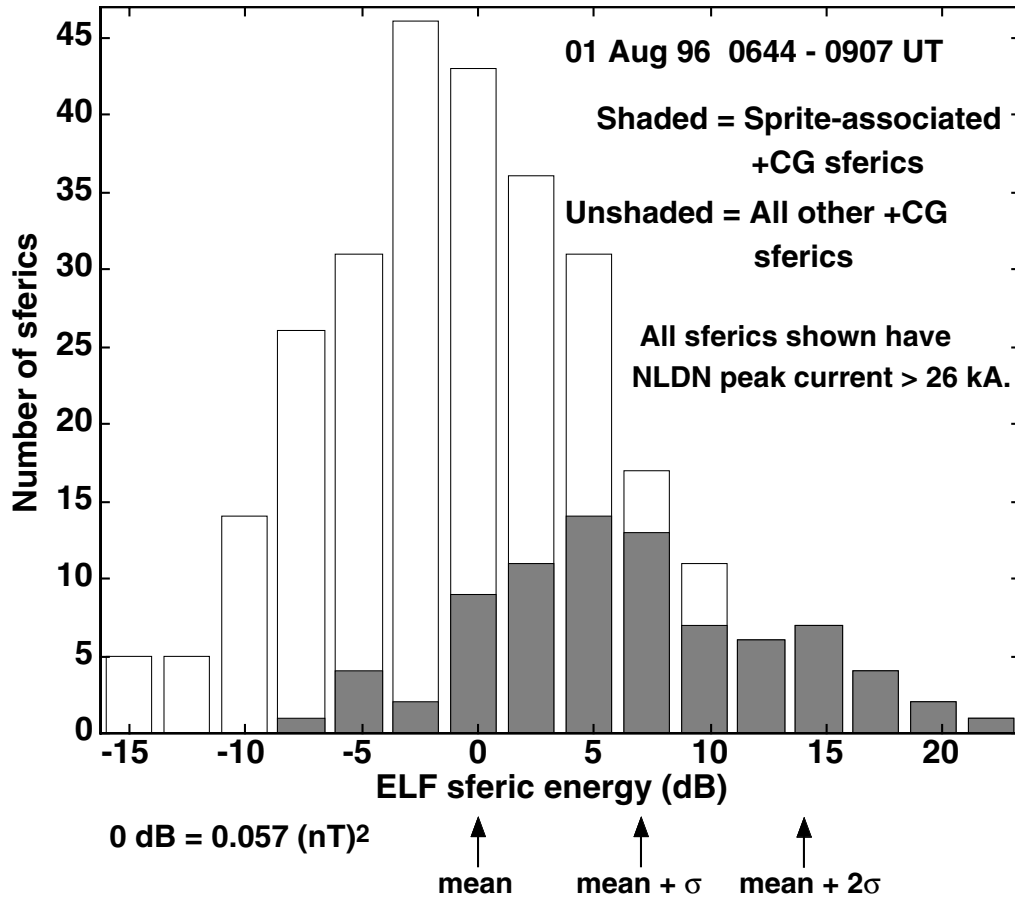
Figure 4.4: Histogram of the number of sferics as a function of ELF sferic energy, plotted on a dB (log) scale. Sprite-associated sferics are shown as shaded bars, and all other positive CGs are shown as unshaded bars. This histogram includes the same flashes as the histogram in Figure 4.3.

to 49 / 0.83 = 59% of the total Sprites produced. This number can be rescaled by 1 / 0.59 = 1.7 to provide an estimate of the total number of Sprites produced during this period. Other Sprite-producing storms in the continental U.S. exhibit similar distributions of ELF sferic energy (see Section 4.3). We apply this proxy indicator for Sprite occurrence to a lower-latitude mesoscale convective system in Mexico in Section 4.3.4. We expect that in general this technique will allow prediction of the number of Sprites produced by a mid-latitude mesoscale convective system to $\pm 25\%$ precision.
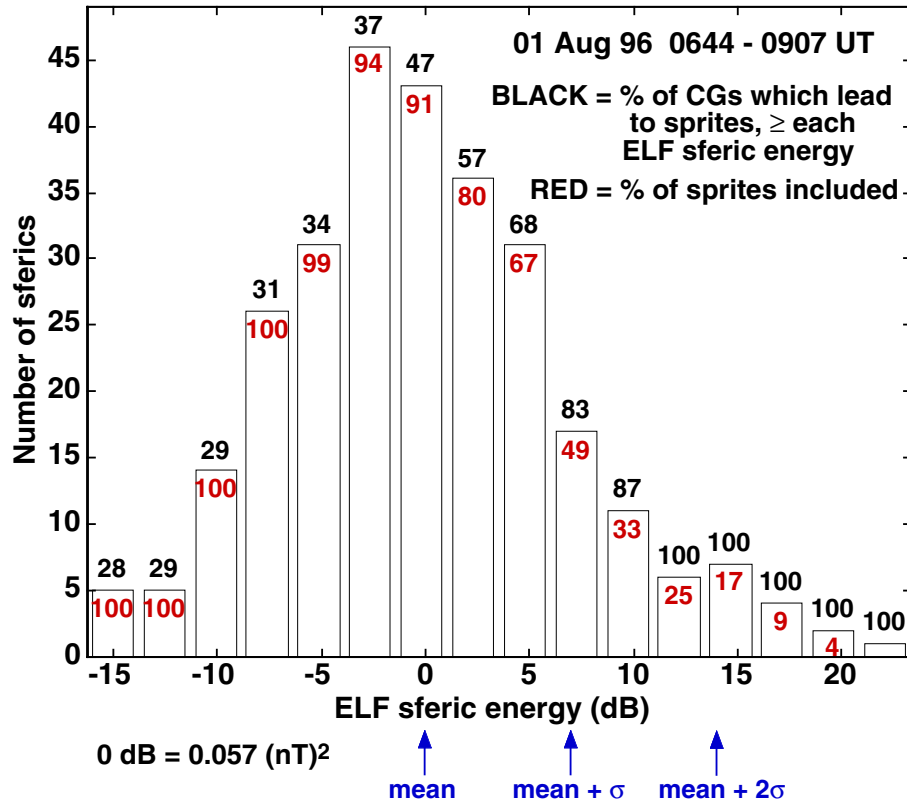
Figure 4.5: Histogram of all sferics shown in Figure 4.4, with the addition of cumulative distribution statistics for the percent of CGs greater than or equal to each ELF sferic energy which lead to Sprites (black numbers). The red numbers give the percent of Sprites included when using each histogram bar as an absolute threshold predictor for Sprite occurrence.

[*Reising et al.*, 1996]. The propagation time from Nebraska to Palmer Station is $\sim$40 ms at VLF frequencies. However, this delay is consistent among sferics originating in the same thunderstorm. The identification of sferic occurrence times to <1 ms precision, along with the identification of arrival azimuth of sferics to $\pm 1°$ (see Section 2.4), allows the unambiguous identification of sferics arising from individual NLDN flashes. In the following section, we use the result that enhancement of the ELF sferic, called a "slow tail" at large (>5,000 km) distances from the source, is due to continuing current following the CG return stroke (see Section 1.3).

4.3.1 Continuing Currents in Sprite-Associated Lightning Flashes

Measurements of sferics at Palmer Station, Antarctica, show that those sferics launched by Sprite-producing CG flashes exhibit enhanced ELF "slow tails" following the initial VLF portion [*Reising et al.*, 1996]. The "slow tail" is the ELF portion which,
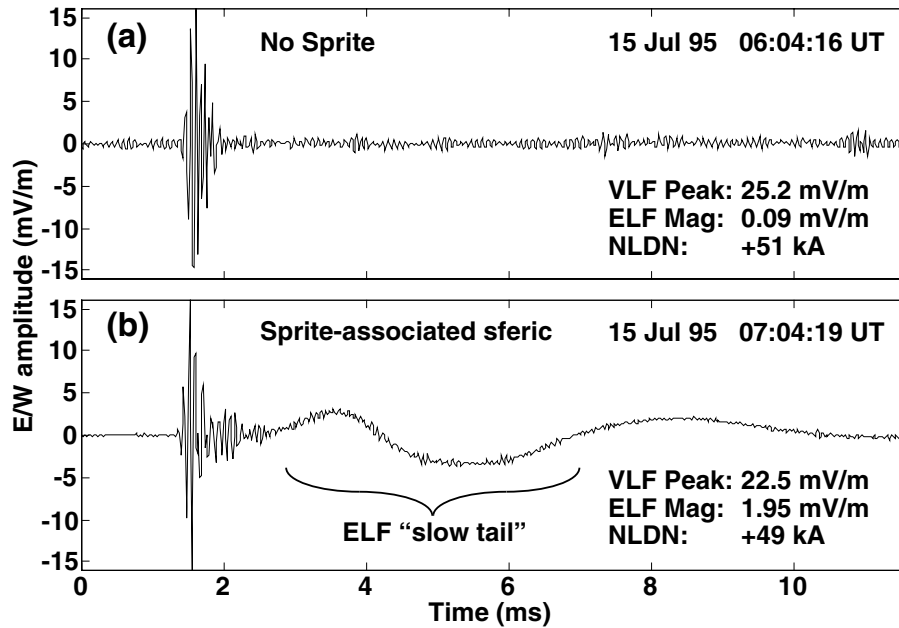
Figure 4.6: From [*Reising et al.*, 1996]. Two sferics originating in the same U.S. Great Plains thunderstorm and recorded at Palmer Station with similar peak values of VLF magnitude but markedly different ELF "slow tail" average magnitudes. The waveform in (b) exhibits an average ELF magnitude more than 20 times greater than that of the one in (a). The sferic with the large slow tail (b) was generated by a Sprite-associated CG flash, whereas the one without a measurable slow tail (a) was not.

flashes. In the following section, we use the result that enhancement of the ELF sferic, called a "slow tail" at large (>5,000 km) distances from the source, is due to continuing current following the CG return stroke (see Section 1.3).

4.3.1 Continuing Currents in Sprite-Associated Lightning Flashes

Measurements of sferics at Palmer Station, Antarctica, show that those sferics launched by Sprite-producing CG flashes exhibit enhanced ELF "slow tails" following the initial VLF portion [*Reising et al.*, 1996]. The "slow tail" is the ELF portion which, over a ~12,000 km propagation path, is significantly delayed in time from the initial VLF oscillating portion due to its slower phase velocity (see Figure 4.6 and Section 1.3). For the two sferics shown in Figure 4.6, the characteristics of the propagation path were essentially constant, so the factor of 20 difference between their average ELF magnitudes is to due to difference in their sources, which in the ELF frequency

band are continuing currents (see Section 1.3). In Figure 4.6 the sferics measurements are displayed in terms of the electric field (E), even though the measured quantity is the wave magnetic field (B). For ground measurements of waves propagating in free space, the magnitudes E and B are related by $E = cB$, where c is the speed of light. This relationship is also correct for the quasi-transverse electric and quasi-transverse magnetic modes (VLF sferic) in the waveguide. For the quasi-transverse electromagnetic mode (ELF sferic), the phase velocity is $\sim$0.9 c [*Sukhorukov and Stubbe*, 1997], so the relationship is approximately true. Under these conditions, the following conversion:

$$30 \, \frac{\text{mV}}{\text{m}} \iff 0.1 \text{ nT}$$

can be used to convert from quantities given in E for Palmer Station measurements to quantities given in B for Yucca Ridge measurements.

The observation that those sferics launched by Sprite-producing CG flashes exhibit enhanced ELF "slow tails" compared to non Sprite-producing sferics indicates that significant continuing currents on the time scale of $\sim$1-5 ms are a necessary condition for Sprite production [*Reising et al.*, 1996]. This interpretation of slow-tail enhancement (see Section 1.3) is consistent with the requirement of continuing current in order to lower large amounts of charge from the cloud to ground, which is believed to be necessary for Sprite production (see Sections 1.2.2 and 1.1).

4.3.2   Sprite-Producing Storm on July 12, 1994

Two cases studied by *Reising et al.* [1996] demonstrate the usefulness of the proxy indicator at $\sim$12,000 km range from the Sprite-producing mesoscale convective system. In the first case, on July 12, 1994, 44 Sprites were observed at Yucca Ridge between 0510 and 0712 UT, at the rate of just less than one Sprite every 3 minutes. Figure 4.7a shows the locations of all positive CG flashes recorded by NLDN, and the circles in Figure 4.7c show the locations of those positive CGs which produced Sprites. At Palmer, sferics were detected in association with 42 of the 44 (95%) Sprites. The NLDN recorded positive CG flashes in 31 of the 44 (70%) events within $\pm$100 ms of the period between the onset of the Sprite and the end of its observed luminosity, as recorded by the intensified CCD camera at Yucca Ridge. The peak current distribution of these 31 flashes is shown in shaded bars in the left panel of Figure 4.8. These Sprite-associated CGs have a wide variation of peak currents, nearly spanning the
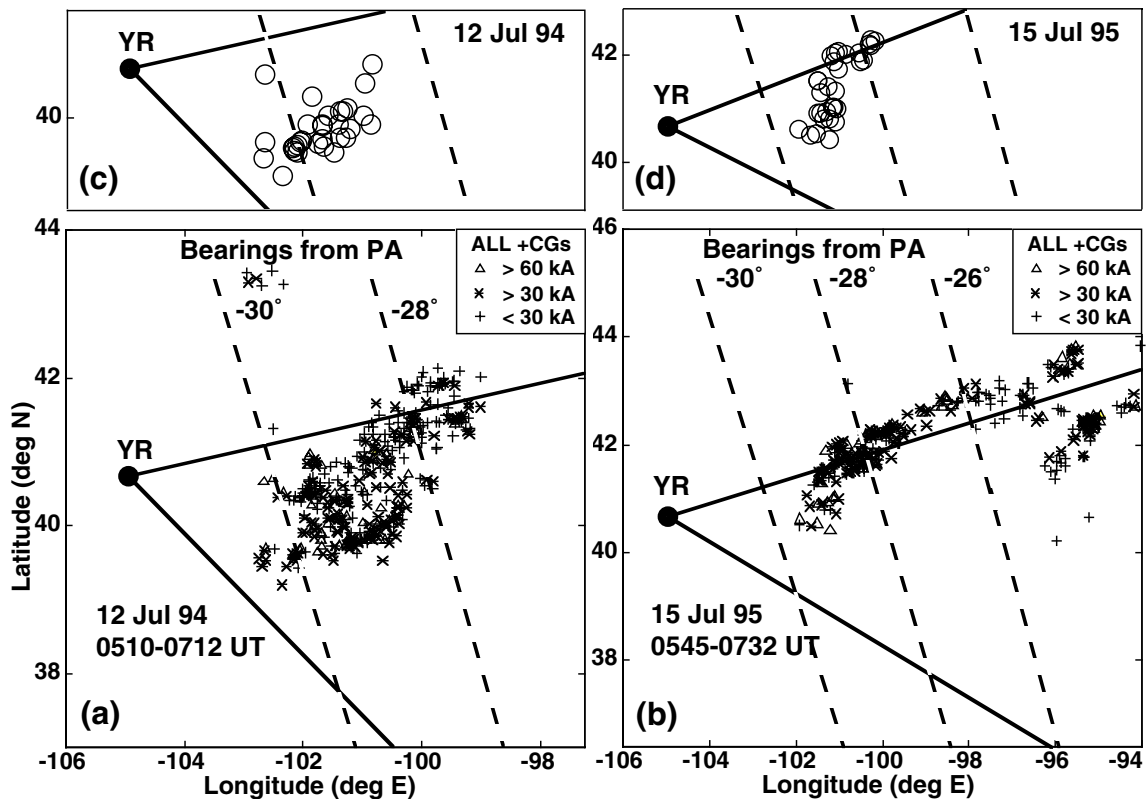
Figure 4.7: From [*Reising et al.*, 1996]. Panel (a) shows all positive CG flashes recorded by NLDN from a mesoscale convective system in central/SW Nebraska and NE Colorado, from 0510-0712 UT on July 12, 1994. The locations of Sprite-producing positive CGs recorded by NLDN are denoted by circles in (c). Panel (b) shows the positive CG flashes from 0545-0732 UT on July 15, 1995, from a mesoscale convective system with strong activity in central/SW Nebraska, with weaker positive CGs in Iowa. Sprite-producing positive CGs are shown as circles in panel (d). The intensified CCD camera fields-of-view are shown as rays extending from Yucca Ridge (YR). The dotted lines are lines of constant bearing from Palmer Station, Antarctica. The NLDN data is provided by courtesy of NASA/MSFC and the Global Hydrology Resource Center.
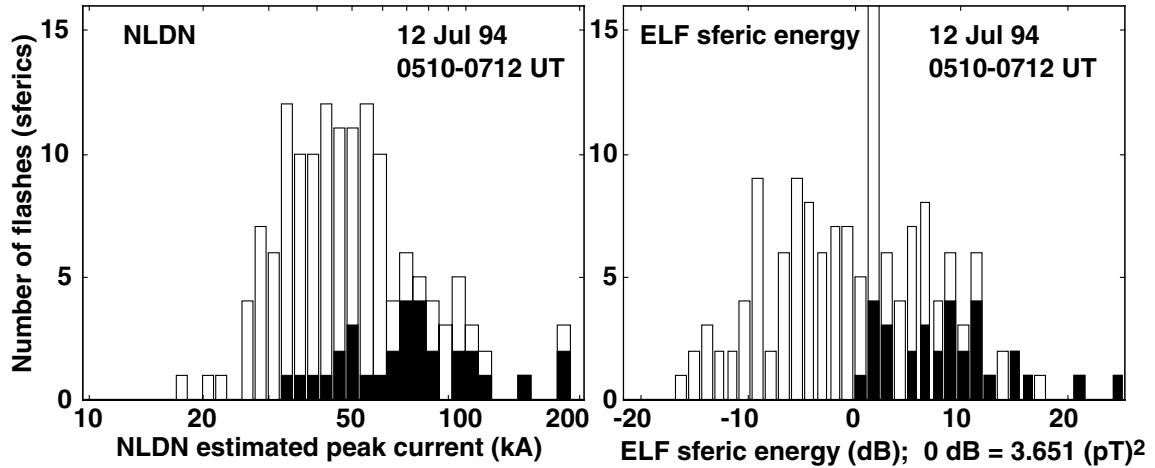
Figure 4.8: Adapted from [*Reising et al.*, 1996]. Distributions of NLDN peak current (left panel) and corresponding Palmer ELF sferic energy (right panel) for all 144 positive CGs on July 12, 1994, within the intensified CCD camera field-of-view. The vertical scales are number of first strokes for the left panel, and number of sferics for the right panel. Sprite-associated CGs are shown as shaded bars, and non Sprite-associated CGs are shown as unshaded bars.

entire distribution of 144 positive CGs within the field of view (shown as unshaded bars). The ELF sferic energy distribution of the same 144 positive CGs is shown in the right panel of Figure 4.8, with the 31 Sprite-associated CGs denoted by shaded bars. The ELF sferic energy is an average over the first 10 ms of the sferic, as in *Reising et al.* [1996]. The distribution demonstrates that Sprite-producing CGs generate sferics with large ELF energy, indicative of large continuing currents on the time scale of several milliseconds [*Reising et al.*, 1996].

4.3.3   Sprite-Producing Storm on July 15, 1995

In the second case, on July 15, 1995, 35 Sprites were observed at Yucca Ridge between 0545 and 0732 UT, at the rate of one Sprite every ∼3 minutes. Figure 4.7b shows the locations of all positive CG flashes recorded by NLDN, and the circles in Figure 4.7d give the locations of those positive CGs which produced Sprites. At Palmer Station, sferics were detected in association with 34 of the 35 (97%) Sprites. The NLDN recorded positive CG flashes in 29 of the 35 (83%) events within ±100 ms of the period between the onset of the Sprite and the end of its observed luminosity.
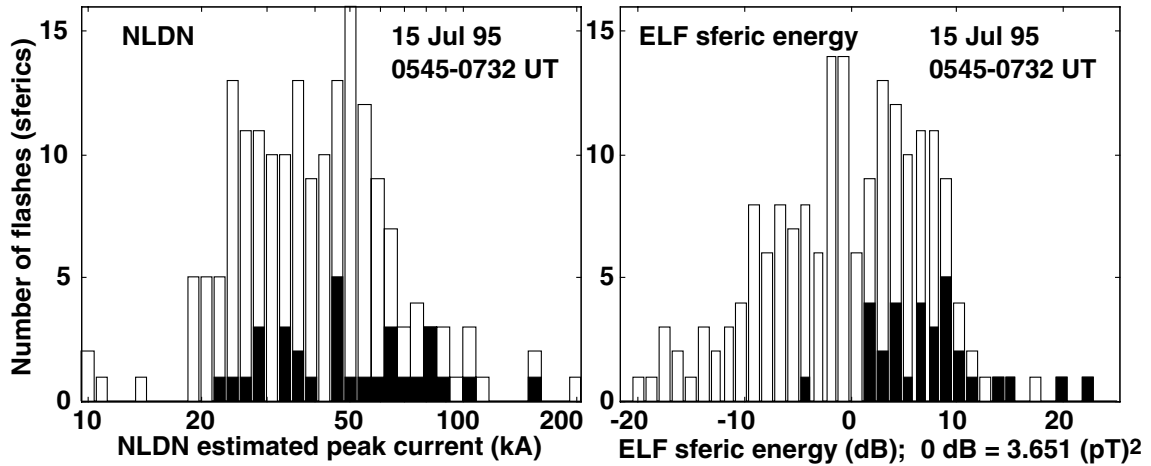
Figure 4.9: Adapted from [*Reising et al.*, 1996]. Distributions of NLDN peak current (left panel) and corresponding Palmer ELF sferic energy (right panel) for all 184 positive CGs on July 15, 1995, within the intensified CCD camera field-of-view. The vertical scales are number of first strokes for the left panel, and number of sferics for the right panel. Sprite-associated CGs are shown as shaded bars, and non Sprite-associated CGs are shown as unshaded bars.

The peak current distribution of these 31 flashes is shown in shaded bars in the left panel of Figure 4.9. These Sprite-associated CGs exhibit a wide variation of peak currents, nearly spanning the full distribution of 184 positive CGs within the field of view. The ELF sferic energy distribution of the same 184 positive CGs is shown in the right panel of Figure 4.9, with the 29 Sprite-associated CGs denoted by shaded bars. The ELF energy is an average over the first 10 ms of the sferic, the same as that reported in Section 4.3.2. The distribution demonstrates that Sprite-producing CGs generate sferics with large ELF energy, indicative of large continuing currents on the time scale of several milliseconds [*Reising et al.*, 1996].

4.3.4 Application of ELF Proxy to Multiple Storms

We studied sferics received at Palmer Station from multiple thunderstorms during the same period of observation on August 1, 1996. This study demonstrates the usefulness of ELF sferic energy as a proxy indicator for Sprite occurrence associated with thunderstorms for which optical recordings of Sprites were not available. The NLDN-recorded lightning activity during the period 0644-0800 UT is shown in the
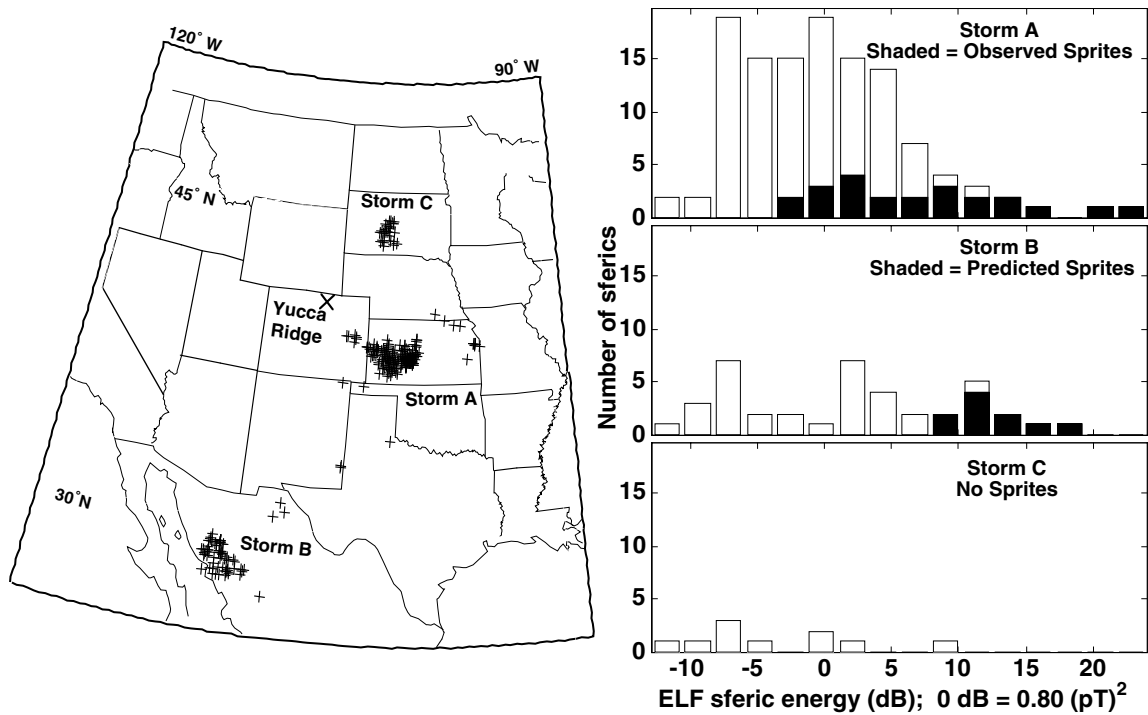
Figure 4.10: (Left) Locations of positive cloud-to-ground flashes observed by the NLDN with peak current exceeding 23 kA from 0644-0800 UT on August 1, 1996, identical to Figure 2.7. (Right) Distributions of ELF sferic energy for sferics recorded at Palmer from Storms A, B and C from 0644 to 0745 UT on August 1, 1996. All sferics are generated by positive CGs recorded by the NLDN with peak current $\geq$23 kA. In the top panel, shaded bars indicate Sprite-associated sferics, as verified by optical observations at Yucca Ridge (see Section 3.2).

left panel of Figure 4.10, where pluses denote positive CG flashes with peak currents exceeding 23 kA. Storm A is the Sprite-producing storm in western Kansas described in detail in Sections 3.2 and 4.2. Storm B is in Sonora, Mexico, just to the east of the Gulf of California. Storm C is a smaller thunderstorm in South Dakota. The GOES 8 infrared brightness temperature data at 0702 UT for the same region is shown in Figure 4.11. The areas of coldest cloud tops are shown in purple and white (Storms A and B), indicating the presence of mixed-phase regions, which are known to be important for thunderstorm electrification and for the generation of large stratiform regions, above which Sprites are observed to occur (see Section 1.2.5).

By matching arrival azimuth and propagation delay separately for each storm (see Section 2.4), we measured sferics in association with many of the NLDN positive CGs with peak currents >23 kA, for storms A, B and C (see Figure 4.10). The distributions of ELF sferic energy for sferics measured from 0644 to 0745 UT in each of the three storms are shown in the right panel of Figure 4.10. In this case the ELF

energy is an average over the first 20 ms of the sferic, as in Section 4.2, so the mean sferic energy is smaller than that shown in Figures 4.8 and 4.9. In the top right panel of Figure 4.10, the shaded bars show the ELF energy of sferics generated by Sprite-associated positive CGs, as determined from optical measurements at Yucca Ridge. Storm B shows an overall distribution which is similar to Storm A, and we infer from the sferic energy distribution of the detected Sprites in Storm A that Storm B most likely produced at least as many Sprites as shown by the shaded bars in the middle right panel. We note that Sprites were measured optically during the summer of 1997 above storms in the same region as Storm B, with a higher rate of Sprite production than many of the Great Plains storms [*Barrington-Leigh et al.*, 1997]. Storm C was a smaller storm with a lower rate of positive CGs, and our measurements indicate that it produced very few or no Sprites at all.

Based on ground-based observations of thousands of Sprites, *Lyons* [1996] gives meteorological criteria for thunderstorms in the U.S. Great Plains which are likely to produce Sprites. His initial evidence indicates that a necessary, but not sufficient, condition for Sprite production is a mesoscale convective system with >20,000 km^2 radar echo area having a large stratiform precipitation region containing numerous positive CG flashes [*Lyons*, 1996]. Storm A meets these criteria, and Storm B has radar echoes >100,000 km^2, putting it into the category of a mesoscale convective complex (see Section 1.2.5). Storm C covers >60,000 km^2, but it has only 0.25 positive CGs per minute during this period, as opposed to 0.6 and 1.7 positive CGs per minute in Storm B and Storm A, respectively. The flash rate in Storm B is likely greater than the 0.6 positive CGs per minute measured by NLDN, because Storm B is located near the edge of the NLDN coverage area [*Cummins et al.*, 1998]. Sprites have been observed above smaller thunderstorms in Florida [*Stanley et al.*, 1997] and in South America [*Sentman et al.*, 1996], so, as *Lyons* [1996] points out, the criteria for a Sprite-producing thunderstorm need to be modified for different climatological regimes.

4.4 ELF Radiation from Electrical Currents in Sprites

In this section we return to analysis of sferics measurements performed at Yucca Ridge during Summer 1996, at ∼500-600 km distance from Sprite-producing mesoscale convective systems in Kansas and Nebraska. At this range, the ELF component of a
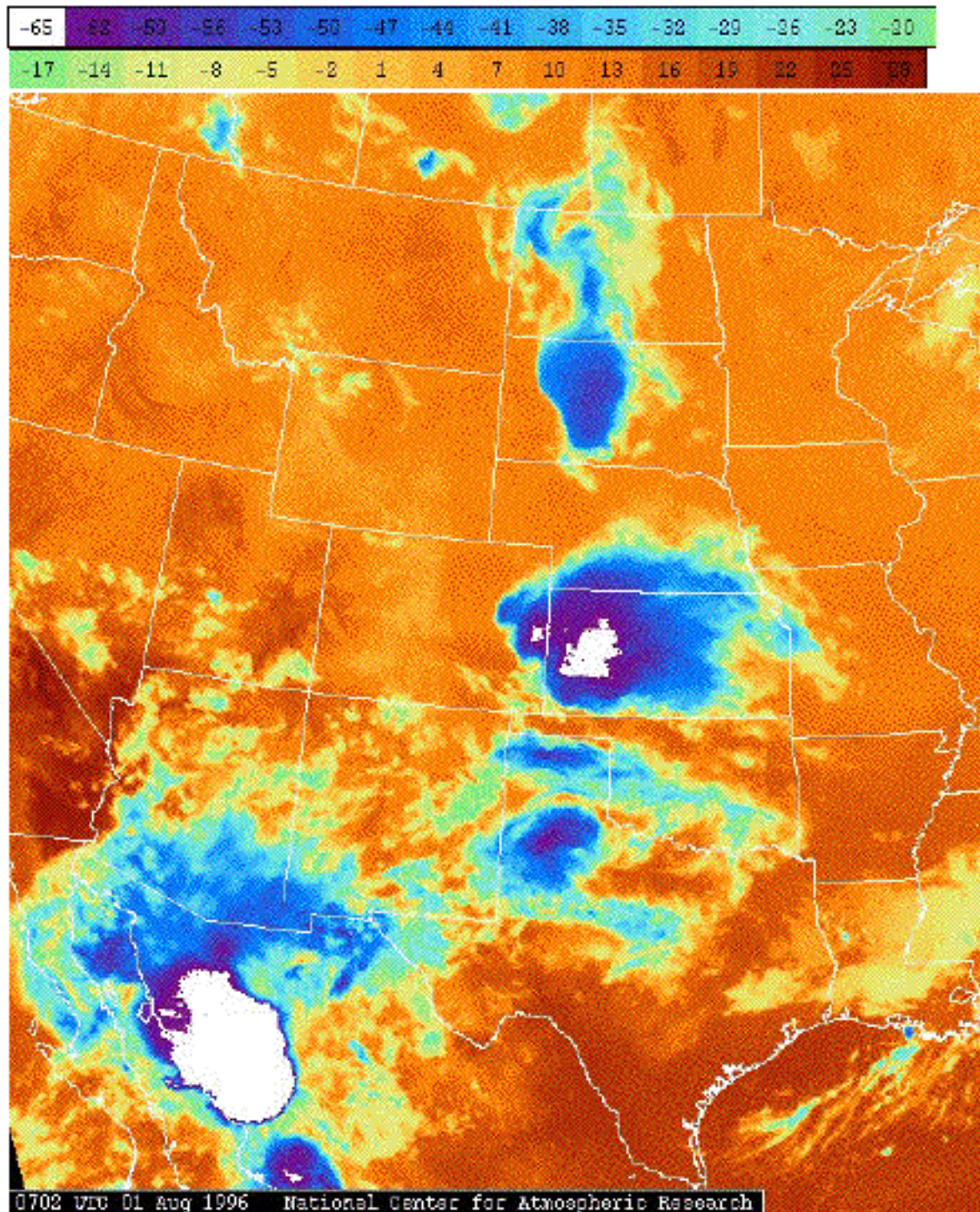
Figure 4.11: Infrared brightness temperature measured on the GOES 8 geosynchronous satellite at 0702 UT on August 1, 1996. The area of coverage is the same as that shown in the left panel of Figure 4.10. Courtesy of the National Center for Atmospheric Research.
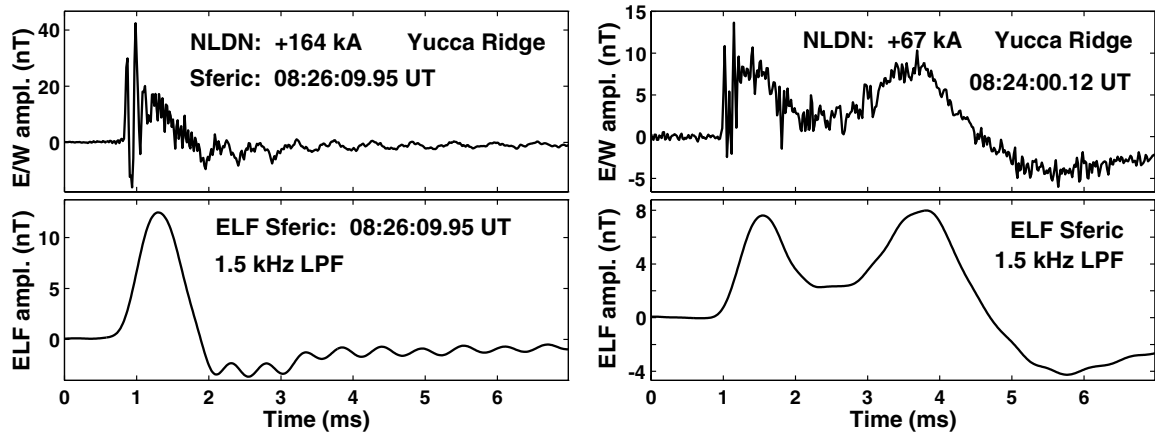
Figure 4.12: (Top Left) The sferic waveform launched by a 164-kA positive CG discharge and measured at Yucca Ridge at 08:26:09 UT on August 1, 1996. (Top Right) The sferic waveform launched by a 67-kA positive CG discharge and measured at Yucca Ridge at 08:24:00 UT on August 1, 1996. (Bottom Panels) The ELF components of both sferics after digital lowpass filtering with a cutoff frequency of 1.5 kHz.

typical Sprite-associated sferic consists of a positive-going pulse of half width 0.5-1 ms followed by a negative-going pulse of much smaller magnitude which recovers to zero in <20 ms, as shown in the lower left panel of Figure 4.12. However, in ∼20% of the Sprite-associated sferics, a second positive-going ELF pulse is observed, clearly separated in time from the first positive ELF pulse, as shown in the lower right panel of Figure 4.12. Simultaneous photometric observations of Sprite luminosity at high time resolution (∼30 μs) verified that the Sprite luminosity rises and falls nearly simultaneous with the source current which radiated the second ELF pulse [*Cummer et al.*, 1998]. The lack of a VLF oscillation at the beginning of the second ELF pulse (see top right panel of Figure 4.12) indicates that this pulse is not generated by a CG return stroke nor by an intracloud lightning discharge. The authors conclude that the temporal association strongly suggests that the source of the second ELF pulse is current flowing in the body of the Sprite itself. In the context of our study, it is important to recognize that the second ELF pulse is included in the proxy indicator described in Section 4.2. As seen in Figure 4.4, the ELF energy distribution of Sprite associated sferics is not strictly Gaussian, but rather bimodal, where the rightmost peak is likely influenced by the presence of the second ELF pulse. This effect is not observed in Figures 4.8 and 4.9 because the time window for measurement of ELF energy extends to $t = 10$ ms, as opposed to $t = 20$ ms for Figure 4.4. Secondly, at ∼12,000 km propagation distance the ELF slow tail is delayed by ∼3 ms from the
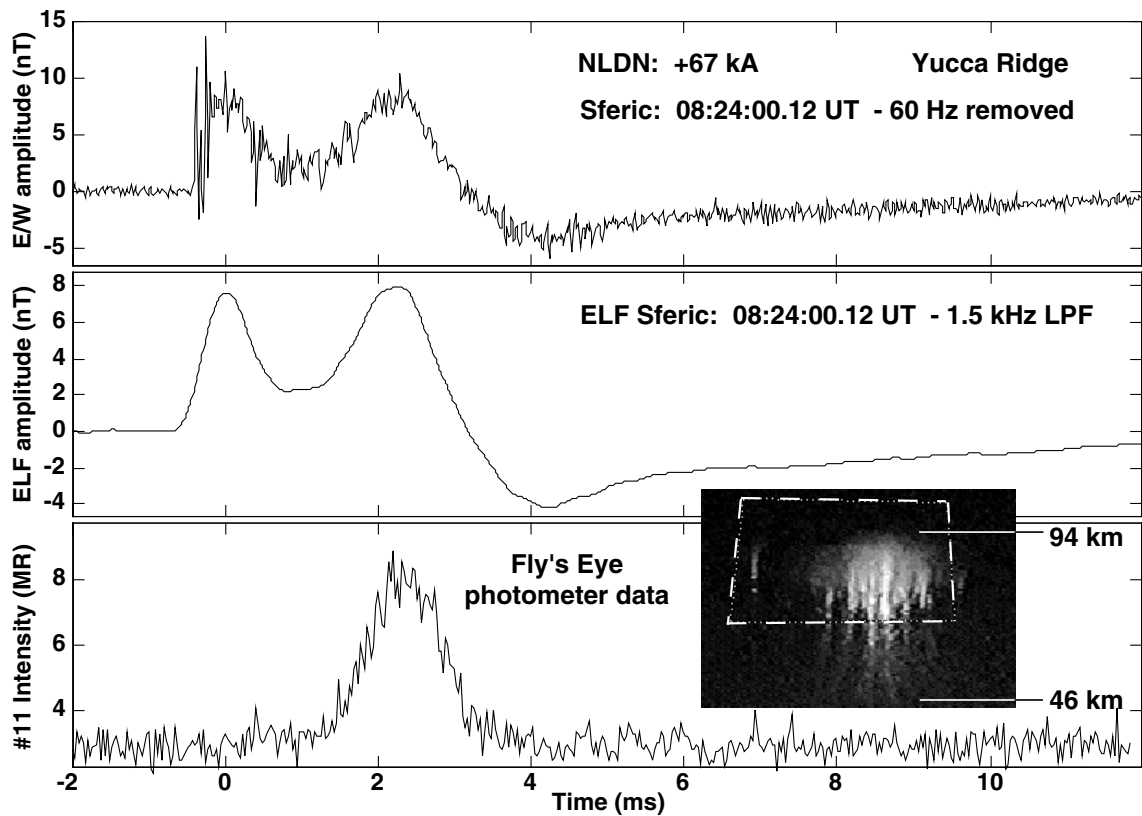
Figure 4.13: (Top) The sferic waveform launched by a 67-kA positive CG discharge and measured at Yucca Ridge at 08:24:00 UT on August 1, 1996. (Middle) The ELF component of the same sferic after digital lowpass filtering with a cutoff frequency of 1.5 kHz. (Bottom) Optical intensity data measured by the Fly's Eye photometer #11. The inset shows the field of view of the photometer by dotted lines overlaid on the image of the Sprite associated with this sferic.

VLF onset, so many of the second ELF pulses are delayed past $t = 10$ ms.

We present simultaneous photometric and sferic observations made at Yucca Ridge of Sprites and lightning produced by the mesoscale convective system in western Kansas on August 1, 1996 (see Section 4.2), which are consistent with the results of *Cummer et al.* [1998]. Photometric observations were conducted with an array of photometers as part of the Stanford / Lockheed Fly's Eye experiment [*Inan et al.*, 1997]. This array consisted of Hamamatsu HC124-01 integrated photomultiplier assemblies with light shields, lenses, and precision-cut focal-plane screens to provide specific views of the sky [*Inan et al.*, 1997]. In this work we show results from photometer #11, which had a 6.6° wide by 3.3° high field of view, denoted by dotted lines on the inset in Figure 4.13. This figure shows a sferic launched by a 67-kA

Figure 4.14: (Top) The sferic waveform launched by a 83-kA positive CG discharge and measured at Yucca Ridge at 08:39:30 UT on August 1, 1996. (Middle) The ELF component of the same sferic after digital lowpass filtering with a cutoff frequency of 1.5 kHz. (Bottom) Optical intensity data measured by the Fly's Eye photometer # 11. The inset shows the field of view of the photometer by dotted lines overlaid on the image of the Sprite associated with this sferic.

positive CG at 08:24:00 UT (top panel), the ELF component of the sferic (middle panel) and the photometer #11 data (bottom panel) showing Sprite luminosity (see inset). These data confirm simultaneity (within ± 0.2 ms) of the second pulse of the ELF sferic and the Sprite luminosity, consistent with *Cummer et al.* [1998]. The second ELF pulse has slightly larger amplitude and longer duration than the first, indicating a larger charge-moment associated with the charge transfer in the Sprite than in the cloud-to-ground continuing current which produced the first pulse. A second example is the sferic launched by a 83-kA positive CG at 08:39:30 UT presented in Figure 4.14, in the same format as this previous figure. In this case the second pulse is of much smaller amplitude than the first, but the simultaneity of the second ELF pulse and the Sprite luminosity is again apparent.
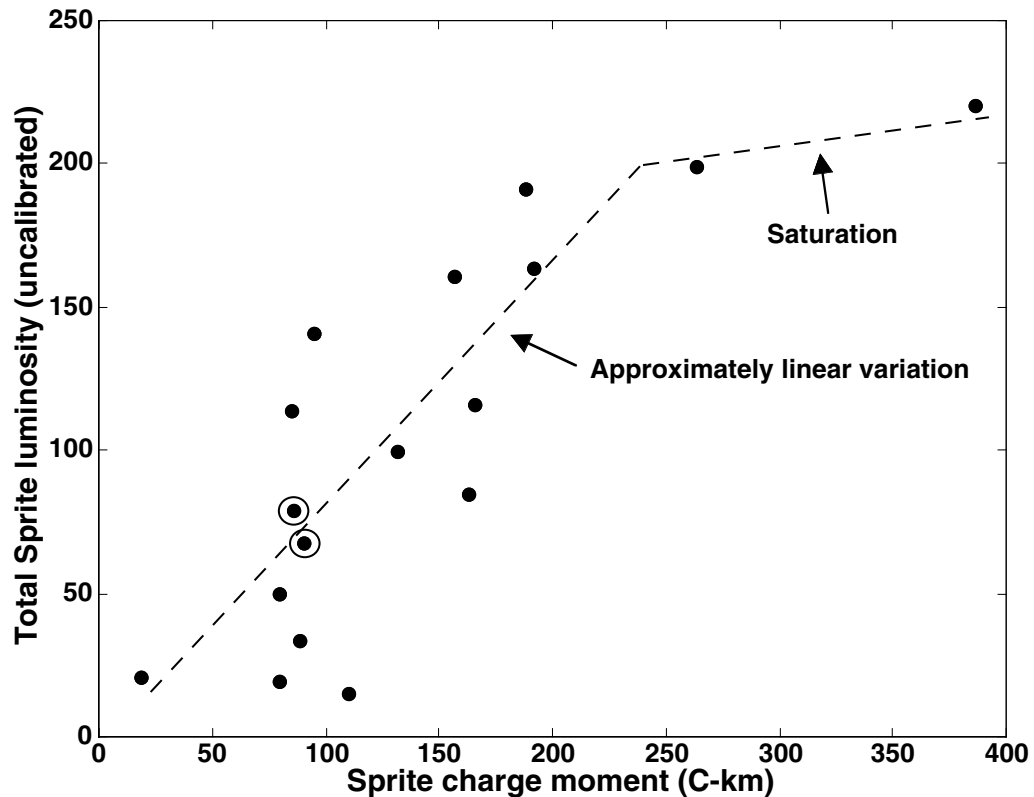
Figure 4.15:   The quantitative relationship of Sprite charge moment and total Sprite luminosity for 17 Sprites on July 24, 1996. The moment of charge transfer in the Sprite is inferred from the second ELF pulse, as measured at Yucca Ridge. The Sprite luminosity is calculated from intensified CCD video recordings of Sprites, as observed at Yucca Ridge.

The dipole moment associated with charge transfer in the source of the second ELF pulse can be calculated using a method applied to estimation of the continuing current from the first ELF pulse by *Bell et al.* [1996; 1998] and discussed in Section 3.3. To obtain a lower bound for the moment of charge transfer in the Sprite itself, we reduced the calculated charge moment by 25% because some of the energy in the second ELF pulse may be generated by weak continuing currents flowing from the cloud to the ground at the time of Sprite occurrence, as suggested by *Cummer et al.* [1998]. We applied this procedure to sferics measurements on July 24, 1996, from an unusually extensive mesoscale convective system covering western Kansas and Oklahoma, and extending deep into the Texas panhandle. Video observations at Yucca Ridge on July 24 recorded at least 140 Sprites from 05:19 to 08:56 UT, giving a rate of one Sprite every ∼90 seconds, occurring to the southeast at ∼500-650 km range from Yucca Ridge. Several interesting sequences were recorded on July 24,
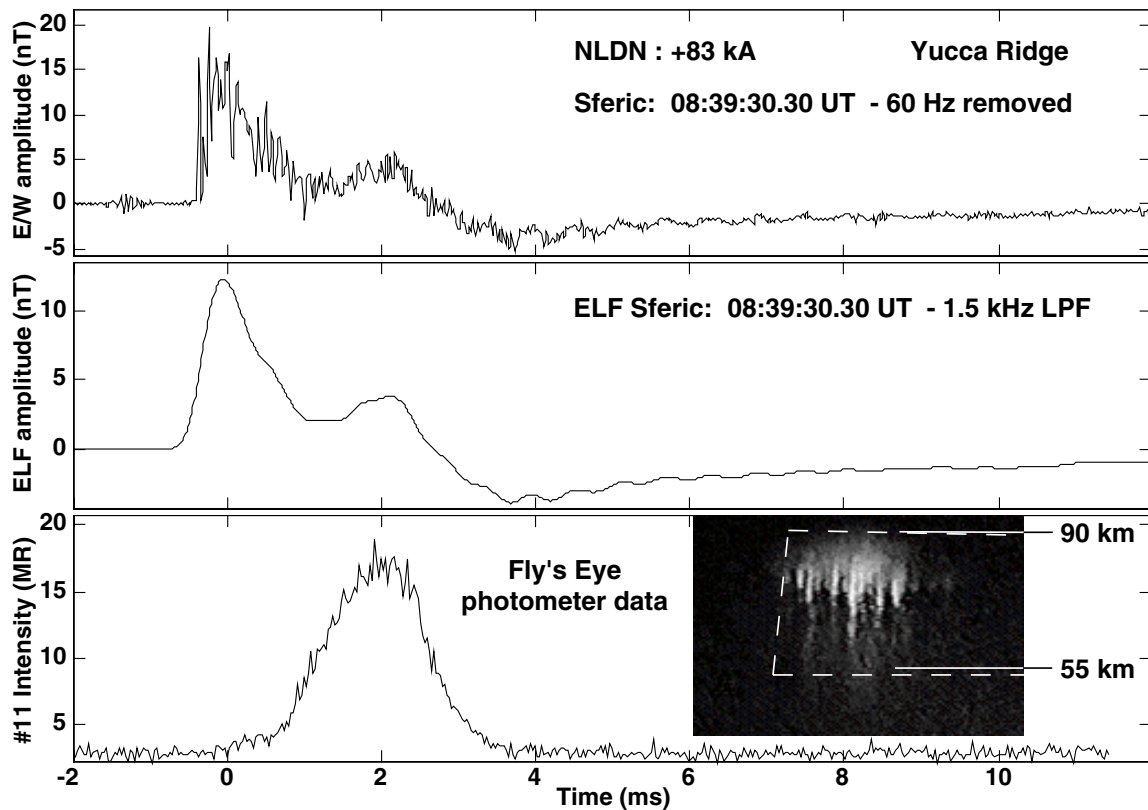
Figure 4.16: (Top) The sferic waveform launched by a 48-kA positive CG discharge and measured at Yucca Ridge at 07:43:48 UT on July 24, 1996. (Bottom) The ELF component of the same sferic after digital lowpass filtering with a cutoff frequency of 1.5 kHz.
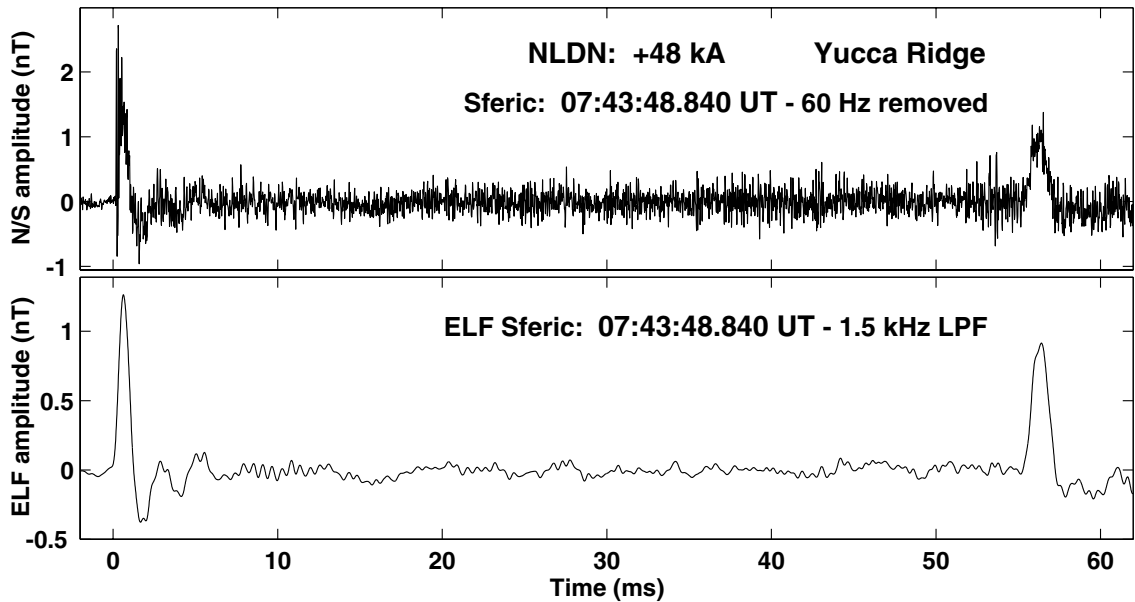
where up to eight Sprites appear to "dance" laterally across the camera field of view in a duration of only 0.5-1.0 seconds (e.g., [*Nelson et al.*, 1997]).

On July 24, at least 17 Sprite-associated sferics exhibited second ELF pulses. Using simultaneous intensified CCD camera images, we measured the total Sprite luminosity as the product of the number of Sprite-illuminated CCD pixels and the average luminosity in each of those pixels. To compensate for varying range between the camera and the Sprite, the measurement was scaled by the square of the range from the camera to the Sprite-associated CG. The assumption of Sprite occurrence near the location of its associated CG has been shown to be valid to within ∼40 km in most cases [*Winckler et al.*, 1996; *Lyons,* 1996], and was used to assign altitude scales to all of the Sprite images shown in this chapter. For these 17 cases, we show an approximately linear relationship between Sprite charge moment and total Sprite luminosity in Figure 4.15. The Sprite luminosity exhibits saturation at the largest two values of Sprite charge moment. The individual CCD pixels were not saturated, so further data are needed to establish the physical cause of the saturation.

The circles in Figure 4.15 denote two examples in which the delay between the occurrence of the associated positive CG and the Sprite onset is >50 ms. In all other
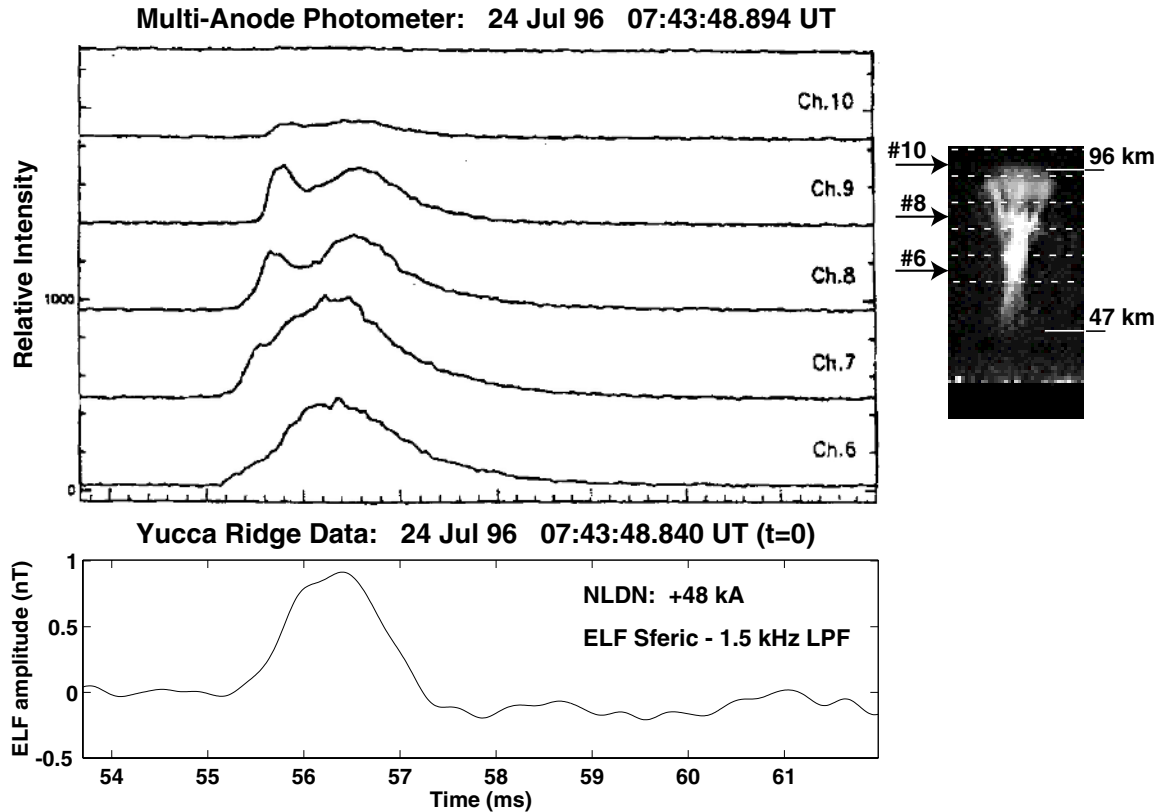
Figure 4.17: (Top) The optical intensity of the Sprite at 07:43:48 UT on July 24, 1996, as recorded by the multi-anode photometer channels #6-10 (Courtesy of Dr. Y. Takahashi). The fields of view of the multi-anode photometer channels are indicated by dotted lines in the associated Sprite image at right. (Bottom) A time-expanded view of the bottom panel of Figure 4.16 from $t = \sim 54$ to $t = 62$ ms, including the second ELF pulse.

cases shown in Figure 4.15, the CG-to-Sprite delay was <18 ms. For the two cases of >50 ms delay, we compared ELF sferics to simultaneous data from multi-anode photometer measurements performed at Yucca Ridge by our colleagues from Tohoku University in Sendai, Japan [*Takahashi et al.*, 1997]. The multi-anode photometer instrument was deployed to resolve the vertical development of Sprites at high time resolution (~ 20 μs). The instrument consists of a 16-element vertical column of photometers, each of which has a $\sim 9°$ wide by $1°$ high field of view (see right panel of Figure 4.17). Figure 4.16 shows a sferic produced by a 48-kA positive CG at 07:43:48 UT on July 24, 1996, and measured at Yucca Ridge. The lower panel shows the ELF sferic, where the first ELF pulse follows the return stroke (in <1 ms), and the second ELF pulse occurs ~ 56 ms later. The high signal-to-noise ratio of the Yucca Ridge observations is evident, even for a modest-sized positive CG of 48 kA, and the peak
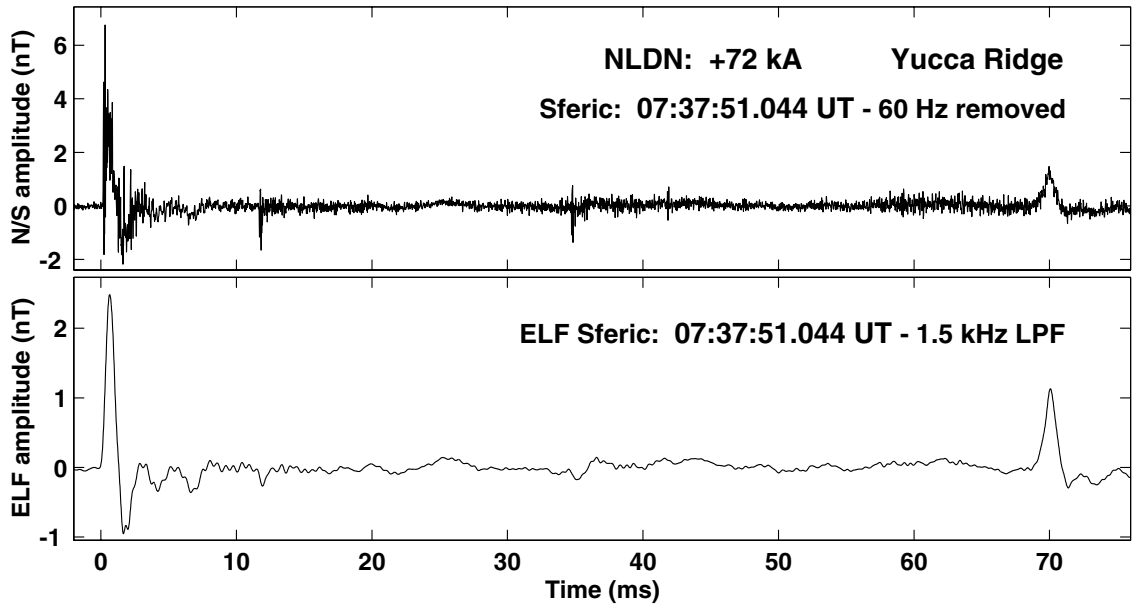
Figure 4.18: (Top) The sferic waveform launched by a 72-kA positive CG discharge and measured at Yucca Ridge at 07:37:51 UT on July 24, 1996. (Bottom) The ELF component of the same sferic after digital lowpass filtering with a cutoff frequency of 1.5 kHz.

amplitude of the second ELF pulse is about 70% of that of the first ELF pulse. An expanded view of the second ELF pulse on $\sim$8 ms time scale is shown in the bottom panel of Figure 4.17. The upper panel shows the intensity measurements of channels #6-10 of the multi-anode photometer on the same time scale, with corresponding fields of view as delineated by dotted lines in the image on the right [*Takahashi et al.*, 1997]. The second ELF pulse occurs simultaneously with the Sprite luminosity and has a similar form to the optical data from channels #6 and #7, consistent with the results shown in Figures 4.13 and 4.14. Figure 4.18 shows a sferic waveform produced by a 72-kA positive CG at 07:37:51 UT. The lower panel shows the ELF sferic, where the second ELF pulse lags the first ELF pulse by $\sim$70 ms and reaches approximately half its peak amplitude. The multi-anode photometer signatures and ELF data are shown on identical time axes in Figure 4.19. The second ELF pulse exhibits a similar time development to the luminosity recorded by multi-anode photometer channel #9.

The coincident photometric and sferic measurements presented in Figures 4.13, 4.14, 4.17, and 4.19 show that the second ELF pulse occurs at the time of Sprite appearance to better than $\pm$0.2 ms. Every observation of the second ELF pulse in the Yucca Ridge continuous sferic data has two characteristics: (1) it is accompanied

Figure 4.19: (Top) The optical intensity of the Sprite at 07:37:51 UT on July 24, 1996, as recorded by the multi-anode photometer channels #6-10 (Courtesy of Dr. Y. Takahashi). The fields of view of the multi-anode photometer channels are indicated by dotted lines in the associated Sprite image at right. (Bottom) A time-expanded view of the bottom panel of Figure 4.18 from $t = {\sim}63$ to $t = {\sim}76$ ms, including the second ELF pulse.
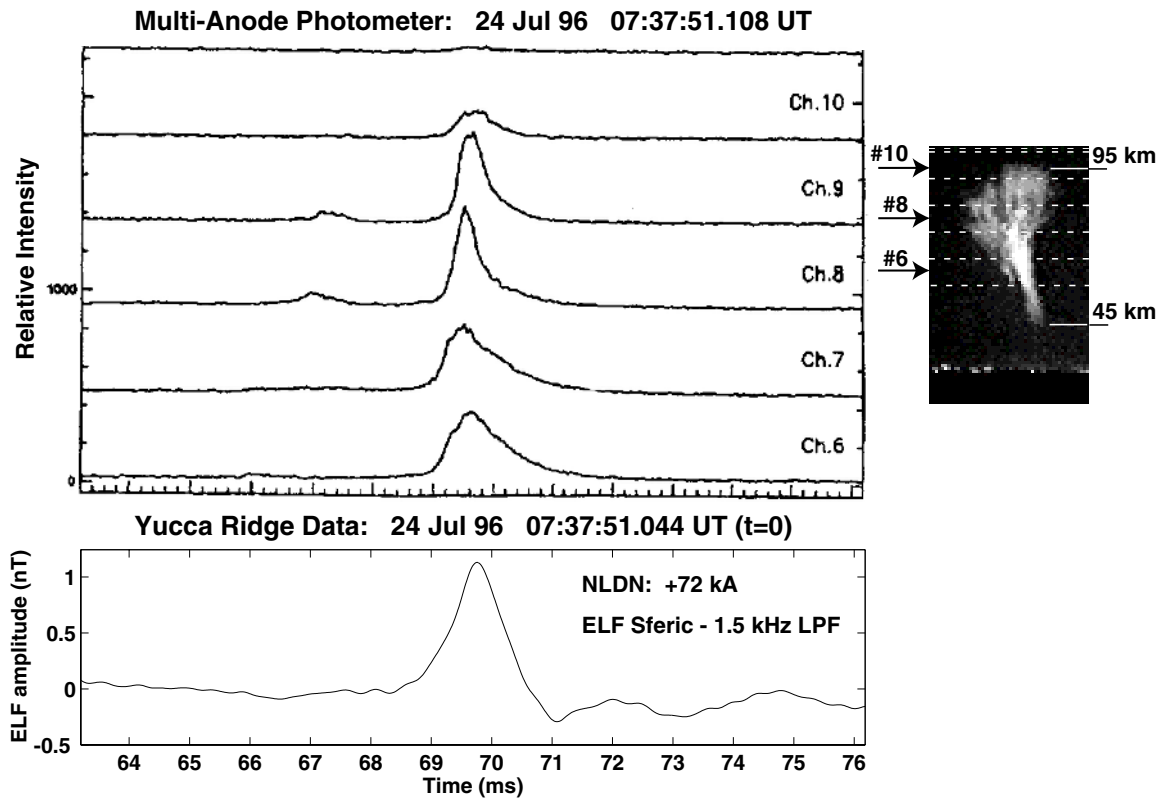
by the occurrence of a Sprite, and (2) it is *not* accompanied by a VLF oscillation at its onset, as opposed to sferics generated by conventional lightning discharges [*Inan et al.*, 1996b; *Reising et al.*, 1996; *Cummer et al.*, 1998]. Consequently, every occurrence of the second ELF pulse allows measurement of the delay between the positive CG and Sprite onset with ±0.2 ms precision. The second ELF pulse is clearly observed at Yucca Ridge in ∼20% of Sprite cases detected by the intensified CCD camera. This measurement of the CG-to-Sprite delay is nearly 50 times more precise than the 16.7 ms resolution provided by intensified CCD measurements (see Section 3.3).

In order to verify and extend the results of *Bell et al.* [1998], we identified 17 sferics on July 24, 1996, which had a clearly observed second ELF pulse and which were associated with optically detected Sprites. To find the relationship between CG-to-Sprite delay and continuing current following each positive CG, we applied the method of *Bell et al.* [1996; 1998] (see Section 3.3) to the *first* ELF pulse to
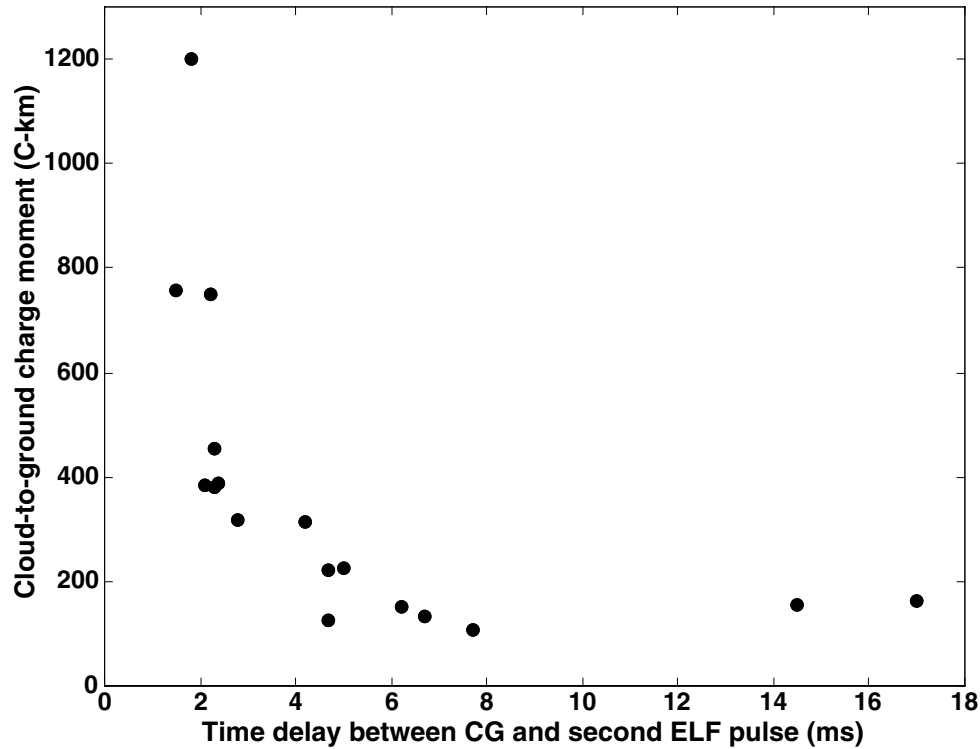
Figure 4.20: The relationship of continuing current charge moment and CG-to-Sprite delay for 17 Sprites on July 24, 1996. The moment of positive charge transfer from the cloud to the ground in the continuing current is inferred from measurements at Yucca Ridge of the first ELF pulse of each sferic. The CG-to-Sprite delay is the time between the peak of the first ELF pulse (within 1 ms of sferic onset) and the peak of the second ELF pulse.

obtain an estimate of the charge moment in the continuing current. The results for the 17 cases analyzed are shown in Figure 4.20. If the length of the cloud-to-ground channel is 10 km, these values range from ∼10 to 120 C. In all cases with charge transfer exceeding 30 C, the CG-to-Sprite delay was <4.5 ms. For smaller charge transfers (<25 C), the delay time until Sprite appearance ranges from ∼4 to 17 ms for this data set. From the two examples shown in Figures 4.16 to 4.19, we know that the maximum delay may be as large as 50-70 ms. These results indicate that if a large quantity of charge is lowered from the cloud to the ground in the continuing current, then a Sprite is produced in <5 ms. Smaller charge transfers to ground in the continuing current may require associated, yet weaker, intracloud currents to flow for a longer time in order to move sufficient positive charge for Sprite production (see Sections 1.2.5 and 3.3). These results agree with those of *Bell et al.* [1998] and extend their measurements of CG-to-Sprite delay to sub-millisecond time precision.

Chapter 5

Summary and Suggestions for Future Work

5.1   Summary

Novel digital signal processing techniques were developed for automated identification and arrival azimuth determination of radio atmospherics ("sferics") in broadband ELF/VLF data on a continuous basis. Sferics are identified in the presence of non-stationary interference produced by natural and anthropogenic sources, based on criteria of threshold intensity and of coherence among multiple sensors. Identification of the time of occurrence of sferics to ∼1 ms precision allows the identification of individual lightning discharges as the sources of individual sferics. The arrival azimuth of each sferic is determined using the VLF Fourier Goniometry technique [*Burgess*, 1993]. Based on broadband ELF/VLF measurements at Palmer Station, Antarctica, we measure the arrival azimuths of individual sferics and compare them with the expected arrival azimuths based on known locations of the individual source lightning discharges. The locations of lightning flashes in the continental U.S. are identified by the National Lightning Detection Network (NLDN) within ∼0.5 km precision. Comparison of expected and measured arrival azimuths demonstrates arrival azimuth determination to ±1° precision for sferics propagating from Nebraska to Palmer Station, Antarctica, a source-to-receiver distance of ∼12,000 km.

Broadband ELF/VLF measurements of sferics at Palmer Station, Antarctica, show that the ELF "slow tails" of Sprite-associated sferics have large energy in relation

to the slow tails of non Sprite-associated sferics at a range of ∼12,000 km [*Reising et al.*, 1996]. Since ELF slow tails are enhanced by continuing current flowing on ∼1-3 ms time scales, these measurements provide the first evidence that continuing currents are a necessary component of *those* positive cloud-to-ground (CG) discharges which lead to Sprite production [*Reising et al.*, 1996]. Continuing current of >1 ms duration after the first return stroke of a flash is necessary to transfer >120 C of charge from the cloud to the ground. Evidence for continuing current in Sprite-producing lightning flashes is consistent with predictions based on quasi-electrostatic models of Sprite production. *Pasko et al.* [1997] predict that the cloud-to-ground charge moment change in a lightning discharge must exceed a threshold value in order for a Sprite to be produced.

Broadband ELF/VLF measurements of sferics near Ft. Collins, Colorado, demonstrate that the ELF sferic energy is a proxy indicator for Sprite occurrence that can be used to estimate the number of Sprites produced by a thunderstorm with an accuracy of ±25%. Our results are in agreement with previous criteria for Sprite-producing thunderstorms in the U.S. Great Plains [*Lyons*, 1996], extend these predictions to other geographical regions and provide an estimate of the number of Sprites produced by each thunderstorm.

Video observations of Sprites, simultaneous with broadband ELF/VLF measurements, confirm that Sprites are uniquely associated with positive CG lightning flashes. The identification of Sprite onset time with ∼17 ms resolution reveals variable delays of 1-100 ms between the positive CG lightning discharge and the Sprite [*Bell et al.*, 1996; 1998]. When photometer measurements are available, they enable the identification of Sprite onset time with sub-millisecond resolution. Comparison of photometer measurements and ELF sferics demonstrates the simultaneity of Sprite luminosity and an ELF "second pulse" radiated by currents within the body of the Sprite [*Cummer et al.*, 1998]. In our study, we confirm the simultaneity of Sprite luminosity and the ELF second pulse in cases where the Sprite is delayed by 50-70 ms after the Sprite-associated positive CG. Our measurements of the ELF second pulse are used to identify an approximately linear relationship between the current within the Sprite body and the total luminosity of the Sprite.

Measurements of sferics from multiple storms at Palmer Station, Antarctica, show that the ELF sferic energy is a useful indicator of Sprite occurrence, even at large distances (∼12,000 km) from the source lightning. Video observations are not always

practical, so the proxy indicator is needed for identification of Sprite-producing storms and assessment of Sprite occurrence rates on a global basis. Our results suggest that a few appropriately placed ELF/VLF sferics receivers are sufficient for estimation of global Sprite occurrence rates.

5.2 Suggestions for Future Work

5.2.1 Assessment of the Global Distribution of Sprite Occurrence

Sprites have been measured from the ground over thunderstorms in the U.S. Great Plains [*Lyons,* 1996], the Midwest [*Winckler et al.*, 1996], Florida [*Stanley et al.*, 1997], Mexico [*Barrington-Leigh et al.*, 1997] and northern Australia [*R. Dowden, personal communication*, 1997]. In addition, Sprites have been measured from aircraft over the central U.S. [*Sentman et al.*, 1995] and over Central America and Peru [*Sentman et al.*, 1996]. Observations from the Space Shuttle have revealed Sprite occurrence over thunderstorms in equatorial Africa, Brazil and central South America, Indonesia and northern Australia [*Boeck et al.*, 1995]. However, with fewer than 20 observations of Sprites, the sample size of the Space Shuttle data is too small for assessment of the geographical distribution of Sprite occurrence.

Since continuous optical monitoring of Sprite occurrence on large spatial scales is not practical, an alternative proxy indicator for Sprite occurrence is needed. Measurements of the ELF energy of sferics can be used as a proxy indicator for Sprite occurrence over large areas of the Earth. A multistation sferics network can be implemented to identify the storm of origin for each detected sferic, as described in Section 2.4. The proxy indicator can provide estimates of Sprite occurrence at ranges of at least ∼12,000 km (see Section 4.3.4). As a result, the global rate of Sprite occurrence can be assessed from a coordinated four or five station network of broadband ELF/VLF receivers (see Section 5.2.3).

The global rate of Sprite occurrence is needed in order to assess the global effect of the electrodynamic coupling of lightning energy to the mesosphere and to the lower ionosphere. The runaway acceleration of electrons [*Bell et al.*, 1995] and ambient electron heating [*Pasko et al.*, 1997] which participate in the creation of the optical emissions of Sprites may also influence reaction rates and lead to the production

of different types of ions, potentially affecting mesospheric chemistry and dynamics. Additionally, quasi-electrostatic thundercloud fields may maintain the ionosphere at a persistently heated level [*Inan et al.*, 1996d], possibly producing persistent infrared glow [*Picard et al.*, 1997], and affecting ionospheric chemistry and dynamics. Assessment of these global effects requires knowledge of the occurrence of Sprites and of the characteristics of their associated lightning discharges. This can be accomplished on a global scale using a network consisting of a few appropriately placed broadband ELF/VLF receivers.

5.2.2   ELF/VLF Proxy Indicator for the Occurrence of Elves

Using methods similar to those discussed in Chapter 4 of this dissertation, a proxy indicator for the occurrence of elves may be developed and verified. "Elves" are optical emissions produced in the lower ionosphere ($\sim$80-95 km altitude) which develop on sub-millisecond time scales and which have horizontal extents of at least 300 km and possibly as large as 600 km [*Boeck et al.*, 1992; *Inan et al.*, 1997]. Elves are thought to be produced by the heating of lower ionospheric electrons by electromagnetic pulses produced by lightning [*Inan et al.*, 1996c; *Glukhov and Inan*, 1996], and predictions based on that mechanism agree with measurements of the rate of horizontal expansion of elves performed as part of the Stanford University Fly's Eye Experiment [*Inan et al.*, 1997]. Even though their peak brightness is similar to that of Sprites [*Fukunishi et al.*, 1996], elves are more difficult to identify based on low light level video observations because of their extremely short duration compared to the $\sim$17 ms integration times of conventional video cameras. Consequently, validation of any proxy indicator developed from ELF/VLF measurements of sferics requires the use of a data set for which existence or absence of elves is clearly verifiable. Example data sets are the Fly's Eye photometer data [*Barrington-Leigh et al.*, 1997] and multi-anode photometer data conducted by experimenters at Tohoku University [*Takahashi et al.*, 1997]. The optical intensity threshold for detection of elves depends upon the particular instrument used. Improvements in sensitivity were accomplished by using a red-sensitive filter to modify the broadband response of standard photomultiplier tubes [*Inan et al.*, 1997; *Barrington-Leigh et al.*, 1997]. It is likely that only a subset of elves is detectable with current instruments and that further improvements will result in the discovery of lower-luminosity elves.

Elves were observed first in association with positive CGs, but recent measurements show association with negative CGs as well [*Barrington-Leigh et al.*, 1997]. Because negative CGs occur at a much higher rate than positive CGs in summer thunderstorms, it is likely that the occurrence rate of elves exceeds that of Sprites. The occurrence of elves apparently does not require the large cloud-to-ground charge transfers that occur in Sprite-producing lightning discharges. Modeling of the interaction of electromagnetic pulses due to lightning with the ionosphere indicates that the maximum optical emission rates depend upon the maximum values of the electric field in the pulse. Therefore, one would anticipate that the peak current of the lightning flash would play an important role in the production of the optical emissions known as elves. As expected, elves detected using the Fly's Eye instrument were associated with positive and negative CGs which have NLDN-recorded peak currents primarily exceeding 75 kA [*Barrington-Leigh et al.*, 1997]. Preliminary studies indicate that those sferics generated by lightning discharges which lead to the production of elves do not necessarily have large ELF energies, but instead have large peak amplitudes in the VLF frequency range (here 1.5-22 kHz). The peak VLF amplitude tends to increase with increasing NLDN-recorded peak current, but the two measurements are not linearly related, especially for high NLDN-recorded peak currents. Consequently, VLF sferics are expected to provide substantially more information on the occurrence of elves than the NLDN-recorded peak current does.

5.2.3 Multistation Measurements of Global Lightning Flash Rates

A multistation network of broadband ELF/VLF sferics receivers has the potential to document thunderstorm locations and flash rates on a global basis. To find the precision of lightning location using multiple receivers, we envision four equidistant stations as an "ideal" four-station global sferics network. Any lightning flash would be within ∼6,700 km of at least one station in the ideal network. For two stations with orthogonal great circle paths to a source at ∼6,700 km from each station, the location of the source could be determined within 110 km in each direction, which is ∼1° in latitude and ∼1.5° in longitude, at middle latitudes. In most cases, one station would be further than 6,700 km from the source lightning, and the other station would be closer. Consequently, the location determination would be substantially better along

one axis than the other. The average error ellipse would have an area similar to a rectangle $\sim1°$ in latitude by $\sim1.5°$ in longitude, at middle latitudes. Implementation of the ideal four-station global network would require five or six stations due to practical considerations limiting possible receiver locations.

A multistation network for continuous detection of global or even Western Hemisphere lightning has the potential to greatly improve our current knowledge of the occurrence properties of lightning. A few of the myriad applications of continuous detection and location of lightning are the following: (1) validation and application of a continuous proxy indicator for convective rainfall with applications in climatology and hydrology; (2) formation of a proxy indicator for convective available potential energy, which may be a sensitive indicator for global climate change; and (3) assessment of the contribution of lightning to the production of nitrogen oxides (NO_y) in the troposphere and lower stratosphere. These applications are explained in the following three paragraphs.

There is extensive evidence indicating a spatial and temporal relationship between flash rates and rainfall rates [*Goodman and Christian*, 1993]. *Petersen and Rutledge* [1996] found quantitative relationships between convective rainfall and CG lightning, differing with storm type and land/ocean differences. These relationships are useful in estimating total rainfall using CG lightning data on $1°$ latitude by $1°$ longitude spatial scales and one-month time scales. Recent observations using an East Coast sferics network implemented by NASA Goddard Space Flight Center and Resolution Displays, Inc., show that areas of high lightning activity coincide with areas of heavy rain, based on Defense Meteorological Satellite Program passive microwave radiometry data [*Morales et al.*, 1997]. A continuous proxy indicator for convective rainfall is needed to fill temporal gaps between the overpasses of the Tropical Rainfall Measuring Mission satellite, launched in November 1997, and other satellites in low earth orbit. Infrared brightness data on cloud top temperature from the geostationary satellites is insufficient for quantitative derivation of the distribution and intensity of precipitation because identification of areas of rainfall is often obscured by residual cirrus clouds [*Arkin and Xie*, 1994].

Continuous lightning location and flash rate data provided by a multistation sferics network and analyzed in conjunction with satellite-based radar, passive microwave and infrared brightness temperature measurements, can yield new climatic insights. *Williams* [1992] showed that lightning flash rates were a strong function of convective

available potential energy, which he suggested could be a sensitive indicator of global temperature. Lightning measurements in the tropics have revealed up to a factor of ten increase in lightning flash rates when surface wet bulb temperature increased by only 1-2°C [*Williams et al.*, 1992]. Similarly, *Goodman and Christian* [1993] noted that global lightning activity provides a signature of tropical moisture and convective updraft velocity and is a proxy indicator for convective available potential energy (CAPE). Additionally, quantitative measurement of lightning activity on a global scale is needed as an input to and for verification of global circulation models [*Price and Rind*, 1994].

The need for continuous large-scale lightning observations has been emphasized by recent work on assessment of the contribution of lightning to the production of tropospheric nitrogen oxides (NO_y). Continuous lightning monitoring is needed for verification of global models of lightning as a source of tropospheric nitrogen oxides [*Levy et al.*, 1996]. Due to the importance of the concentration of nitrogen oxides in chemical processes affecting the concentration of stratospheric ozone, NASA has implemented programs such as the Subsonic Assessment, Ozone and Nitrogen Oxide Experiment in order to assess the relative contributions of jet aircraft, boreal fires, lightning and other sources of nitrogen oxides in the upper troposphere [*Thompson et al.*, 1996]. Because they occur in the proximity of the tropopause, intracloud flashes are believed to have a greater contribution to stratospheric chemistry than CG flashes. Intracloud lightning produces sferics with different waveform characteristics than those produced by CG lightning, but further analysis of sferics measurements is needed to enable continuous monitoring of intracloud lightning flash rates.

In summary, an envisioned global network of sferics receivers would document all lightning using five or six receiving stations and identify location within ∼1° in latitude and ∼1.5° in longitude, at middle latitudes. The continuous monitoring of global lightning has myriad applications in fields such as meteorology, hydrology, atmospheric chemistry and climatology.

Bibliography

[*Arkin and Xie*, 1994]   Arkin, P. A., and P. Xie, The Global Precipitation Climatology Project: first Algorithm Intercomparison Project, *Bull. Amer. Meteor. Soc., 75*, 401, 1994.

[*Barrington-Leigh et al.*, 1997]   Barrington-Leigh, C. P., M. Stanley, and U. S. Inan, Fast multi-channel photometry, broadband sferics, and intensified video observations of sprites and elves over southwestern United States and Mexico, *1997 AGU Fall Meeting Abstracts. EOS, 78*, F69, 1997.

[*Barry and Chorley*, 1987]   Barry, R. G., and R. J. Chorley, *Atmosphere, Weather and Climate*, 5th ed., Methuen, London, 1987.

[*Bell et al.*, 1995]   Bell, T. F., V. P. Pasko, and U. S. Inan, Runaway electrons as a source of Red Sprites in the mesosphere, *Geophys. Res. Lett., 22*, 2127, 1995.

[*Bell et al.*, 1996]   Bell, T. F., and S. C. Reising, Continuing currents determined from broadband ELF/VLF magnetic fields radiated by positive cloud-to-ground discharges associated with red sprites, *1996 AGU Fall Meeting Abstracts. EOS, 77*, F61, 1996.

[*Bell et al.*, 1998]   Bell, T. F., S. C. Reising, and U. S. Inan, Intense continuing currents following positive cloud-to-ground lightning associated with Red Sprites, *Geophys. Res. Lett., 25*, 1285, 1998.

[*Berger et al.*, 1975]   Berger, K., R. B. Anderson, and H. Kroninger, Parameters of lightning flashes, *Electra, 80*, 23, 1975.

[*Boccippio et al.*, 1995]   Boccippio, D. J., E. R. Williams, S. J. Heckman, W. A. Lyons, I. T. Baker, and R. Boldi, Sprites, ELF transients, and positive ground strokes, *Science, 269*, 1088, 1995.

[*Boeck et al.*, 1992]   Boeck, W. L., O. H. Vaughan Jr., R. J. Blakeslee, B. Vonnegut, and M. Brook, Lightning induced brightening in the airglow layer, *Geophys. Res. Lett., 19*, 99, 1992.

[*Boeck et al.*, 1995]   Boeck, W. L., O. H. Vaughan Jr., R. J. Blakeslee, B. Vonnegut, M. Brook, and J. McKune, Observations of lightning in the stratosphere, *J. Geophys. Res., 100*, 1465, 1995.

[*Brook et al.*, 1982]   Brook, M., M. Nakano, P. Krehbiel, and T. Takeuti, The electrical structure of the Hokuriku winter thunderstorms, *J. Geophys. Res., 87*, 1207, 1982.

[*Brook et al.*, 1989]   Brook, M., R. W. Henderson, and R. B. Pyle, Positive lightning strokes to ground, *J. Geophys. Res., 94*, 13,295, 1989.

[*Brooks*, 1925]   Brooks, C. E. P., The distribution of thunderstorms over the globe, *Geophys. Mem. London, 13*, 147, 1925.

[*Budden*, 1961]   Budden, K. G., *The Wave-Guide Mode Theory of Wave Propagation*, Logos, London, 1961.

[*Budden*, 1962]   Budden, K. G., The influence of the Earth's magnetic field on radio propagation by wave-guide modes, *Proc. Roy. Soc. A, 265*, 538, 1962.

[*Burgess*, 1993]   Burgess, W. C., Lightning-induced coupling of the radiation belts to geomagnetically conjugate ionospheric regions, Ph. D. Thesis, Stanford University, Stanford, California, 1993.

[*Burgess and Inan*, 1993]   Burgess, W. C., and U. S. Inan, The role of ducted whistlers in the precipitation, loss and equilibrium flux of the nighttime D-region, *J. Geophys. Res., 98*, 15,643, 1993.

[*Burke*, 1996]   Burke, M. W., *Image Acquisition*, Chapman and Hall, London, 1996.

[*Christian et al.*, 1996]   Christian, H. J., K. T.Driscoll, S. J. Goodman, R. J. Blakeslee, D. A. Mach, and D. E. Buechler, The Optical Transient Detector (OTD), *Proc. 10th Int'l Conf. on Atmospheric Electricity*, Osaka, Japan, 368, June 10-14, 1996.

[*Cousins*, 1972]   Cousins, M. D., Direction finding on whistlers and related VLF signals, *Tech. Rep. 3432-2*, Stanford Electronics Laboratories, Stanford, California, 1972.

[*Cummer*, 1997]   Cummer, S. A., Lightning and ionospheric remote sensing using VLF/ELF radio atmospherics, Ph. D. Thesis, Stanford University, Stanford, California, 1997.

[*Cummer and Inan*, 1997]   Cummer, S. A., and U. S. Inan, Measurement of charge transfer in sprite-producing lightning using ELF radio atmospherics, *Geophys. Res. Lett., 24*, 1731, 1997.

[*Cummer et al.*, 1998] Cummer, S. A., U. S. Inan, T. F. Bell, and C. P. Barrington-Leigh, ELF radiation produced by electrical currents in Sprites, *Geophys. Res. Lett., 25*, 1281, 1998.

[*Cummins et al.*, 1998] Cummins, K. L., M. J. Murphy, E. A. Bardo, W. L. Hiscox, R. B. Pyle, and A. E. Pifer, A combined TOA/MDF technology upgrade of the U.S. National Lightning Detection Network, *J. Geophys. Res., 103*, 9035, 1998.

[*Davies*, 1990] Davies, K., *Ionospheric Radio*, Peregrinus, London, 1990.

[*Dowden et al.*, 1994] Dowden, R. L., C. D. C. Adams, J. B. Brundell, and P. E. Dowden, Rapid onset, rapid decay (RORD), phase and amplitude perturbations of VLF subionospheric transmissions, *J. Atmos. Terr. Phys., 56*, 1513, 1994.

[*Fernsler and Rowland*, 1996] Fernsler, R. F., and H. L. Rowland, Models of lightning-produced sprites and elves, *J. Geophys. Res., 101*, 29,653, 1996.

[*Fishman et al.*, 1994] Fishman, G. J., P. N. Bhat, R. Malozzi, J. M. Horack, T. Koshut, C. Kouveliotou, G. N. Pendleton, C. A. Meegan, R. B. Wilson, W. S. Paciesas, S. J. Goodman, and H. J. Christian, Discovery of intense gamma-ray flashes of atmospheric origin, *Science, 264*, 1313, 1994.

[*Franz et al.*, 1990] Franz, R. C., R. J. Nemzek, and J. R. Winckler, Television image of a large upward electric discharge above a thunderstorm system, *Science, 249*, 48, 1990.

[*Fukunishi et al.*, 1996] Fukunishi, H., Y. Takahashi, M. Kubota, K. Sakanoi, U. S. Inan, and W. A. Lyons, Lightning-induced transient events in the lower ionosphere, *Geophys. Res. Lett., 23*, 2157, 1996.

[*Fukunishi et al.*, 1997] Fukunishi, H., Y. Takahashi, M. Sato, A. Shone, M. Fujito, and Y. Watanabe, Ground-based observations of ULF transients excited by strong lightning discharges producing elves and sprites, *Geophys. Res. Lett., 24*, 2973, 1997.

[*Füllekrug and Reising*, 1997] Füllekrug, M., and S. C. Reising, Promising regions of Sprite occurrence in North America, *1997 AGU Fall Meeting Abstracts. EOS, 78*, F83, 1997.

[*Glukhov and Inan*, 1996] Glukhov, V. S., and U. S. Inan, Particle simulation of the time-dependent interaction with the ionosphere of rapidly varying lightning EMP, *Geophys. Res. Lett., 23*, 2193, 1996.

[*Goodman and Christian*, 1993] Goodman, S. J., and H. J. Christian, Global observations of lightning, in R. J. Gurney, J. L. Foster and C. L. Parkinson, eds., *Atlas of Satellite Observations Related to Global Change*, Cambridge University Press, 1993.

[*Goto and Narita*, 1995] Goto, Y., and K. I. Narita, Electrical characteristics of winter lightning, *J. Atmos. Terr. Phys., 57*, 449, 1995.

[*Greifinger and Greifinger*, 1986] Greifinger, C., and P. Greifinger, Noniterative procedure for calculating ELF mode constants in the anisotropic Earth-ionosphere waveguide, *Radio Science, 21*, 981, 1986.

[*Hakeman et al.*, 1993] Hakeman, D. J., S. C. Reising, U. S. Inan and V. S. Sonwalkar, Long range thunderstorm location using a broadband VLF sferics detection technique, *1993 AGU Fall Meeting Abstracts. EOS, 74 Suppl.*, 165, 1993.

[*Helliwell*, 1965] Helliwell, R. A., *Whistlers and Related Ionospheric Phenomena*, Stanford University Press, Stanford, California, 1965.

[*Hepburn*, 1957] Hepburn, F., Atmospheric waveforms with very low frequency components below 1 kc/s known as slow tails, *J. Atmos. Terr. Phys., 10*, 266, 1957.

[*Idone et al.*, 1993] Idone, V. P., A. B. Saljoughy, R. W. Henderson, P. K. Moore, and R. B. Pyle, A reexamination of the peak current calibration of the National Lightning Detection Network, *J. Geophys. Res., 98*, 18,323, 1993.

[*Idone et al.*, 1998a] Idone, V. P., D. A. Davis, P. K. Moore, Y. Wang, R. W. Henderson, M. Ries, and P. F. Jamason, Performance evaluation of the U.S. National Lightning Detection Network in eastern New York: 2. Location accuracy, *J. Geophys. Res., 103*, 9057, 1998a.

[*Idone et al.*, 1998b] Idone, V. P., D. A. Davis, P. K. Moore, Y. Wang, R. W. Henderson, M. Ries, and P. F. Jamason, Performance evaluation of the U.S. National Lightning Detection Network in eastern New York: 1. Detection efficiency, *J. Geophys. Res., 103*, 9045, 1998b.

[*Inan et al.*, 1988] Inan, U. S., D. C. Shafer, W. Y. Yip, and R. E. Orville, Subionospheric VLF signatures of nighttime D-region perturbations in the vicinity of lightning discharges, *J. Geophys. Res., 93*, 11,455, 1988.

[*Inan et al.*, 1991] Inan, U. S., T. F. Bell, and J. V. Rodriguez, Heating and ionization of the lower ionosphere by lightning, *Geophys. Res. Lett., 18*, 705, 1991.

[*Inan et al.*, 1993] Inan, U. S., J. V. Rodriguez, and V. P. Idone, VLF signatures of lightning-induced heating and ionization of the nighttime D-region, *Geophys. Res. Lett., 20*, 2355, 1993.

[*Inan et al.*, 1995] Inan, U. S., T. F. Bell, V. P. Pasko, D. D. Sentman, E. M. Wescott, and W. A. Lyons, VLF signatures of ionospheric disturbances associated with Sprites, *Geophys. Res. Lett., 22*, 3461, 1995.

[*Inan et al.*, 1996a] Inan, U. S., A. Slingeland, V. P. Pasko, and J. V. Rodriguez, VLF signatures of mesospheric / lower ionospheric response to lightning discharges, *J. Geophys. Res., 101*, 5219, 1996a.

[*Inan et al.*, 1996b] Inan, U. S., S. C. Reising, G. J. Fishman, and J. M. Horack, On the association of terrestrial gamma-ray bursts with lightning and implications for sprites, *Geophys. Res. Lett., 23*, 1017, 1996b.

[*Inan et al.*, 1996c] Inan, U. S., W. A. Sampson, and Y. N. Taranenko, Space-time structure of lower ionospheric optical flashes and ionization changes produced by lightning EMP, *Geophys. Res. Lett., 23*, 133, 1996c.

[*Inan et al.*, 1996d] Inan, U. S., V. P. Pasko, and T. F. Bell, Sustained heating of the ionosphere above thunderstorms as evidenced in "early/fast" VLF events, *Geophys. Res. Lett., 23*, 1067, 1996d.

[*Inan et al.*, 1997] Inan, U. S., C. Barrington-Leigh, S. Hansen, V. S. Glukhov, and T. F. Bell, Rapid lateral expansion of optical luminosity in lightning-induced ionospheric flashes referred to as 'elves', *Geophys. Res. Lett., 24*, 583, 1997.

[*Krider et al.*, 1976] Krider, E. P., R. C. Noggle, and M. A. Uman, A gated, wide-band magnetic direction finder for lightning return strokes, *J. Appl. Meteor., 15*, 301, 1976.

[*Krider et al.*, 1980] Krider, E. P., R. C. Noggle, A. E. Pifer, and D. L. Vance, Lightning direction-finding systems for forest fire detection, *Bull. Amer. Meteor. Soc., 61*, 980, 1980.

[*Lehtinen et al.*, 1996] Lehtinen, N. G., M. Walt, U. S. Inan, T. F. Bell, and V. P. Pasko, γ-ray emission produced by a relativistic beam of runaway electrons accelerated by quasi-electrostatic thundercloud fields, *Geophys. Res. Lett., 23*, 2645, 1996.

[*Lehtinen et al.*, 1997] Lehtinen, N. G., T. F. Bell, V. P. Pasko, and U. S. Inan, A two-dimensional model of runaway electron beams driven by quasi-electrostatic thundercloud fields, *Geophys. Res. Lett., 24*, 2639, 1997.

[*Levy et al.*, 1996] Levy, H., W. J. Moxim, and P. S. Kasibhatla, A global three-dimensional time-dependent lightning source of tropospheric NO_x, *J. Geophys. Res., 101*, 22,911, 1996.

[*Lyons*, 1994] Lyons, W. A., Characteristics of luminous structures in the stratosphere above thunderstorms as imaged by low-light level video, *Geophys. Res. Lett., 21*, 875, 1994.

[*Lyons*, 1996] Lyons, W. A., Sprite observations above the U.S. High Plains in relation to their parent thunderstorm systems, *J. Geophys. Res., 101*, 29,641, 1996.

[*Lyons et al.*, 1989] Lyons, W. A., D. A. Moon, J. S. Schuh, N. J. Petit and J. R. East-
man, The design and operation of a national lightning detection network using
time-of-arrival technology, *Proc. 1989 Int'l Conf. on Lightning and Static Elec-
tricity*, Bath, England, Sept. 1989.

[*Mach et al.*, 1986] Mach, D. M., D. R. MacGorman, W. D. Rust, and R. T. Arnold,
Site errors and detection efficiency in a magnetic direction-finder network for
locating lightning strikes to ground, *J. Atmos. Ocean. Tech., 3*, 67, 1986.

[*Marshall et al.*, 1996] Marshall, T. C., M. Stolzenburg, and W. D. Rust, Electric
field measurements above mesoscale convective systems, *J. Geophys. Res., 101*,
6979, 1996.

[*Morales et al.*, 1997] Morales, C. A., J. A. Weinman, J. S. Kriz, and G. D. Alexan-
der, Thunderstorm distributions from the NASA/RDI sferics observing system,
1997 AGU Fall Meeting Abstracts. EOS, 78, F255, 1997.

[*Moran and Morgan*, 1997] Moran, J. M., and M. D. Morgan, *Meteorology: The
Atmosphere and the Science of Weather*, 5th ed., Prentice-Hall, Upper Saddle
River, New Jersey, 1997.

[*Milikh et al.*, 1995] Milikh, G. M., K. Papadopoulos, and C. L. Chang, On the
physics of high altitude lightning, *Geophys. Res. Lett., 22*, 85, 1995.

[*Nelson et al.*, 1997] Nelson, T. E., W. A. Lyons, M. Stanley, P. Krehbiel, M. Brook,
R. A. Armstrong, E. R. Williams, D. M. Suszcynsky, S. C. Reising, K. Cummins,
J. B. Brundell, J. L. Bahr, and R. L. Dowden, A detailed multi-sensor investi-
gation of a complex Sprite event, *1997 AGU Fall Meeting Abstracts. EOS, 78*,
F69, 1997.

[*Oppenheim and Schafer*, 1989] Oppenheim, A. V., and R. W. Schafer, *Discrete-
Time Signal Processing*, Prentice-Hall, Englewood Cliffs, NJ, 1989.

[*Orville*, 1994] Orville, R. E., Cloud-to-ground lightning flash characteristics in the
contiguous United States: 1989-1991, *J. Geophys. Res., 99*, 10,833, 1994.

[*Orville and Henderson*, 1986] Orville, R. E., and R. W. Henderson, Global distri-
bution of midnight lightning: September 1977 to August 1978, *Mon. Weather
Rev., 114*, 2640, 1986.

[*Orville et al.*, 1983] Orville, R. E., R. W. Henderson, and L. F. Bosart, An east
coast lightning detection network, *Bull. Amer. Meteor. Soc., 64*, 1029, 1983.

[*Orville et al.*, 1988] Orville, R. E., R. W. Henderson, and L. F. Bosart, Bipole
patterns revealed by lightning locations in mesoscale storm systems, *Geophys.
Res. Lett., 15*, 129, 1988.

[*Orville Jr.*, 1987] Orville Jr., R. E., An analytical solution to obtain the optimum source location using multiple direction finders on a spherical surface, *J. Geophys. Res., 92*, 10,877, 1987.

[*Paschal*, 1988] Paschal, E. W., The design of broad-band VLF receivers with air-core loop antennas, (internal report), Stanford Electronics Laboratories, Stanford, CA, 1988.

[*Pasko et al.*, 1995] Pasko, V. P., U. S. Inan, Y. N. Taranenko, and T. F. Bell, Heating, ionization and upward discharges in the mesosphere due to intense quasi-electrostatic thundercloud fields, *Geophys. Res. Lett., 22*, 365, 1995.

[*Pasko et al.*, 1996] Pasko, V. P., U. S. Inan, and T. F. Bell, Sprites as luminous columns of ionization produced by quasi-electrostatic thundercloud fields, *Geophys. Res. Lett., 23*, 649, 1996.

[*Pasko et al.*, 1997] Pasko, V. P., U. S. Inan, T. F. Bell, and Y. N. Taranenko, Sprites produced by quasi-electrostatic heating and ionization in the lower ionosphere, *J. Geophys. Res., 102*, 4529, 1997.

[*Petersen and Rutledge*, 1996] Petersen, W. A., and S. A. Rutledge, Characteristic differences in cloud-to-ground lightning flash densities and rain-yields for different climate regimes, *Proc. 10th Int'l Conf. on Atmospheric Electricity*, Osaka, Japan, 396, June 10-14, 1996.

[*Picard et al.*, 1997] Picard, R. H., U. S. Inan, V. P. Pasko, J. R. Winick, and P. P. Wintersteiner, Infrared glow above thunderstorms?, *Geophys. Res. Lett., 24*, 2635, 1997.

[*Price and Rind*, 1994] Price, C., and D. Rind, Modeling global lightning distributions in a general circulation model, *Mon. Weather Rev., 122*, 1994.

[*Rakov and Uman*, 1990] Rakov, V. A., and M. A. Uman, Long continuing current in negative lightning ground flashes, *J. Geophys. Res., 95*, 5455, 1990.

[*Reising et al.*, 1996] Reising, S. C., U. S. Inan, T. F. Bell, and W. A. Lyons, Evidence for continuing current in Sprite-producing cloud-to-ground lightning, *Geophys. Res. Lett., 23*, 3639, 1996.

[*Rogers and Peden*, 1975] Rogers, J. C., and I. C. Peden, The VLF complex permittivity of deep Antarctic ice measured *in situ*, *Radio Science, 10*, 763, 1975.

[*Roussel-Dupré and Blanc*, 1997] Roussel-Dupré, R. A., and E. Blanc, HF echoes from ionization potentially produced by high-altitude discharges, *J. Geophys. Res., 102*, 4613, 1997.

[*Rowland et al.*, 1995]   Rowland, H. L., R. F. Fernsler, J. D. Huba, and P. A. Bernhardt, Lightning driven EMP in the upper atmosphere, *Geophys. Res. Lett., 22*, 361, 1995.

[*Rowland et al.*, 1996]   Rowland, H. L., R. F. Fernsler, and P. A. Bernhardt, Breakdown of the neutral atmosphere in the *D*-region due to lightning driven electromagnetic pulses, *J. Geophys. Res., 101*, 2297, 1996.

[*Rust et al.*, 1981]   Rust, W. D., D. R. MacGorman, and R. T. Arnold, Positive cloud-to-ground lightning flashes in severe storms, *Geophys. Res. Lett., 8*, 791, 1981.

[*Rutledge et al.*, 1990]   Rutledge, S. A., C. Lu, and D. R. MacGorman, Positive cloud-to-ground lightning in mesoscale convective systems, *J. Atmos. Sci., 47*, 2085, 1990.

[*Rutledge et al.*, 1993]   Rutledge, S. A., E. R. Williams, and W. A. Petersen, Lightning and electrical structure of mesoscale convective systems, *Atmos. Res., 29*, 27, 1993.

[*Sentman and Wescott*, 1993]   Sentman, D. D., and E. M. Wescott, Observations of upper atmospheric optical flashes recorded from an aircraft, *Geophys. Res. Lett., 20*, 2857, 1993.

[*Sentman et al.*, 1995]   Sentman, D. D., E. M. Wescott, D. L. Osborne, D. L. Hampton, and M. J. Heavner, Preliminary results from the Sprites94 aircraft campaign: 1. Red Sprites, *Geophys. Res. Lett., 22*, 1205, 1995.

[*Sentman et al.*, 1996]   Heavner, M. J., D. L. Hampton, D. D. Sentman, and E. M. Wescott, Sprites over Central and South America, *1996 AGU Fall Meeting Abstracts. EOS, 77*, F115, 1996.

[*Stanley et al.*, 1997]   Stanley, M., P. Krehbiel, W. Rison, and C. B. Moore, Observations of sprites and their parent lightning discharges in Florida storms, *1997 AGU Fall Meeting Abstracts. EOS, 78*, F69, 1997.

[*Stolzenburg et al.*, 1994]   Stolzenburg, M., T. C. Marshall, W. D. Rust, and B. F. Smull, Horizontal distribution of electrical and meteorological conditions across the stratiform region of a mesoscale convective system, *Mon. Weather Rev., 122*, 1777, 1994.

[*Strum and Kirk*, 1988]   Strum, R. D., and D. E. Kirk, *First Principles of Discrete Systems and Digital Signal Processing*, Addison-Wesley, Reading, MA, 1988.

[*Sukhorukov*, 1992]   Sukhorukov, A. I., On the excitation of the Earth-ionosphere waveguide by pulsed ELF sources, *J. Atmos. Terr. Phys., 54*, 1337, 1992.

[*Sukhorukov and Stubbe*, 1997] Sukhorukov, A. I., and P. Stubbe, On ELF pulses form remote lightnings triggering sprites, *Geophys. Res. Lett., 24*, 1639, 1997.

[*Takahashi et al.*, 1997] Takahashi, Y., M. Fujito, Y. Watanabe, and H. Fukunishi, Multi-anode array photometer observations of the intensity ratio of N_2 1st and 2nd positive bands in sprites and elves, *1997 AGU Fall Meeting Abstracts. EOS, 78*, F69, 1997.

[*Taranenko and Roussel-Dupré*, 1996] Taranenko, Y. N., and R. A. Roussel-Dupré, High altitude discharges and gamma-ray flashes: a manifestation of runaway air breakdown, *Geophys. Res. Lett., 23*, 571, 1996.

[*Taranenko et al.*, 1993] Taranenko, Y. N., U. S. Inan, and T. F. Bell, Interaction with the lower ionosphere of electromagnetic pulses from lightning: Heating, attachment and ionization, *Geophys Res. Lett., 19*, 1815, 1993.

[*Taylor and Sao*, 1970] Taylor, W. L. and K. Sao, ELF attenuation rates and phase velocities observed from slow-tail components of atmospherics, *Radio Science, 5*, 1453, 1970.

[*Thomson*, 1993] Thomson, N. R., Experimental daytime VLF ionospheric parameters, *J. Atmos. Terr. Phys., 55*, 173, 1993.

[*Thompson et al.*, 1996] Thompson, A. M., K. E. Pickering, D. P. McNamara, M. R. Schoeberl, R. D. Hudson, J. H. Kim, E. V. Browell, V. Kirchoff, and D. Nganga, Where did tropospheric ozone over southern Africa and the tropical Atlantic come from in October 1992? Insights from TOMS, GTE TRACE A, and SAFARI 1992, *J. Geophys. Res., 101*, 24,251, 1996.

[*Uman*, 1987] Uman, M. A., *The Lightning Discharge*, International Geophysics Series - Vol. 39, Academic Press, Orlando, 1987.

[*Wait*, 1960] Wait, J. R., On the theory of the slow tail portion of atmospheric waveforms, *J. Geophys. Res., 65*, 1939, 1960.

[*Weidman and Krider*, 1986] Weidman, C. D., and E. P. Krider, The amplitude spectra of lightning radiation fields in the interval from 1 to 20 MHz, *Radio Science, 21*, 964, 1986.

[*Wescott et al.*, 1995] Wescott, E. M., D. Sentman, D. Osborne, D. Hampton, and M. Heavner, Preliminary results from the Sprites94 aircraft campaign: 2. Blue Jets, *Geophys. Res. Lett., 22*, 1209, 1995.

[*Wescott et al.*, 1996] Wescott, E. M., D. D. Sentman, M. J. Heavner, D. L. Hampton, D. L. Osborne, and O. H. Vaughan Jr., Blue starters: brief upward discharges from an intense Arkansas thunderstorm, *Geophys. Res. Lett., 23*, 2153, 1996.

[*Williams*, 1992]   Williams, E. R., The Schumann resonance: A global tropical ther-mometer, *Science, 256*, 1184, 1992.

[*Williams*, 1995]   Williams, E. R., Meteorological aspects of thunderstorms, Ch. 2 of H. Volland, Ed., *Handbook of Atmospheric Electrodynamics, Vol. I*, CRC, Boca Raton, 1995.

[*Williams et al.*, 1992]   Williams, E. R., S. A. Rutledge, S. G. Geotis, N. Renno, E. Rasmussen, and T. Rickenbach, A radar and electrical study of tropical "hot towers," *J. Atmos. Sci., 49*, 1386, 1992.

[*Wilson*, 1925]   Wilson, C. T. R., The electric field of a thundercloud and some of its effects, *Proc. Phys. Soc. London, 37*, 32D, 1925.

[*Winckler et al.*, 1996]   Winckler, J. R., W. A. Lyons, T. E. Nelson, and R. J. Nemzek, New high-resolution ground-based studies of sprites, *J. Geophys. Res., 101*, 6997, 1996.